

**GIS-Based Predictive Mapping of Gold Prospectivity: A case  
Study in the Busia Goldfield, Southeastern Uganda.**

**Henry Ngada**

**March, 2009**

GIS-Based Predictive Mapping of Gold Prospectivity: A case Study in the Busia Goldfield,  
South-eastern Uganda

By

Henry Ngada

Thesis submitted to the International Institute for Geo-information Science and Earth Observation in partial fulfilment of the requirements for the degree of Master of Science in Geo-information Science and Earth Observation, Specialisation: ***Earth Resources Exploration***

Thesis Assessment Board

- |                               |                    |
|-------------------------------|--------------------|
| 1. Prof.Dr. F.D. van der Meer | Chair              |
| 2. Dr. P.M. van Dijk          | Examiner           |
| 3. Dr. J. Carranza            | Supervisor         |
| 4. Dr. F.J.A. van Ruitenbeek  | Supervisor         |
| 5. Drs. T.M. Loran            | Programme Director |



**INTERNATIONAL INSTITUTE FOR GEO-INFORMATION SCIENCE AND EARTH  
OBSERVATION ENSCHEDE, THE NETHERLANDS**

**Disclaimer**

This document describes work undertaken as part of a programme of study at the International Institute for Geo-information Science and Earth Observation. All views and opinions expressed therein remain the sole responsibility of the author, and do not necessarily represent those of the institute.

## Abstract

---

Lode gold mineralization occurs in the Busia Goldfield. However there is poor understanding of the mineralization model due to lack of publications. To contribute to a better definition of the mineralization model, the geological, geochemical and structural features were investigated so as to identify which features are spatially associated with the known gold occurrences. This was achieved by: 1) qualitatively synthesizing knowledge from geosciences literature about gold mineralization controls, 2) quantification of gold favourability with respect to each evidential feature, 3) generation of a gold prospectivity map via a knowledge-guided data-driven approach and 4) validation of the gold prospectivity map generated by overlaying of known gold occurrences onto the map.

Results show that: 1) the Busia gold field is a potential area for lode gold mineralization whose recognition requires the use of structures and lode gold pathfinder elements, 2) the Lode gold mineralization in the Busia goldfield is structurally controlled with the NW, NNW and NS faults being the principal geological features with which lode gold mineralization is associated, 3) although the multi-element association Fe-Ti-V-Cr-Ni-Cu-Zn as well as the individual uni-elements appear to be spatially associated with the gold anomalies and known gold occurrences, there is no significant linear association between Au and these elements and hence, they are only of lithological significance (i.e. amphibolites) which hosts the gold-bearing quartz veins and 4) the Amphibolites (mafic metavolcanics) in the Busia gold field are spatial vectors to shear/fracture zones with which lode gold mineralization is associated.

Additionally, the conformance of the current results to results of past gold prospectivity work in the Busia goldfield suggests that: 1) inverse distance weighting is a good method for interpolating geochemical data provided the data is auto-correlated, 2) the wildcat method is a good technique for quantifying and scoring the spatial association between geological features and zones of high prospectivity for mineral deposits such as lode gold mineralization/deposits, 3) Fuzzy algebraic product is a good method for integrating evidential maps to generate an overall mineral (e.g. gold) prospectivity map, 4) ground-collected and remotely-sensed datasets are useful for mapping geological features that are essential predictors for lode gold prospectivity and finally 5) GIS-based data representation and integration techniques are useful for mapping mineral prospectivity which can guide in decision making during mineral exploration.

**Key words:** lode gold, evidential features, knowledge-guided data-driven and GIS.

## Acknowledgements

---

I wish to express my sincere gratefulness to the Government of Uganda for financing my MSc programme through the ongoing Sustainable Management of Mineral Resources Project (SMMRP) in the Ministry of Energy and Mineral Development.

Special thanks go to the Commissioner of the Department of the Geological Survey and Mines (Mr. J. Tuhumwire), SMMRP Coordinators (Mr. J. Nyakana (RIP) and Mr. E. Katto) and the entire SMMRP management for all the assistance rendered. Thanks to my colleagues at the DGSM especially Mr. Peter Turyasigura, Mr. E.M. Isabirye, Mr. E Kahwa and Mr. Wabbi for all their support during my studies.

I am very grateful to my supervisors: Dr. John Carranza and Dr. F.J.A. van Ruitenbeek for their constructive criticisms and guidance which led to quality of this work.

My appreciation also goes to the entire ITC staff for all the services provided without which my study at ITC would not have been possible. Particular acknowledgement goes to programme Director (Drs. Tom Loran) for the parental care right from the Netherlands Embassy in Uganda while applying for a resident permit in The Netherlands. Thanks to Drs. B. de Smith and Dr. P.M. van Dijk for their parental care too.

I thank my fellow classmates, ITC Fellowship, St. Jacobus and St. Paul congregations, the Ugandan and East African student communities, Rev. Fr. F. Vester and Rev. Fr. Wiel Eggen and all friends for their social, cultural, and spiritual nourishment which made the Netherlands a home away from home.

I acknowledge my family members especially my mother Perepetwa K. Miti, my in-laws Mr & Mrs Lule and family for their love, prayers and encouragement before and during my studies. Thanks to my brothers Bakalikwira, Miti and Dr. Dhirumuka and my sister Anoonya for taking care of the family which provided a favourable environment for my studies. Special thanks to my dear and lovely wife Sylvia. N.K. Ngada for her tireless prayers for me as well as enduring the pains of long distance love and taking care of the home alone.

And to the Almighty God-the giver of life and wisdom and to my Lord and Saviour Jesus and to the Holy Spirit-my comforter and counsellor to whom this thesis is dedicated, be the glory for ever and ever, Amen.



## Table of contents

---

1.	Introduction .....	1
1.1.	Background .....	1
1.2.	Research problem .....	2
1.3.	Research questions .....	2
1.4.	Research objectives.....	3
1.5.	Methodology.....	3
1.6.	Thesis outline .....	4
2.	The study area .....	6
2.1.	Location and accessibility .....	6
2.2.	Geology and gold mineralization.....	8
2.2.1.	Regional Geological Setting.....	11
2.2.1.1.	Basement complex (GC).....	11
2.2.1.2.	Nyanzian-Kavirondian System (NZK) .....	11
2.2.1.3.	Buganda-Toro System (BT).....	11
2.2.1.4.	Karagwe-Ankolean System (KA) .....	12
2.2.1.5.	Upper Proterozoic Sediments .....	12
2.2.1.6.	Cenozoic-Mesozoic rocks .....	12
2.2.1.7.	Palaeozoic rocks .....	12
2.2.2.	Local geology of the BGF.....	12
2.2.2.1.	Basement/gneissic complex (GC >2930 Ma) .....	13
2.2.2.2.	Nyanzian-Kavirondian System .....	13
2.2.2.3.	Tertiary and Mesozoic .....	14
2.2.2.4.	Cenozoic rocks .....	14
2.2.2.5.	Intrusives .....	15
2.2.2.6.	Iganga-Irimbi granitoids complex (A3, 2930 Ma) .....	15
2.2.2.7.	Metamorphism .....	15
2.2.2.8.	Tectonics and structures.....	16
2.2.2.9.	Geochronology .....	16
2.2.3.	Lode gold deposits .....	16
2.2.3.1.	General characteristics of lode gold deposits.....	16
2.2.3.2.	Lode gold deposits characteristics in the Nyanzian greenstone belts.....	18
2.2.3.3.	Lode gold characteristics in the BGF.....	18
2.3.	Description of datasets and expected geoinformation .....	19
2.3.1.1.	Geological and topographical Maps.....	19
2.3.2.	Remote sensing (RS) data.....	20
2.3.3.	Airborne Magnetic and radiometric data.....	20
2.3.4.	Stream sediment geochemical data .....	21
2.3.5.	Field data .....	21
3.	Geological mapping with multispectral, magnetic and radiometric data.....	22
3.1.	Introduction.....	22
3.2.	Lithological mapping .....	22
3.3.	Lineament mapping .....	25

3.3.1.	Mapping of Lineaments using DEM.....	25
3.3.2.	Mapping of Lineaments using airborne magnetic data .....	26
3.4.	Discussion and conclusions .....	29
4.	Geochemical anomaly mapping with stream sediment geochemical data.....	30
4.1.	Quality assessment.....	30
4.2.	Univariate data analysis .....	31
4.2.1.	Exploratory data analysis of geochemical data (EDA) .....	31
4.2.1.1.	Descriptive statistics .....	31
4.2.1.2.	Univariate anomalies in stream sediment geochemical data.....	34
4.2.1.3.	Spatial distribution of uni-elements in stream sediment geochemical data.....	36
4.2.2.	Multivariate anomalies in stream sediment geochemical data.....	39
4.2.2.1.	Principle component analysis (PCA).....	39
4.3.	Discussion and conclusions .....	48
5.	Mapping of prospectivity for Au deposits.....	50
5.1.	Introduction.....	50
5.2.	Spatial association analysis to define prospectivity recognition criteria .....	51
5.3.	Knowledge-guided data-driven mapping of prospectivity for Au deposits .....	52
5.3.1.	Introduction.....	52
5.3.2.	Preparation of evidential features for gold prospectivity mapping.....	52
5.3.2.1.	Structural evidential maps .....	52
5.3.2.2.	Lithological evidential map.....	57
5.3.2.3.	Geochemical evidential map .....	58
5.3.2.4.	Integration of the evidential map .....	61
5.4.	Discussion and conclusions .....	64
6.	Overall Conclusions and Recommendations .....	65
6.1.	Overall conclusions.....	65
6.2.	Recommendations .....	66
7.	References: .....	67
8.	Appendices .....	70

## List of figures

---

Figure 1.1: Flow chart summarizing the methodology followed in Mapping Gold Prospectivity in the BGF.....	4
Figure 2.1 : Simplified regional geological features of Precambrian age (Hester et al., 2006) showing the area under study. Note also the Archean greenstone belts of Kenya and Tanzania neighbouring the BGF. ....	7
Figure 2.2: Photos of part of the BGF showing the topography. LL is low land area whereas the Carbonatite (C), Granite (B) and ferruginous quartzites (BIF) form a few of the isolated hills in the area. ....	8
Figure 2.3: Regional geology of Uganda (modified from an extract from the Atlas of Uganda, 1995).....	9
Figure 2.4: Geological map of the Busia Goldfield (Compiled from: (GARS-DBM-TEAM et al., 1998; Isabirye, 2005; Mroz et al., 1991a) .....	10
Figure 2.5: Orogenic gold deposits (Groves et al., 1998). Note the accretionary environment and associated vein-hosted gold deposits typical of greenstone belts (e.g. Busia gold field). ....	19
Figure 3.1: Lithological map modification. 3.1A shows lithological boundaries overlaid on radiometric ternary grid map and 3.1B is a modified lithological map. Note the offset of the Masaba granite (P) boundaries in 3.1A and the modified boundaries in 3.1B. The geomorphology added by the SRTM DEM underlying the ternary map improves the visual interpretation of the lithological boundaries.....	24
Figure 3.2: Extraction of Faults from an ASTER shaded relief DEM image (3.2A), 3.2B is the finished map of faults interpreted. Note the dominant NW lineament trend from the Rose diagram. ....	27
Figure 3.3: Extraction of lineaments (3.3A) using a 1 <sup>st</sup> vertical derivative from an RTP magnetic grid map and 3.3B is a finished lineaments map. ....	28
Figure 4.1: Au anomalies in log <sub>e</sub> transformed geochemical data. Figure: 4.2A and 4.2B are bulb plots and IDW interpolation Au data. Black triangles are respectively Au mines and Au prospects. ....	38
Figure 4.2: scatter plot of Log <sub>e</sub> excluding Au censored values versus PC1, PC2 and PC3 scores for both the felsic and mafic rock suites. ....	44
Figure 4.3: scatter plot of Log <sub>e</sub> excluding Au censored values versus PC4, PC5 and PC6 scores for both the felsic and mafic rock suites.....	45
Figure 4.4: Box and Whiskers plots for raw and Log <sub>e</sub> transformed Au excluding censored values for both felsic and mafic rock suites. N = 38 and 112 for felsic and mafic rock suites respectively. All units are in ppb and natural logarithmic numbers for raw and Log <sub>e</sub> transformed Au data respectively. The number assigned to each outlier is its corresponding sample location number for easy identification and followed up.....	46
Figure 4.5: Scatter plots of log <sub>e</sub> Fe <sub>2</sub> O <sub>3</sub> versus Log <sub>e</sub> PC1 scores of standardized stream sediment geochemical data for both felsic and mafic rock suites. Note the linear (R <sup>2</sup> =83.8% and 75.8% for felsic and mafic suites respectively) association between Fe and the PC1 scores. ....	47
Figure 5.1: Graph of class median of proximity to NS trending faults versus scores.....	54

Figure 5.2: Au prospectivity map based on the NW faults. The black triangles are known gold occurrences.....	55
Figure 5.3: Graph of scores versus class median of proximity to NS trending faults.....	56
Figure 5.4: Au prospectivity map based on the NS faults. The black triangles are known gold occurrences.....	56
Figure 5.5: Possible stratigraphic column with respect to Amphibolites, Banded Iron quartzites (BIFs) and Undifferentiated Nyanzian-Kavirondian metavolcanics and metasediments. Direction of younging is upwards.....	58
Figure 5.6: Au prospectivity map based on lithology. The black triangles are known gold occurrences.....	58
Figure 5.7: Histogram and box plots showing populations in the loge transformed Au data excluding censored values (N =150).....	59
Figure 5.8: Graph showing the variation of Au scores with the Au class median.....	60
Figure 5.9: Au prospectivity map based on Au geochemical data. The black triangles are known gold occurrences. Note that the maximum favourability score is 0.7071 but for visualization purpose, the favourability scores were stretched between 0.00 and 0.15. ....	61
Figure 5.10: Overall gold prospectivity map for the Busia gold field base on all evidential features. Black triangles are known gold occurrences. N1 and N2 zones are predicted as favourable.....	63

## List of tables

---

Table 4.1: Descriptive Statistics of raw stream sediment geochemical data for 1924 samples. Loge Skewness demonstrates the reduction in the skewness in the data. All units in ppm except for Au (ppb) and SiO <sub>2</sub> , Al <sub>2</sub> O <sub>3</sub> , Fe <sub>2</sub> O <sub>3</sub> , MgO and TiO <sub>2</sub> (%) .....	33
Table 4.2: Upper class boundaries of Uni-element background and anomaly based on threshold = Median+2MAD for both mafic and felsic facies in the BGF. All units are in ppm except for Au (ppb) and SiO <sub>2</sub> , Al <sub>2</sub> O <sub>3</sub> , Fe <sub>2</sub> O <sub>3</sub> , MgO and TiO <sub>2</sub> (%).....	35
Table 4.3: PCA of standardised (z) Log <sub>e</sub> transformed stream sediment data for 1924 samples, i.e. 492 and 1432 samples from mafic and felsic rock suits respectively.....	43
Table 5.1: proximity classes and scores of the distance to NW trending faults .....	54
Table 5.2: proximity classes and scores of the distance to NS trending faults .....	55
Table 5.3: Au data classes and scores .....	60

# 1. Introduction

## 1.1. Background

For many developing countries mineral resources are essential for socio-economic development. Investment in mineral resource exploration and exploitation leads to infrastructure development, creation of jobs as well as foreign exchange earning. In Uganda for example, the contribution of mineral resource development to the national foreign exchange earnings reached 30% between 1955 and 1976. Mineral resources are however non-renewable natural resources, i.e. any deposit, whatever its size, will eventually be depleted. Therefore, for sustainable developing of mineral resources, there is need to discover more mineral deposits. This in turn requires adequate mineral-resource geoinformation as well as relevant spatial datasets.

Mineral deposits are often discovered by comparing geology of different areas. For example, if some geological environment somewhere is mineralized, then, there is a high possibility that a similar geological setting elsewhere hosts mineral deposits of the same type. Thus, by applying geological knowledge from well-explored areas to poorly explored areas, mineral prospectivity can be mapped to guide in further exploration in the latter. Geological knowledge such as mineral deposit models (e.g. lode gold deposit model) is a guide to prospective areas for minerals. Mineral prospectivity of an area refers to the likelihood (<http://www.wordwebsoftware.com/>) of finding a given mineral in an area provided the necessary conditions exist.

A conceptual mineral deposit model describes the typical characteristics of a group of deposits (Bonham-Carter, 1994). These characteristics (depending on the deposit-type) may be spatial characteristics (Carranza and Hale, 2002e) such as: presence of or proximity to lineaments (faults/fractures, dykes etc), presence of or proximity to particular lithology, chemical elements spatial association, proximity to intrusive plutonic rocks, remote sensing spectral response, radiometric distribution, magnetic susceptibility etc. Applying a mineral deposit model of well explored areas to poorly explored areas may lead to the discovery of mineral deposits of the same type in the latter, given similar geological setting

Establishing a mineral deposit model is therefore crucial not only to field-based mineral exploration but also to mineral prospectivity mapping (MPM) in a Geographic Information

System (GIS), where mineral exploration is carried out on a remote basis. In this computer based software system (i.e. GIS) (often including hardware and personnel), spatial information can be captured, stored, analyzed, displayed and retrieved (Bonham-Carter, 1994). GIS-based MPM can be carried out to estimate the likelihood for mineral deposit occurrences at every location within a study area,(Carranza et al., 2008b). Consequently, GIS-based MPM can provide useful geoinformation for decision making in mineral exploration.

There are two GIS-based mineral prospectivity mapping methods: 1) conceptual and 2) empirical. Whereas conceptual methods involve subjective (i.e. knowledge-driven) weighting of evidential maps based on geological expertise, empirical methods involve objective (i.e. data-driven) weighting of evidential maps based on measured spatial association between locations of known mineral deposits and indicative geologic features, (Bonham-Carter, 1994). Therefore, empirical methods can be adopted in areas with a significant number of known mineral deposits while for areas with few known mineral deposits , a conceptual approach is appropriate.

## **1.2. Research problem**

Lode gold mineralization occurs in the Busia Goldfield (BGF) with Tiira (mechanized) gold mine, Amonikakinei and Syanyonja being well known gold producing areas in the BGF. Despite the number of geological studies and availability of geodata sets, the conceptual model for the lode Au mineralization at a goldfield-scale in the BGF is poorly understood due to the lack of publications of work done in the area. The poor understanding of the conceptual model of Au mineralization presents problems of: 1) data selection, 2) deciding which gold predictive features to enhance and 3) weighting the relative importance of the gold predictive features during exploring for gold in the area. Further more; sustainability of gold mining investment in the BGF is at risk if no other gold prospective areas are revealed. This research therefore seeks to make a contribution to a better defined conceptual model for the gold mineralization in the BGF.

## **1.3. Research questions**

To address the above problem there is need to find answers to the following questions:

- 1) What geological features and geochemical/geophysical anomalies are spatially associated with gold mineralization in the BGF?

- 2) How can the spatial association between the various geological features and geochemical/geophysical anomalies and known gold occurrences be quantified and combined in order to produce a gold predictive model?

#### **1.4. Research objectives**

To contribute to a better definition of the conceptual model of gold mineralization in the BGF by synthesizing the:

- 1) Qualitative knowledge from geosciences literature about gold mineralization controls
- 2) Quantitative knowledge of the spatial distribution of known gold occurrences and the spatial associations between the various geological features and geochemical/geophysical anomalies and known gold occurrences
- 3) To demonstrate the usefulness of ground-collected and remotely-sensed datasets for mapping geological features that can be used as predictors of gold prospectivity
- 4) To demonstrate GIS-based data representation and integration techniques for creating a gold predictive model.

#### **1.5. Methodology**

To realize the research objectives, the following steps (Figure1.1) were taken:

- 1) The geological literature about lode gold deposits in general and about previous works on gold deposits in the BGF and LVGF was reviewed, followed by a field survey, in order to define geological features that probably controlled and/or are indicative of lode gold mineralization in the BGF. A conceptual gold model (chapter 5) was also defined to guide in the collection of pertinent spatial datasets ( chapter 2) from which to extract features relevant to lode gold deposits
- 2) A spatial database for BGF was as a result developed to aid in the data analysis for gold prospectivity mapping
- 3) Data processing and analysis to enhance, extract, reclassify and buffer the features relevant to lode gold mineralization was carried out to generate binary predictor maps
- 4) Finally, the binary predictor maps were integrated (by the fuzzy algebraic product) to produce the final gold prospectivity map.

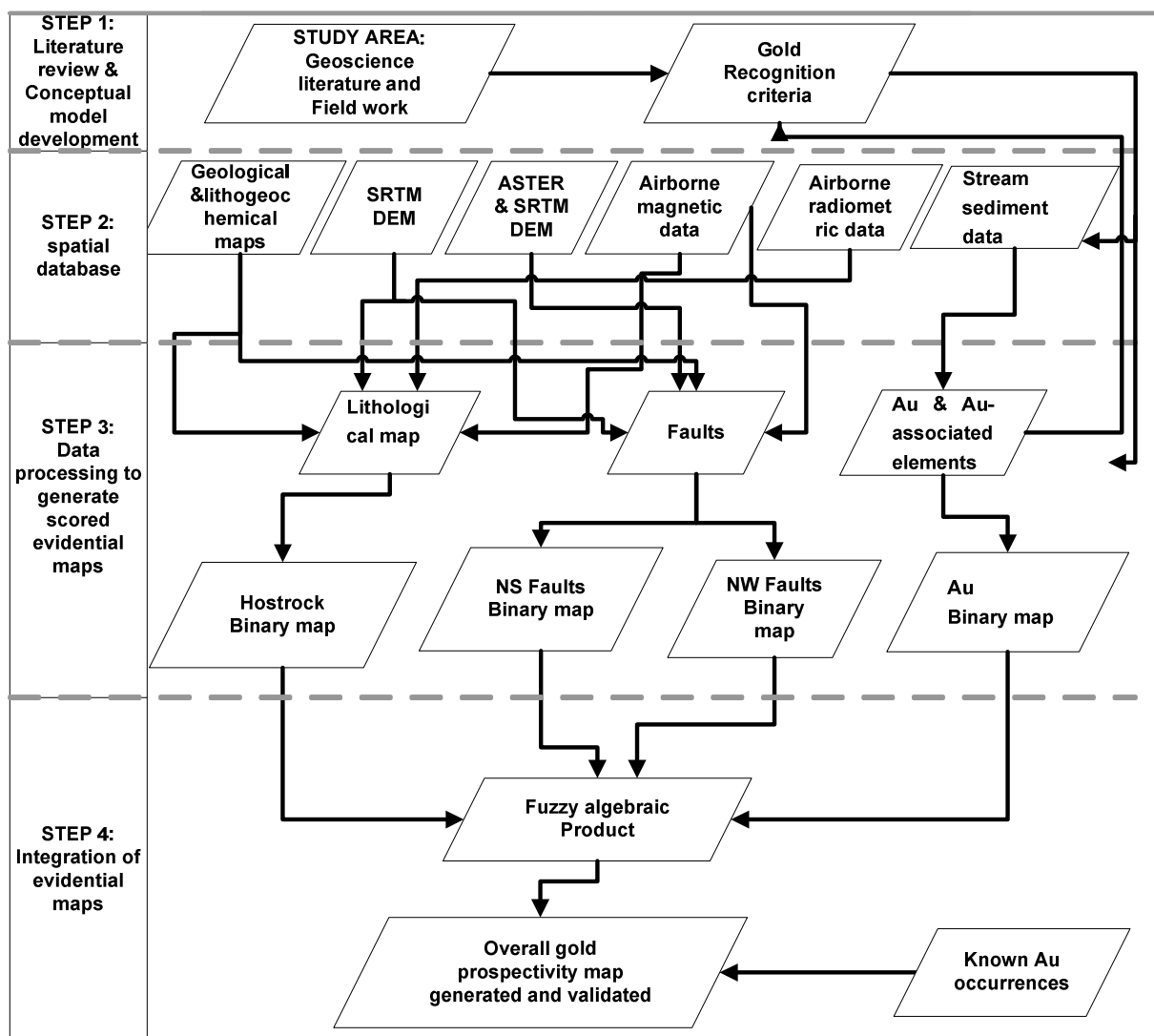


Figure1.1: Flow chart summarizing the methodology followed in Mapping Gold Prospectivity in the BGF

## 1.6. Thesis outline

This thesis presents a compilation of all the preliminary steps and findings of this research in six chapters. After this introductory Chapter 1, follows description of the study area in Chapter 2 including: location and accessibility, previous work in the area and the geodata sets used in the research. Chapter 3 presents the results of geologic interpretation in the study area with particular emphasis on lithological and lineament mapping. Chapter 4 deals with geochemical anomaly mapping using radiometric and stream sediment geochemical datasets. Chapter 5 focuses on the integration of the gold predictive features for gold

prospectivity mapping. Chapter6 finally outlines the overall conclusions and recommendations.

## **2. The study area**

### **2.1. Location and accessibility**

The study area (~2500 Km<sup>2</sup>) is situated at the extreme south-eastern part of Uganda, (Figure 2.1). Busia gold field extends eastwards to Kenya's south-western border with Uganda and continues southwards to Lake Victoria shores. It is located by UTM coordinates (575 000mE, 020 000mN), (630 000mE, 020 000mN), (630 000mE, 070 000mN) and (575 000mE, 070 000mN). It is located about 210 Km east of Kampala, the capital city of Uganda and can be accessed by taking the Kampala-Tororo or Kampala-Busia all-weather tarmac roads. Busia and Tororo are the biggest and nearest towns in the area and from them it is possible to reach all parts of the BGF by using motorable feeder roads. The area is relatively low lying with a few isolated hills formed by ferruginous quartzites (BIFs), Carbonatite and granites, (Figure 2.2A-D).

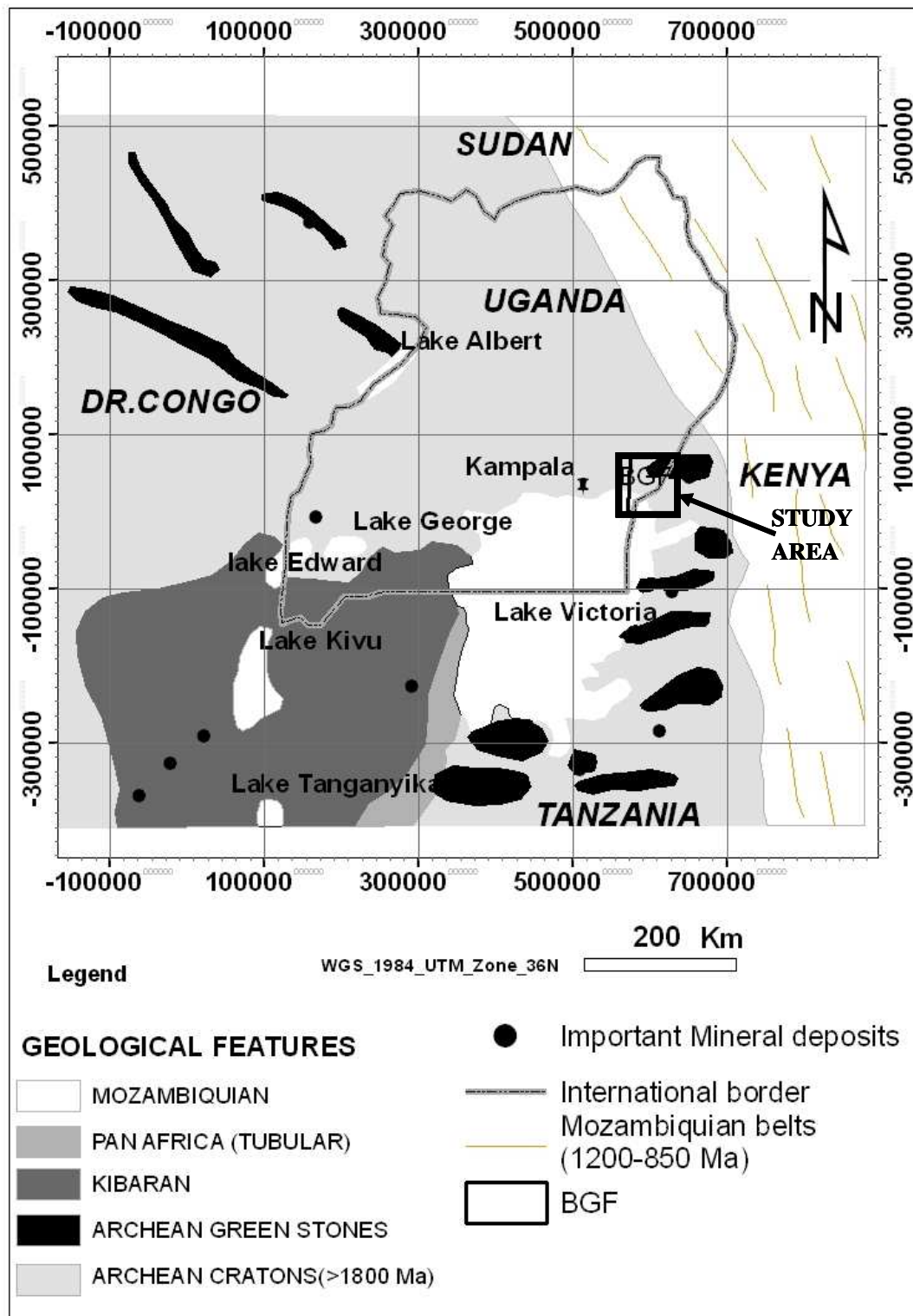


Figure 2.1 : Simplified regional geological features of Precambrian age (Hester et al., 2006) showing the area under study. Note also the Archean greenstone belts of Kenya and Tanzania neighbouring the BGF.

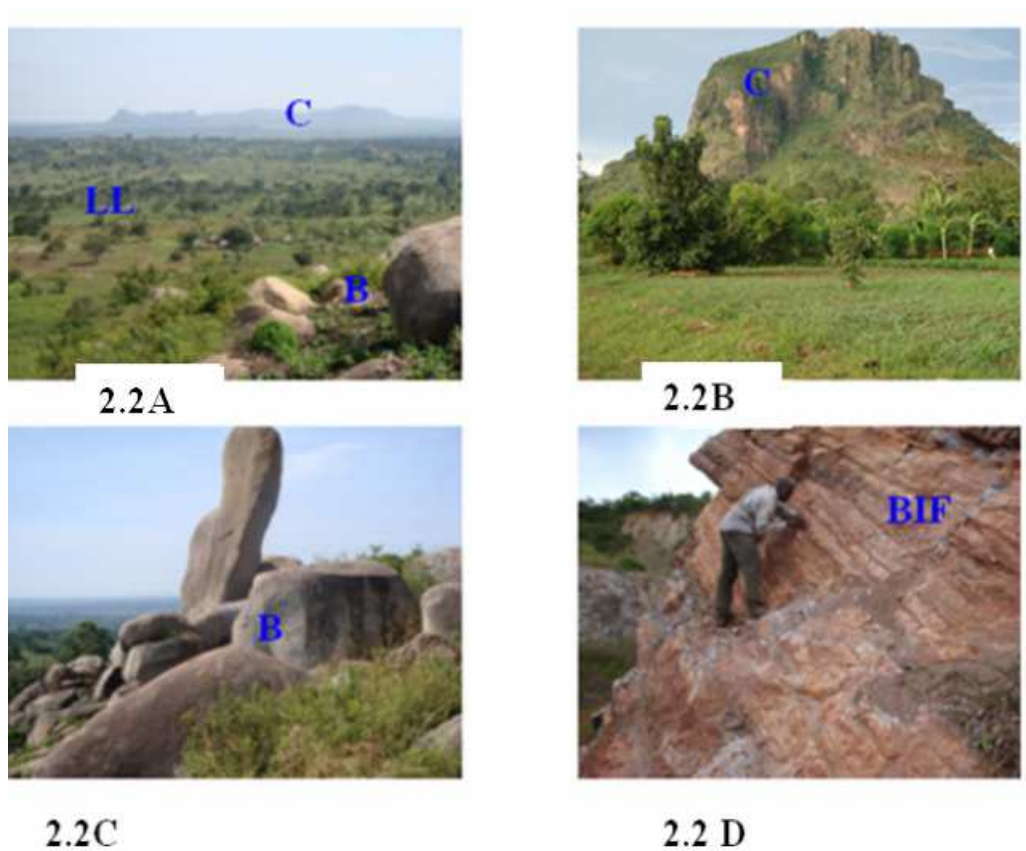


Figure 2.2: Photos of part of the BGF showing the topography. LL is low land area whereas the Carbonatite (C), Granite (B) and ferruginous quartzites (BIF) form a few of the isolated hills in the area.

## 2.2. Geology and gold mineralization

Mineralization is a process by which valuable minerals (e.g. Au) are introduced into a rock, resulting into an ore (Lapidus, 2003). Mineralization is therefore a geological phenomenon which can only be understood studying geology of the area under investigation. Consequently, this section reviews both the regional and local geological setting in which the BGF is situated in order to understand the factors underlying the Au mineralization in the area. Figures 2.3 and 2.4 are respectively the regional and local geology of the BGF.

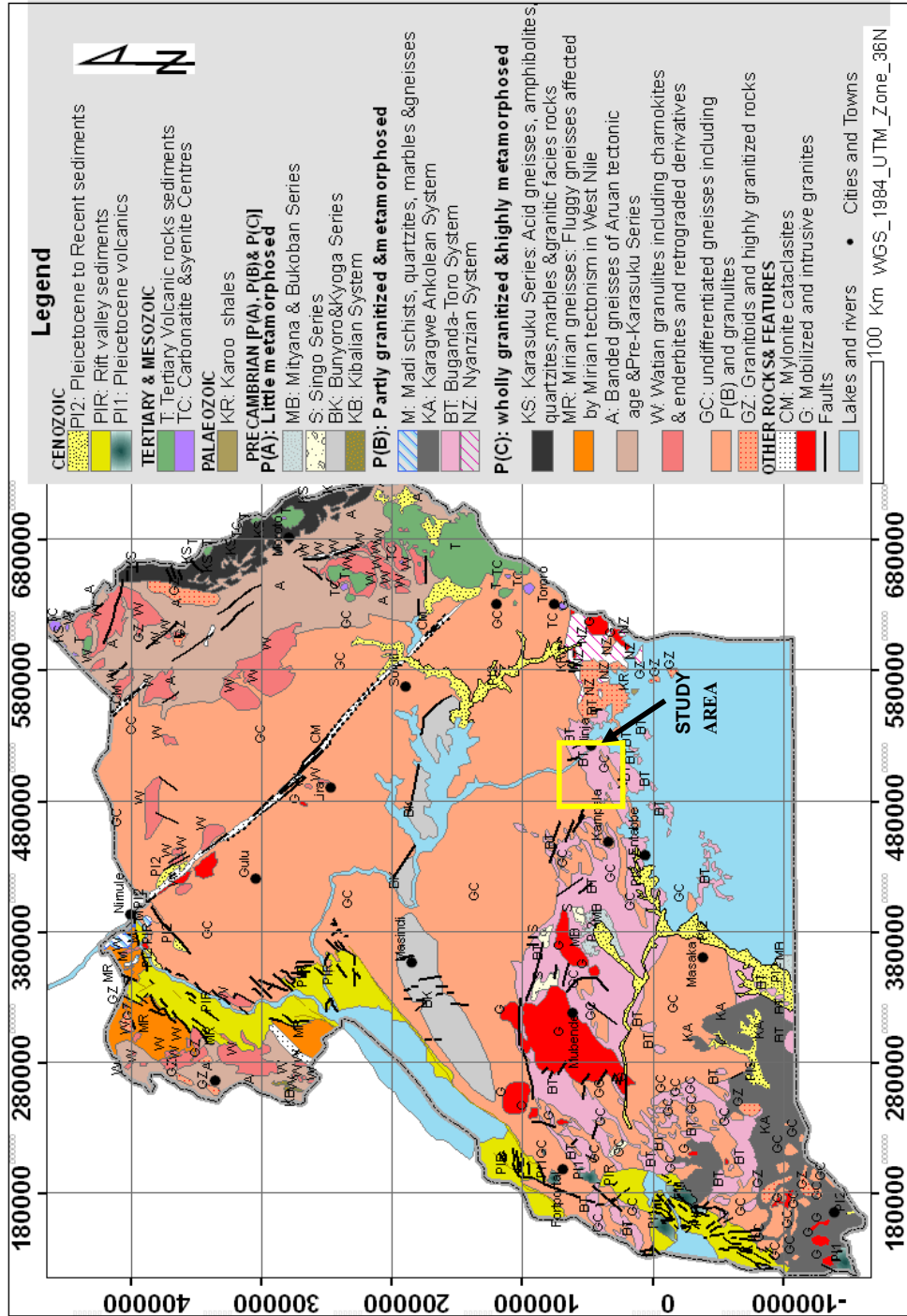


Figure 2.3: Regional geology of Uganda (modified from an extract from the Atlas of Uganda, 1995).

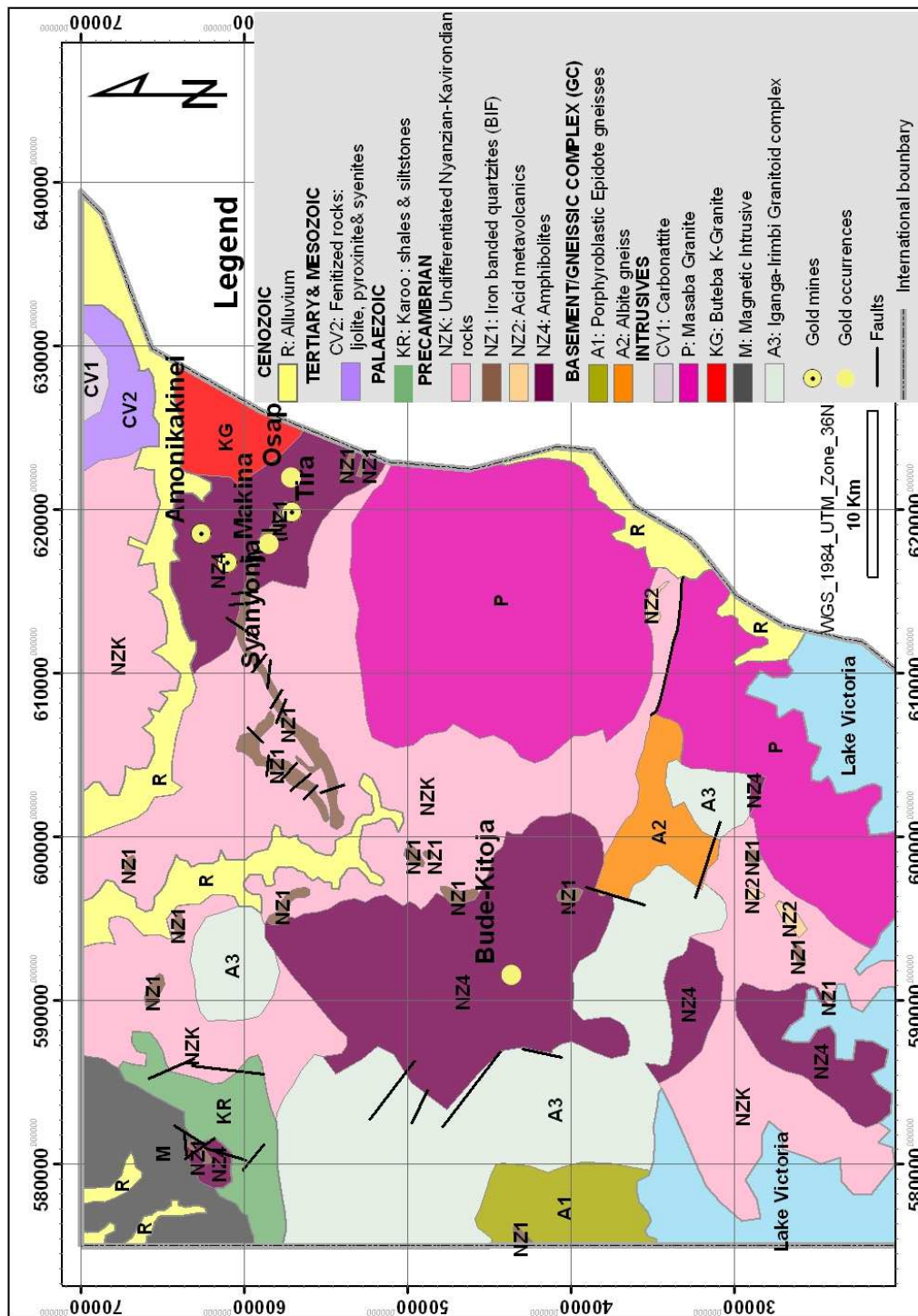


Figure 2.4: Geological map of the Busia Goldfield (Compiled from: (GARS-DBM-TEAM et al., 1998; Isabirye, 2005; Mroz et al., 1991a)

## **2.2.1. Regional Geological Setting**

Uganda covers an area of about 235,000 km<sup>2</sup>. However, only about 1/3 has been geologically mapped (Figure 2.3) and the following geological formations can be distinguished: 1) the Gneissic complex (GC), 2) Nyanzian-Kavirondian System (NZK), 3) Buganda-Toro System (BT), 4) Karagwe-Ankolean System, 5) Upper Proterozoic Sediments, 6) Cenozoic-Mesozoic rocks, (7) Palaeozoic rocks and 8) Cenozoic rocks. The dominant rocks consist of Archean-Proterozoic granitoids, granulites, metavolcanics, metasediments and Cenozoic rocks and limited Palaeozoic rocks. Below is a brief overview.

### **2.2.1.1. Basement complex (GC)**

The GC covers the central to northern parts of Uganda. It comprises the oldest rocks in Uganda and consists of high-grade granulites facies rocks, gneisses, migmatites amphibolites, and granitoids (GZ) which have been affected by a number of tectonometamorphic events. The Watian (W) (2900 Ma) and Aruan Group (A) (2675-2550) groups of gneisses together with Mirian (~950 Ma) and the Karusuku (650 Ma) are (possibly) testimonial to these tectonometamorphic events.

### **2.2.1.2. Nyanzian-Kavirondian System (NZK)**

Overlying the GC is the Nyanzian-Kavirondian System (>2700-2500 Ma). Although they occur as separate sequences in the neighbouring Kenya and Tanzania, the Nyanzian and Kavirondian systems seem to form one undifferentiated sequence (Old, 1968) in Uganda (Figure 2.4). The predominant rocks of the NZK (see details in 2.2.2) include: the acid-basic metavolcanic rocks with tuff, metasediments (e.g. phyllites, greywackes, conglomerates etc) and banded iron formations (BIFs).

### **2.2.1.3. Buganda-Toro System (BT)**

Buganda-Toro System (Lower Proterozoic mobile belts ~1800ma) occurs in the central, southern and western parts of Uganda. The BT system unconformably overlies the NK system and comprise of quartzites, amphibolites and argillaceous rocks varying from phyllites to mica schists. Granites, pegmatites as well as young basic-intermediate dykes are also common.

#### **2.2.1.4. Karagwe-Ankolean System (KA)**

The Karagwe-Ankolean System overlies the BT System. It represents Kibaran mobile belt (~1400-950 Ma), which extends from southwestern Uganda, through northwestern Tanzania, Rwanda, Burundi into the Democratic Republic of Congo. The KA system is composed of acid gneisses, migmatites, folded metasediments (originally of argillaceous composition intercalated with arenaceous horizons) and occasionally conglomerates, calcareous and volcanic sequences. The rocks of the KA system have been intruded by biotite granites, pegmatites and acid-basic veins.

#### **2.2.1.5. Upper Proterozoic Sediments**

Singo, Mityana and Bukoban series (MB) are examples of the upper Proterozoic sedimentary sequence in various parts of Uganda. Singo series (as outliers) overlies the BT System (in the west-central Uganda) whereas the Mityana and Bukoban series occur (also as outliers) in central and south-westwards along the shores of Lake Victoria where they continue into Tanzania as Bukoban series. The rocks of these series are arenaceous, not metamorphosed and a little folded.

#### **2.2.1.6. Cenozoic-Mesozoic rocks**

Rift valley sediments (PIR) and volcanics (PI1) in part of western arm of the East African rift valley and Pleistocene-Recent sediments are the representatives of the Cenozoic rocks in Uganda. The Tertiary alkaline volcanics and associated sediments (T) and the carbonatites (TC) align along the eastern Uganda border with Kenya.

#### **2.2.1.7. Palaeozoic rocks**

Very few exposures of Palaeozoic rocks are known in Uganda. Only Karoo shales are exposed near Bugiri (Eastern Uganda), on Dagusi (near Entebbe) and Sigulu Islands.

### **2.2.2. Local geology of the BGF**

The geology (Figure 2.3) of the BGF is characterized by an Archean granite-greenstone belt terrane which extends from northwestern Tanzania through southwestern Kenya into south-eastern Uganda (Figure 2.1). The greenstone belts (comprised of Nyanzian volcano-sedimentary formations) in the BGF predominantly consist of acidic-basic metavolcanic rocks, metasediments and banded iron quartzite formations (BIFs) that form an important

marker horizon (Mroz et al., 1991b) The Nyanzian formations have been intruded by granite bodies (e.g. Masaba and Buteba) and have undergone green schist facies metamorphism. Below are the details of the different lithologies which are distinguishable in the BGF.

#### **2.2.2.1. Basement/gneissic complex (GC >2930 Ma)**

##### **Epidote gneisses (A1)**

Silicic epidote gneisses outcrop in the southwestern part of the study area. They enclose small bodies of epidote and are strongly foliated with planar orientations of subhedral albite crystals. The gneiss is commonly porphyritic with porphyroblasts of non oriented microcline.

##### **Albite gneisses (A2)**

Corresponding to the Lunyo granite of earlier authors, aquartz-albite gneiss outcrops at Lunyo. It is placed in the gneiss family because of the presence of one and commonly two foliations. The gneiss consists (in some places) bands of microcline porphyroblasts. Although it is possible that the gneiss is as a result of granitization of Nyanzian soda-rich volcanic rocks, the pre-tectonic intrusion of the Nyanzian formation theory is still debatable.

#### **2.2.2.2. Nyanzian-Kavirondian System**

Rocks of the Nyanzian-Kavirondian System (2930-2550 Ma) distinguishable in the BGF include: the undifferentiated acid-basic metavolcanics and metasediments, banded cherty quartzites (BIF), acid (silicic) metavolcanics and amphibolites.

##### **Nyanzian-Kavirondian metavolcanics and metasediments (NZK)**

This NZK consists of a variety of undifferentiated metavolcanics and metasediments. These rocks are so spotty to clearly define or map and hence the general grouping. The different lithologies in this group includes: Basaltic pillow lava, andesite, silicic-intermediate tuff, rhyolite, silicic lava, volcanic conglomerate, siltite, greywackes and phyllites.

##### **Banded cherty and ironstones (BIF-NZ1)**

Commonly referred to as ferruginous banded quartzite (because of its iron and quartz bands), the BIF form most of the isolated and elongate (north and west of the Masaba (P)) hills in the BGF area (Figure 2.2) due to its resistance to weathering than other Nyanzian-Kavirondian rock facies. The thickness of the BIF reaches (in some parts e.g. Iwembe) up to 480 m. the banding in the BIF is due to alternating quartz and haematite or limonite beds, the thickness of which vary greatly. Sedimentary structures are very rare. The undulations

(on the BIFs) are of tectonic origin (Old, 1968) i.e. neither secondary growth on the quartz observed on the quartz grains have been observed nor detrital material is seen in thin section.

The origin of the BIF is still debatable. Whereas previous work considers the BIFs to have precipitated in a marine environment from iron and silica derived from associated volcanic rocks under specific pH and Eh conditions (Old, 1968), recent evidences attribute their (BIFs) origin to metasomatism around effusive rocks in a highly tectonic setting . Although the absence of clastic products are (possibly) a fact that the BIFs were deposited in an archipelago environment with volcanic piles that had accumulated and were periodically eroded(Old, 1968), the disappearance of gold-bearing quartz veins over a short distance within the BIFs (Davies, 1934b) supports the formation of BIFs around effusive rocks in a highly tectonic setting such as shear zones.

#### **Acid metavolcanics (NZ2)**

Silicic metavolcanic rocks (characterized by schistosity outlined by quartz and sericite) outcrop at Siavona, Siabwiru and Nebolola hills in the southern part. The schistose features are derived from highly altered and weathered silicic lava and tuff.

#### **Amphibolites (NZ4)**

Amphibolites are very extensive rocks in the BGF. They outcrop to the east of Buteba and south of Bugodo granites as well as in the southwestern parts of the area. These amphibolites are of volcanic origin and are distinguishable from the spotty amphibolites as a result of metamorphism of the basaltic pillow lavas by flow textures in the latter.

#### **2.2.2.3. Tertiary and Mesozoic**

Tertiary and Mesozoic are represented only by the karoo shales and siltstones in the northwestern corner of the study area, just to the west of Bugodo granite.

#### **2.2.2.4. Cenozoic rocks**

Quaternary sediments (alluvial deposits) are limited to very wide swamps (>1Km in places) and are now mainly under rice growing e.g. at Kibimba.

#### **2.2.2.5. Intrusives**

Numerous acid-basic rocks have intruded the Nyanzian system in the BGF. Their age is generally post-Archean. They include a Carbonatite, granites and dolerite dykes. Whereas most dykes are only interpreted as lineaments (chapter 3) on magnetic grid maps (because of their size), the Carbonatite and the granites (Buteba, Masaba and Iganga-Irimbi) clearly stand out.

#### **Carbonatite (CV1)**

A Carbonatite (at Sukulu hill) outcrops in the northeastern part of the study area. It is one of the several Tertiary alkaline ring complexes that align Uganda's eastern border with Kenya (Figure 2.3).

#### **Buteba granite (KG)**

Non-foliated and more potassic than the Masaba granite ( $2430 \pm 100$  Ma), the Buteba granite outcrops to the northeast of Tiira gold mine. It is grey and medium grained (Appendix 3) with microcline, albite and a few ferromagnesian minerals. Its intrusive nature is characterized by the presence of micro-granites e.g. at Amonikakinei and near River Okame.

#### **Masaba granite**

Poorly exposed, Masaba granite (2900 Ma) extends southwards and outcrops only near Siavona Hill towards Lake Victoria shores. It is a grey-pink coarse grained, leucocratic, biotite-orthoclase-albite granite. Comparably, masaba is more sodic than the Buteba granite.

#### **2.2.2.6. Iganga-Irimbi granitoids complex (A3, 2930 Ma)**

Foliated but still with a granitic appearance, the Iganga-Irimbi granitoids complex (A3) has been transformed into a granitic gneiss. It is a pinkish, medium-coarse grained leucocratic rock with microcline, albite and biotite, showing planar orientation of the minerals. It is porphyritic and pegmatitic in some places and the microcline porphyroblasts may represent relatively late recrystallization (Old, 1968).

#### **2.2.2.7. Metamorphism**

Two large groups of metamorphic rocks are distinguishable (Old, 1968) in the BGF. The groups consist of: the Nyanzian volcanic and sedimentary rocks metamorphosed in the greenschist facies and the gneissic facies which are metamorphosed in the upper part of the amphibolite facies. Metamorphic minerals typical of the greenschist facies include: epidote,

chlorite, chlorite and tremolite. The presence of andalusite in certain silicic metavolcanic rocks could indicate the presence of contact metamorphism. Metamorphism in the sediments has resulted in the formation of biotite and sericite giving rise to a very distinctive schistosity to the clayey facies (phyllite) rocks. The greywackes are more coarsely-foliated.

#### **2.2.2.8. Tectonics and structures**

The regional trend of the Nyanzian-Kavirondian mountain range in East Africa is roughly WNW-ESE. This is also the main structural trend in the gneissic facies and some metasedimentary rocks of the Nyanzian system of southeastern Uganda (in BGF). For example majority of the noticeable faults and rivers have a general NNW-SSE trend. Cropping out very poorly of most of the Nyanzian formations, the tectonic structural studies can only be appreciated from the BIF quartzites beds. Two phases of folding are distinguishable: 1) a first phase of recumbent isoclinal type folding with the beds striking WNW-ESE and 2) a second phase with approximately the same strike as the first (N110°E) but with an almost vertical axial plane. The two phases of folding were then followed by the Masaba granite doming (Old, 1968) which is manifested by a reorientation and outward dip of the Nyanzian formations at the contacts with the Masaba granite, e.g. , the BIFs (NZ1) appear to bend around the Masaba granite (Figure 2.4)

#### **2.2.2.9. Geochronology**

Stratigraphically, the Masaba granite ( $2930 \pm 80$  Ma) intrudes the Nyanzian (>2930-2550 Ma). The Buteba granite ( $2430 \pm 100$  Ma) intrudes the Kavirondian (better observed in Kenya) and the Iganga-irimbi granitoids complex (2930 Ma) is associated with the Nyanzian. It is (possible) that the Iganga-irimbi granitoid complex is a result of granitization of the Nyanzian facies (Old, 1968). The gneissic (basement) complex (>2930) stratigraphically underlies the rest of the formations.

### **2.2.3. Lode gold deposits**

#### **2.2.3.1. General characteristics of lode gold deposits**

Various terms such as Au-Ag deposits, lode or reef type, veins in shear zones, stockworks, mineralized wall rocks, mesothermal or mesozonal, low sulphidic gold etc have been used to describe this class of gold deposits, (Campbell and Kerrich, 1998; Hodgson, 1989; Keays et al., 1989). Hodgson (1982) also describes lode gold deposits as “gold only” because of their high enrichment in Au relative to other metals (e.g. Cu, Pb, Zn and Ag) However previous

work (Campbell and Kerrich, 1998) has shown that significant Ag with Au:Ag ratios averaging 5 as well as sporadic enrichments of W and Te are common to these deposits. Lode gold deposits accounts for a worldwide historic gold production in excess of 9,900 tonnes of gold, second only to the Witwatersrand modified paleo-placer gold deposits of South Africa ([http://www.pcgold.ca/en/Deposit\\_Type\\_34.html#](http://www.pcgold.ca/en/Deposit_Type_34.html#))

Various studies of lode gold deposits (Campbell and Kerrich, 1998) have (globally) revealed a number of common principal characteristics, including:

- 1) Deposits are sited proximal to major accretionary structures within, or at the boundaries of, composite metamorphosed volcanic-plutonic or sedimentary terranes. Less commonly, deposits occur internal to terranes with no regional structures evident
- 2) Lode gold deposits are distributed in belts of great geological complexity, with gradients of lithology, strain, and metamorphic grade, reflecting an accretionary environment.
- 3) Lode gold deposits can occur in almost any rock type and age although they may be plentiful in Archean rocks; however, super giant lode gold metallogenic provinces are in greenschist facies metamorphic terranes.
- 4) Deposits are structurally hosted, associated with second or higher order splays of translithospheric faults.
- 5) Deposits are generally restricted to the brittle-ductile transition.
- 6) The alteration mineral paragenesis in greenschist facies domains is dominated by quartz, carbonate, mica, (albite), chlorite, pyrite, scheelite and tourmaline.
- 7) There is a distinctive element association characterized by enrichment in Au, Ag and ( As, Sb, Te, W, Mo, Bi, B), with low enrichments of Cu, Pb, Zn relative to the background abundances. In Phanerozoic deposits Mo and Te are only enriched where veins cut felsic intrusions.
- 8) Ore forming hydrothermal fluids are dilute aqueous carbonic fluids, with uniformly low fluid salinities (typically < 6 wt% NaCl equivalent
- 9) Lode systems may have vertical extents of up to 2 km, with a lack of zoning, or weak zoning, within deposits, albeit with some zoning of metal content at the scale of an entire mining district.
- 10) Mineralization is typically syn- to post-peak metamorphism.
- 11) Lamprophyres are closely associated in space and time with mineralization in many deposits

### **2.2.3.2. Lode gold deposits characteristics in the Nyanzian greenstone belts**

Studies of the Archean lode gold deposits in the East African's (Uganda, Kenya and Tanzania) Nyanzian greenstone belts have revealed mineralization controls common to those at a global scale. The lode gold mineralization controls within the Nyanzian greenstone belts (Gabert, 1990; Kuehn et al., 1990; Sango, 1995) include:

- 1) The greenstone belts (mafic metavolcanics ) form the main host rocks
- 2) The gold occurs as shear-zone-controlled quartz reefs
- 3) Gold mineralization is associated with lineament structures
- 4) associated with Gold mineralization are :sericite, chlorite, carbonate and sulphide (pyrite, chalcopyrite, arsenopyrite, pyrrhotite and galena) minerals

### **2.2.3.3. Lode gold characteristics in the BGF**

Previous work in the BGF (Barnes, 1961; Byamugisha et al., 1994; Davies, 1934b; Mroz et al., 1991b; Schumann, 2007) shows the gold to occur within the rocks of the Nyanzian System, with the main primary deposit features being:

- 1) Gold-bearing quartz veins
- 2) Commonly tectonically controlled (i.e. associated with fractures, shear zones, breccia zone)
- 3) Preferentially located in the basic metavolcanic facies (Amphibolites) although other lithologies may host economic gold mineralization

Detailed work at known gold mines (Tiira mainly) indicates the reefs or lode gold structures to consist mainly of quartz and sometimes with a core of calcite. The reefs are mostly discontinuous, parallel–running, pinch-and-swell and bifurcate along strike and depth. Their widths generally range from 0.3 m to about 1 m, with a maximum observed width of 3 m and a maximum observed strike length of a couple of hundred meters. However field observation (in Amonikakinei and Syanyonja artisanal workings during the current research) indicate that gold-bearing reefs may actually be followed over kilometres provided they are not offset by faults. Minor quartz veins (stringers, usually <0.1 m wide) generally follow similar strike (i.e. NW-SE, NNW-SSE and N-S) often with varying dip angles although they may also form networks. Although the previous work at Tiira mine points to the NW-SE trending faults to have been the preferred pathways for fluids that led to the gold mineralization, recent exploration and assay values of gold-bearing quartz veins along NNW-SSE and N-S trending faults (at the same Mine) give evidence that these faults are as mineralised as the NW-SE. These faults have a sub-vertical dip to the east. The NE-SW to ENE-WSW trending fault

system which offset the gold bearing reefs (Schumann, 2007) seems to document the youngest tectonic event.

The gold mineralization consists of free gold, pyrite and auriferous arsenopyrite, with much rarer galena (PbS) and sphalerite ((Zn, Fe) S). The gold appears as small flakes or coatings on joint surfaces or cracks and is unevenly distributed within the veins, which is typical of shear zone hosted high grade vein deposits, with highest gold assay values well above 200 g/t (Schumann, 2007). Figure 2.5 shows the formation of vein hosted gold deposits which is typical of the Busia gold field.

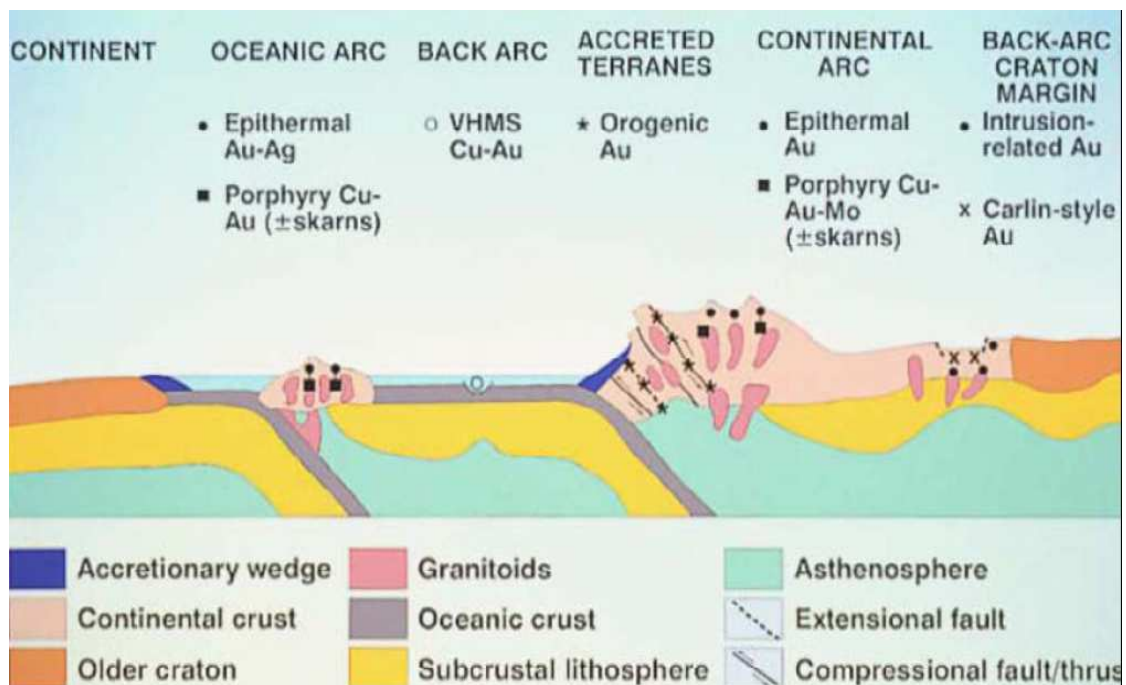


Figure 2.5: Orogenic gold deposits (Groves et al., 1998). Note the accretionary environment and associated vein-hosted gold deposits typical of greenstone belts (e.g. Busia gold field).

## 2.3. Description of datasets and expected geoinformation

### 2.3.1.1. Geological and topographical Maps

Four different geological maps obtained by different workers at different times were used to compile a geological base map to guide in the interpretations. The maps used include:

- 1) 1:50 000 Geology map of parts of Samia (Budama) and Bukoli (Busoga), Eastern Province Uganda Department of Geological Survey and Mines, Entebbe, Uganda.(Davies, 1934a)

- 2) 1:100 000 Lithochemical map of the Busia Goldfield area, Department of Geological Survey and Mines (Mroz et al., 1991a)
- 3) 1:250 000 Geology map of Jinja: compiled by McDonald and published by GARS-DBM-TEAM, GSMD and MARC. Entebbe, Uganda (GARS-DBM-TEAM et al., 1998)
- 4) 1:250 000 Jinja Geology map. Enschede, The Netherlands.(Isabirye, 2005)

### **2.3.2. Remote sensing (RS) data**

Two RS data sets were used i.e. Shuttle Radar Topography Mission (SRTM) and the Advanced Spaceborne Thermal Emission and Reflection Radiometer (ASTER) digital elevation model (DEM) imagery. The SRTM imagery (Path 170 and Row 60) recorded on 2001-02-05, WRS-2, were obtained from the Global Land Cover Facility (<http://glcfapp.umiacs.umd.edu:8080/esdi/index.jsp?productID=11>) whereas ASTER DEM were obtained from ITC. These RS datasets, in combination with the rest of the datasets were used for lithological and structural (lineaments) interpretations.

### **2.3.3. Airborne Magnetic and radiometric data**

Airborne magnetic and radiometric data used here were acquired by FUGRO REF: FCR2417A (in 2007) for the Ministry of Energy and Mineral Development of the Republic of Uganda through the ongoing Sustainable Management of Mineral Resources Project implemented by the Department of Geological Survey and Mines. The following specifications were used by FUGRO in the data acquisition:

#### **Survey Specifications**

Magnetic Data Recording Interval	0.1 seconds
Radiometric Data Recording Interval	1 second
Sensor Mean Terrain Clearance	80 metres
Flight Line Spacing	200 metres
Tie Line Spacing	2000 metres
Flight Line Trend	035 degrees
Tie Line Trend	125 degrees

Whereas magnetic data were used for lithological and structural interpretations, radiometric data were used for lithological and geochemical anomaly mapping.

#### **2.3.4. Stream sediment geochemical data**

Stream sediment geochemical data were collected during a BGRM-DGSM joint geochemical survey between 1990 and 1991 at an average sample density of about 1.5 samples per square Kilometre. The samples were collected from the second and third order streams. Before analysis, the samples were dried in shallow dishes under plastic greenhouses for 5-6 days. After reducing the particle size by pounding in a porcelain mortar, each sample was passed through a number of sieves the last one being with 125  $\mu\text{m}$  and 63  $\mu\text{m}$ . The -63  $\mu\text{m}$  fraction was quartered until only sufficient material remained to fill two Caubre tubes. One of the sample-full Caubre tube was then analysed for 34 elements using the induced coupled plasma spectrometry (ICP) technique while the second one was kept for uncertainties. After an alkaline attack chemical by calcinations in a sodium peroxide ( $\text{Na}_2\text{O}_4$ ) solution, the samples were digested in digested in HCl before excitation in the induced coupled argon plasma. The emitted ion rays were the used in the spectrometry. ICP allows for simultaneous analysis, for multi-elements (e.g. 34 in this case).

Meanwhile analysis for gold was carried out on the -125  $\mu\text{m}$  fraction by Atomic Absorption (AA) technique in a graphite furnace at a detection threshold of 5ppb. In the AA technique the sample is attached in a triacid medium ( $\text{HCl}+\text{HNO}_3+\text{HF}$ ), following which gold is extracted using a meta-Isobutyl-Ketone solution. All the geochemical analyses were carried out in the BGRM laboratories in Orléans, France. Table 4.1 give the descriptive summary of the results. The units of the uni-elements are: Au (ppb), major elements ( $\text{SiO}_2$ ,  $\text{Al}_2\text{O}_3$ ,  $\text{Fe}_2\text{O}_3$ ,  $\text{MgO}$  and  $\text{TiO}_2$ ) are given in % whereas the trace elements ( $\text{P}_2\text{O}_5$ , Li, B, V, Cr, Co, Ni, Cu, Zn, Sr, Nb, Nb, Mo, Ce, Pb and Zr) are in ppm.

After chemical analysis, the uni-elements were sorted according to their relative importance to the objectives of the geochemical survey and out of the 35 elements analysed for, only 23 uni-elements in 1924 out of the 2311 samples taken are used in this research. In this research, the stream sediment dataset is used for mapping geochemical anomalies indicative of the presence of gold mineralization.

#### **2.3.5. Field data**

Lithological, lineament and gold occurrence locations and descriptions in selected parts of the study area were recorded during a field campaign conducted between the 23rd September and 10th October 2008. This facilitated the data interpretation process during the research.

## **3. Geological mapping with multispectral, magnetic and radiometric data**

### **3.1. Introduction**

Mineral prospectivity mapping uses geologic features which are indicative of the mineral under investigation. The better these spatial features are mapped, the better the mineral prospectivity can also be mapped (van Roij et al., 2006). This chapter therefore deals with the compilation of a geological map to be used (in chapter 5) for mapping lode gold prospectivity in the BGF.

### **3.2. Lithological mapping**

With the exception of adjusting the lithological boundaries as could be interpreted, there is no much modification to the lithologies on the geological base map (chapter 2) compiled from different geological maps and lithogeochemical map. An overlay of the lithological boundaries of the base map onto the remotely sensed data (e.g. Figure 3.1), proved fitting to the interpretations that could be made on the data sets. This increases the confidence in the geological maps produced by earlier workers. Therefore, the contribution to the compiled base map involved mainly adjusting the lithological boundaries so as to fit better in accordance with the interpretations that could be made.

Figure 3.1 shows the contribution of radiometric ternary grid map in lithological mapping in this case. The ternary map is a colour composite of three radio-element (K, Th and U) grid maps (Appendix 1) which can be generated by the following steps: Firstly, production of grid maps for each radio-element. Secondly, masking of the water bodies (by using the linear transform option of the Oasis montaj), so as to differentiate the water from the alluvial sediments in the swampy areas in the BGF. Linear transformation allows for the specification of the minimum, maximum and contour interval for the uni-element values of the grid map. The first colour is all values less or equal to the minimum, whereas the last colour represents the maximum value. Individual colour ranges are then evenly spread between the minimum and the maximum. Finally, combining of the modified radio-element grid maps to produce a colour composite ternary map using the R: B: G for K: Th: U visualization.

The first step of gridding uni-element data can be achieved by a number of methods e.g. Bi-directional gridding, minimum curvature as well as Kriging. Based upon the inverse distance averaging of point data within a specified search radius, minimum curvature gridding (randomly) fits a minimum curvature surface to the data points. A minimum curvature surface is the smoothest possible surface that will fit the given data values. Thus minimum curvature suits randomly acquired data.

On the other hand Kriging is a statistical gridding method used to determine a value at each grid point based on the position and data value (i.e. using XYZ coordinates). The first step in Kriging is to calculate a variogram of the data, which shows the correlation of the data as a function of distance. Although Kriging is useful for gridding line data, bi-directional gridding method is a better option. The Bi-directional gridding method is ideal for line oriented data because it inherently tends to strengthen trends perpendicular to the direction of the survey lines. In this way Bi-directional gridding takes advantage of the fundamental characteristics of line-based surveys.

The gridding process is carried out in two principle steps: 1) First, each line is interpolated along the original survey line to yield data values at each required grid line in relation to the observed line and 2) interpolation in the across-line grid direction to produce a value at each required grid point. Hence the method *bi-directional gridding* is directly attributed to the two perpendicular-directional interpolation/gridding of line data.

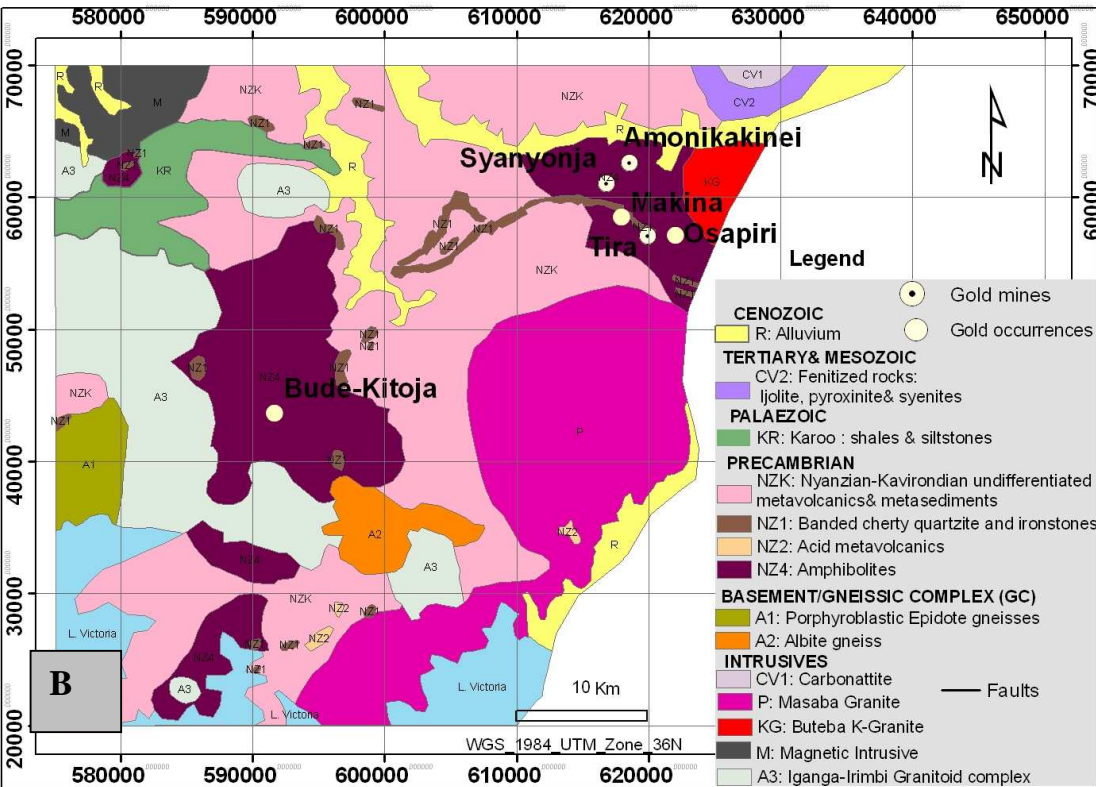
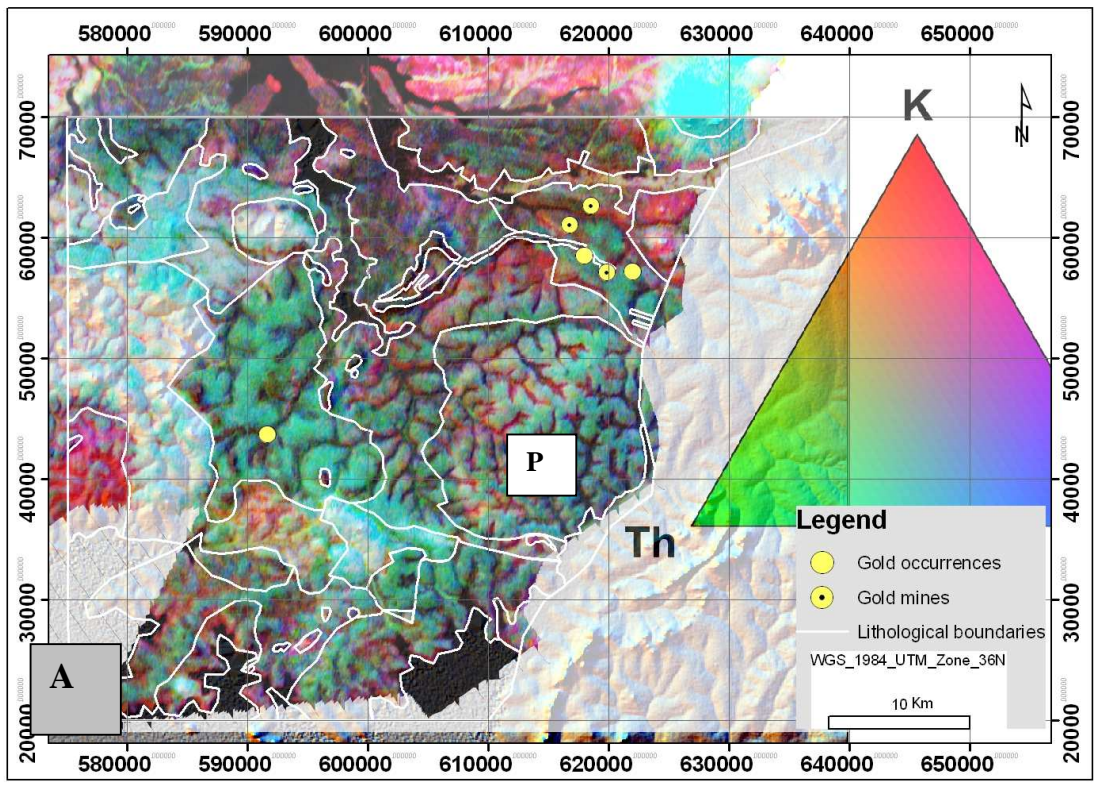


Figure 3.1: Lithological map modification. 3.1A shows lithological boundaries overlaid on radiometric ternary grid map and 3.1B is a modified lithological map. Note the offset of the

Masaba granite (P) boundaries in 3.1A and the modified boundaries in 3.1B. The geomorphology added by the SRTM DEM underlying the ternary map improves the visual interpretation of the lithological boundaries.

Whereas the Iganga-Irimbi granitoid complex is characterised by approximately equal proportions of K, Th and U (white hue), amphibolites and the Carbonatite by high Th, Buteba granite and epidote gneiss by high K, most of the greenstone lithologies and Masaba granite are characterised by mixels (mixed pixels) of the three radio-elements. A mixel in this case refers to the small units (pixels) on the ternary map which are characterized by a mixture K, Th and U whereby it is not possible to identify which one of them predominates. Given the lithologies in the area, these observations are meaningful. The mixels of K, Th and U in greenstone lithologies of the BGF are due to the complex composition of the mixture of the acid-basic metavolcanics and metasediments with various ranges of these radioelements. The high Th in the amphibolites is possibly due to the highly weathering nature of the amphibolites (now laterite), whereby the K is leached out leaving the weathering resistant Th as residuals. While the high K in Buteba granite (KG) is due to its potassic nature (appendix 2), the anomalous K in the epidote gneiss is possibly due to adsorption of K onto clay minerals as a consequence of alteration and or weathering. The fairly unexposed nature of Masaba granite (P) also explains the radio-element distribution in this area which is strongly influenced by the greenstone lithologies overlying it.

### **3.3. Lineament mapping**

A lineaments are topographical features thought to reflect crustal structures e.g. faults, aligned volcanoes, straight stream courses etc (Lapidus, 2003). Lineaments are important channels and catchment zones for mineralizing fluids, and thus, there is a spatial relationship between crustal lineaments and the locations of magmatic centres as well as associated mineral deposits (Chernicoff et al., 2002). Therefore this subsection deals with lineament enhancement and extraction for vein-hosted or lode gold prospectivity mapping in the BGF.

#### **3.3.1. Mapping of Lineaments using DEM**

The elevation above the mean sea level for the BGF ranges between about 1070 to 1400 m. However, both ASTER and SRTM DEM imagery had elevation values as low as negatives. To correct for this, the ASTER and SRTM DEM imagery were separately stretched to eliminate the lower elevation values. Hill shaded relief DEM were then generated using three

different solar azimuth angles, i.e. 270°, 315° and 360° and a constant sun illumination angle of 45°. These parameters are useful in enhancing the entire multidirectional lineaments. Of the two DEM imageries, the higher resolution (30 m) ASTER DEM was the most useful in delineating the lineaments.

### **3.3.2. Mapping of Lineaments using airborne magnetic data**

Depending on their location in the Earth's subsurface, the shapes of magnetic data anomalies differ. For the anomalies at the pole, the peaks are vertically centred over the source and can easily be located. This is not the case on moving from the pole to other locations on the Earth's surface for example at the equator where this case study area is situated. To correct for this, the total magnetic intensity data are reduced-to-the-pole so that the magnetic anomalies appear as if they were observed at the pole. Linear magnetic anomalies may be basic dykes or ductile shear zones. Ductile shear zones are characteristic of an accretionary greenstone belts environment such as the BGF. Figure 3.3 shows the lineaments interpreted from the reduced-to-the-pole (RTP) total magnetic intensity data for the BGF. The parameters used in reducing the magnetic data to the pole include: magnetic inclination ( $I = -22^\circ$ ), magnetic declination ( $D = 0.69^\circ$ ) and amplitude ( $A = 45$ ) I and D were calculated using the latest update of International Geomagnetic Reference (IGRF) model of year 2005.

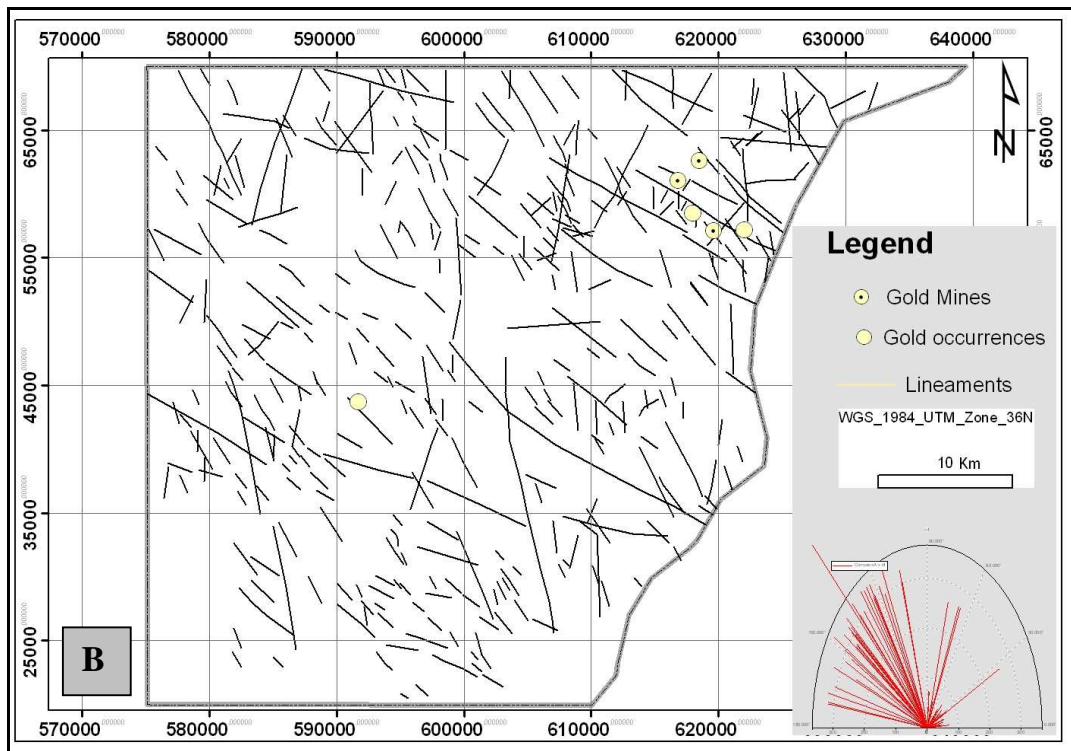
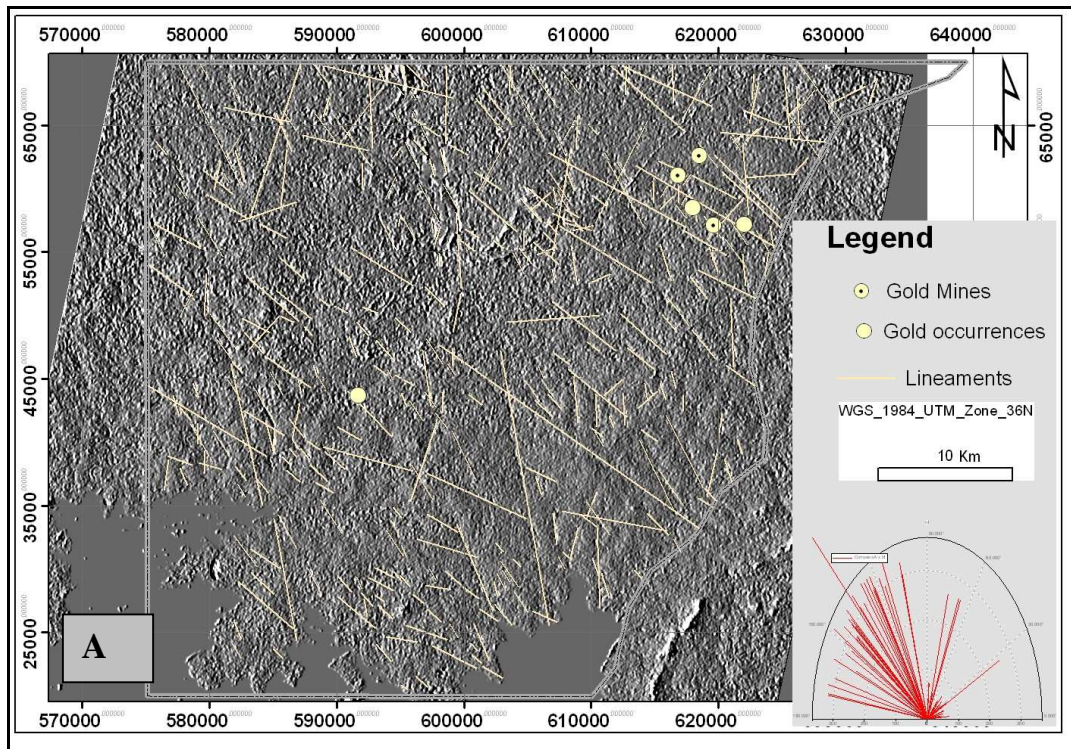


Figure 3.2: Extraction of Faults from an ASTER shaded relief DEM image (3.2A), 3.2B is the finished map of faults interpreted. Note the dominant NW lineament trend from the Rose diagram.

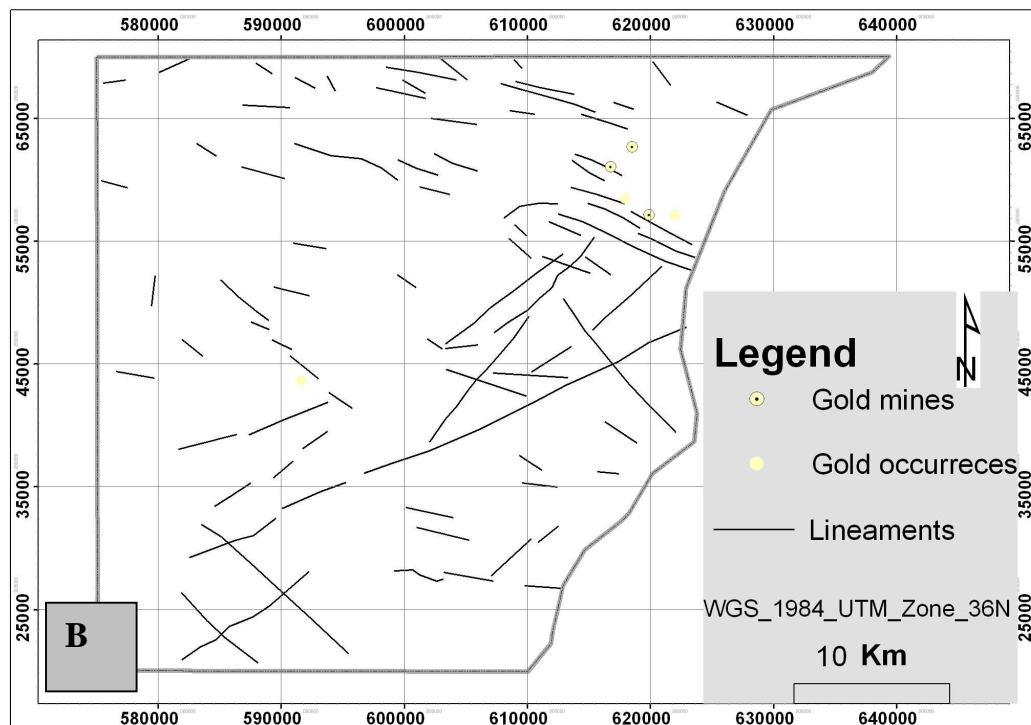
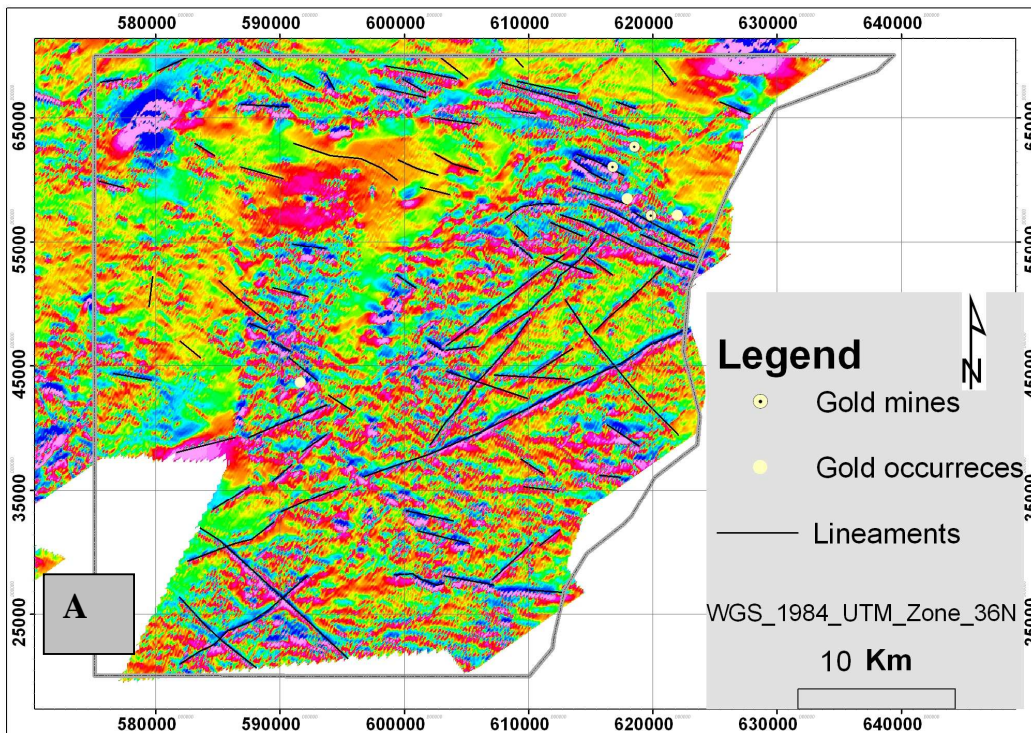


Figure 3.3: Extraction of lineaments (3.3A) using a 1<sup>st</sup> vertical derivative from an RTP magnetic grid map and 3.3B is a finished lineaments map.

### **3.4. Discussion and conclusions**

The BGF is a typical granite-greenstone belt terrane characterized by great geological complexity with gradients of lithology, strain and metamorphic grade reflecting an accretionary environment (Campbell and Kerrich, 1998). The multidirectional strike of lineaments on both the DEM and the 1st vertical derivative from an RTP magnetic grid map imply a highly tectonic setting which has been reactivated several times. Archean greenstone belts are globally known for Archean lode-gold systems (Eilu and Mikucki, 1998a; Eilu et al., 1998; Mikucki, 1998) whereas crustal lineaments are channels for hydrothermal fluids transport and depositional processes responsible for mineralization. The existence of such evidential features for the presence of lode gold deposits in the BGF implies that more lode gold deposits than currently known may exist in the in the BGF and hence worth investigating for the presence of gold or gold-pathfinder-elements anomalies. Therefore, the next step (chapter 4) is geochemical anomaly mapping for gold prospectivity, using stream sediment and radiometric data.

## **4. Geochemical anomaly mapping with stream sediment geochemical data**

### **4.1. Quality assessment**

Geochemical characteristics of mineral deposit occurrences may be masked by substantial errors arising from not only data collection but also laboratory analysis protocols as well as analytical procedures during data interpretation. Such errors (if substantial) may cause variations in geochemical data that are not as a result of geological and geochemical processes. Consequently, it is very important that the quality of a geochemical data set is assessed before any analysis and interpretation are done. Useful statistical techniques in quality assessment include: scatter plot analysis, 10% precision plots as well as analysis of variances. These analyses make use of duplicate samples so that data for comparison. Unfortunately, the geochemical dataset at hand does not include duplicates. It is therefore not possible for quality assessment to determine which elements are satisfactory for geochemical anomaly mapping. Therefore any negative effects in the results of geochemical modelling may be attributed to this.

Analytical procedures undertaken during data interpretation which cause considerable errors include data generalization. Just as it is not meaningful to generalize about the acidity of apples and oranges collectively (since the latter are, in general, more acidic than the former) it is not meaningful to generalize about the Cr content of samples from a suite of mafic rocks such as amphibolite metabasalts and samples from felsic rocks such as rhyolites, granites etc (Amor, <http://dirtbagger.golinfo.com/data1.pdf>). In such a case, subdividing the data into subsets according to the rock type from which the samples were derived (Carranza, 2008; Yusta et al., 1998) and analysing them independently is the solution.

With this quality consideration therefore, the stream sediment geochemical data set was divided into two subsets i.e. 1) mafic, referring to geochemical data from mafic lithological units and 2) Felsic, for geochemical data obtained from felsic lithologies. Because the rock type from which the samples were obtained was not recorded, georeferenced stream sediment sample locations were: 1) overlaid onto the previously compiled lithological map

(Figure 3.1B), 2) selected samples from mafic (amphibolites) lithological units and 3) saved the samples as a separate layer. The same procedure was repeated for the samples originating from felsic rock facies. The two layers were separately imported into ILWIS from where they were copied into an excel sheet for statistical analysis.

## **4.2. Univariate data analysis**

The mostly determined chemical property of each geochemical sample (e.g. stream sediment, water, soil, rock) collected during geochemical surveys is the concentration of one or more elements. The sole aim for this is to find anomalous areas with enriched concentrations of one or more pathfinder elements, which may perhaps be vectors to the presence of geochemical anomalies and or mineral deposits of the type sought. Since geochemical anomalies can easily be delineated once the threshold value in the individual uni-element data sets are determined (Carranza, 2008), the next subsection is therefore aimed at exploring the data so as to determine the threshold concentration for each uni-element for significant geochemical anomaly mapping.

### **4.2.1. Exploratory data analysis of geochemical data (EDA)**

Like an explorer (studies maps before) crossing unknown lands, it is imperative to explore the data so as to understand and describe their main features (Moore and McCabe, 1998). Thus, descriptive statistical and graphical tools in EDA are aimed at: 1) gaining maximum insight in a data set, 2) discovering data distribution structure, 3) defining significant variables in the data, 4) determining outliers and anomalies and 5) identifying possible treatment or transformation in order to analyze and interpret a data set. Hence, EDA is a useful approach to decision making. Of the several EDA techniques, descriptive statistics (Table 4.1) the box and whiskers plots (Appendix 3) and scatter plots were used in this research. This is because these techniques provided sufficient information required for: 1) exploring the data and establishing the data distribution structure, 2) identifying which transformation to apply and 3) identifying the appropriate analytical techniques to use, in order to extract useful the geoinformation required in geochemical anomaly mapping.

#### **4.2.1.1. Descriptive statistics**

The summary statistics of the uni-elements (Table 4.1) shows the distribution of all the uni-elements (raw data) to be asymmetric. With the exception of SiO<sub>2</sub> which is negatively skewed, the rest of the elements are positively skewed. Of all the uni-elements however, Au exhibits the highest skewness. The maxima of almost all uni-elements are several times their corresponding standard deviations. Unless rectified, the asymmetry of this geochemical

data set may have negative effects on the statistical analysis results. Consequently, the data (save SiO<sub>2</sub>) were transformed (using natural logarithm) before further statistical analysis. Logarithmic transformation of the data reduces the inherent asymmetry in geochemical data so as to maximize the contrast in the uni-element data, in order to facilitate geoinformation extraction from the data set. Similarly, logarithmic transformation improved the asymmetry (see Log<sub>e</sub>skewness, Table 4.1) in the stream sediment geochemical data above. The extreme skewness of Au data even after logarithm transformation is attributed to the many censored values which are more than 90% of the Au analyses. Censored values are uni-element analytical values under the analytical detection limit (Grünfeld, 2004) for that uni-element. Cleaning data of the censoring effect is either by removal or replacement of the censored values if only these values are under a tolerable percentage of all analyses for a given uni-element. Because only less than 30% of all analyses for each uni-element can be tolerated as analytical detection limit values (Amor, <http://dirtbagger.golinfo.com/data1.pdf>; Grünfeld, 2004), Au data were not used in multivariate statistics so as to avoid biased or faulty results (Grünfeld, 2004).

On the other hand, elementary descriptive statistics (Table 4.1) further show that elements such as Cr, Cu, V, Ti and Mg except Fe, Ni and Co which are known to be associated with mafic rocks have their concentrations highest in mafic rocks. Similarly, elements such as SiO<sub>2</sub>, Al<sub>2</sub>O<sub>3</sub>, Sr, Ce, Ba etc which are known to be associated with felsic rocks have their concentration in the felsic rock suite. In conformity with subsection (2.2.3.3), the highest Au concentration is associated with the mafic facies. Further spatial association between uni-elements and other geological features is analysed in the next subsection (4.2.1.2), which extensively deals with uni-variate anomaly mapping in stream sediment geochemical data.

Table 4.1: Descriptive Statistics of raw stream sediment geochemical data for 1924 samples. Loge Skewness demonstrates the reduction in the skewness in the data. All units in ppm except for Au (ppb) and SiO<sub>2</sub>, Al<sub>2</sub>O<sub>3</sub>, Fe<sub>2</sub>O<sub>3</sub>, MgO and TiO<sub>2</sub> (%)

	Minimum		Maximum		Median		Mean		Standard deviation		Skewness		Log <sub>e</sub> skewness	
	Felsic	Mafic	Felsic	Mafic	Felsic	Mafic	Felsic	Mafic	Felsic	Mafic	Felsic	Mafic	Felsic	Mafic
SiO <sub>2</sub>	37.3	27	93.6	87.9	74	66.4	72.9	66.4	9.10	8.79	-0.38	-0.24	-	-
Al <sub>2</sub> O <sub>3</sub>	4	6.3	29.3	29	13.3	15.35	13.8	15.8	4.23	4.37	0.66	0.36	-0.42	-1.02
Fe <sub>2</sub> O <sub>3</sub>	1	1.7	37.9	21.2	6.45	9.9	7.2	10.1	4.39	4.12	1.95	0.39	0.67	-0.94
MgO	0.2	0.2	2	2.4	0.4	0.6	0.5	0.7	0.23	0.33	1.19	1.20	0.18	0.18
TiO <sub>2</sub>	0.6	0.7	4.3	3.9	1.3	1.7	1.4	1.8	0.39	0.53	1.00	0.68	0.00	-0.39
P <sub>2</sub> O <sub>5</sub>	70	302	8259	6820	1278	1548.5	1467	1655	869.6	780.0	2.1	2.0	0.8	0.7
Li	5	5	138	50	10	14	12	15	8.6	7.9	3.4	0.9	1.2	-0.1
B	10	7	296	570	48	48	55	59	30.6	50.8	2.6	5.2	1.0	1.6
V	28	59	559	579	118	244.5	127	240	54.9	88.3	1.6	0.0	0.5	-4.7
Cr	1	39	477	511	80	162.5	89	167	42.8	66.0	3.1	0.9	1.1	-0.1
Co	5	10	285	191	25	45	30	48	20.9	22.3	4.2	1.4	1.4	0.3
Ni	16	25	232	216	52	93.5	57	96	22.3	31.7	2.1	0.4	0.8	-0.9
Cu	1	6	218	227	37	80	42	81	22.8	38.4	2.0	0.4	0.7	-0.8
Zn	15	28	219	422	70	96	73	98	27.4	37.2	0.9	2.6	-0.1	0.9
Sr	18	22	302	359	55	55	63	68	31.2	39.6	2.2	2.5	0.8	0.9
Y	12	17	489	122	39	45	44	47	22.9	16.9	6.7	1.1	1.9	0.1
Nb	10	10	427	192	72	79	77	80	28.5	25.1	2.4	0.4	0.9	-0.8
Mo	1	1	17	10	4	3	4	3	2.2	1.8	0.6	0.5	-0.6	-0.8
Ba	77	79	1424	882	287	203	317	250	156.7	142.3	1.7	1.7	0.5	0.5
Ce	10	10	721	240	93	96	112	97	70.0	35.5	2.3	0.5	0.8	-0.7
Pb	1	1	223	71	16	14	18	15	12.4	7.9	4.5	1.3	1.5	0.3
Zr	41	165	2207	1104	451	405.5	506	421	219.9	128.5	2.5	1.4	0.9	0.4
Au	5	5	165	370	5	5	5	12	5.3	31.0	24.1	7.8	3.2	2.1

#### **4.2.1.2. Univariate anomalies in stream sediment geochemical data**

Uni-element anomalies can be distinguished from the background once the threshold concentrations of individual uni-elements are established. Background concentration for a given uni-element is the normal concentration of that uni-element in non-mineralised Earth materials (Carranza, 2008). Since earth materials vary in uni-element concentration, background concentration is a range of values and not just a single value. The estimated upper limit of the range of background values is the. Therefore, a threshold can be regarded as the approximate boundary between the background and anomalous uni-element concentration values.

A number of methods can be used in establishing the threshold concentrations of uni-elements. Examples include: 1) the mean+2standard deviation, 2) Median+2MAD and the box and whisker plot, where MAD (see equation 4.1) is the median absolute deviation. The Median+2MAD together with the box and whisker plot techniques are some of the useful EDA tools in establishing uni-element threshold concentration, classifying uni-element geochemical data and hence geochemical anomaly mapping. Unlike the classical statistical technique (mean-based) which is strongly influenced by outliers and therefore the data distribution structure, the box and whisker plot in addition to the Median+2MAD techniques are robust (Carranza, 2008; Rose et al., 1979) and unaffected by data distribution. Of the three techniques however, the box and Whisker plot performs best (Reimann et al., 2005) in defining the threshold value. This is because; the box and whiskers technique is based on the properties of the middle 50% of the data.

Considering the general rule that, almost all measured variables in regional geochemical data have neither normal nor lognormal data distributions (Grünfeld, 2004), methods that are not strongly based on statistical assumptions (e.g. Median+2MAD and box and Whickers plot) should be first choice (Reimann et al., 2005) in uni-element threshold estimation. However, thresholds based on the box and Whisker plot are normally higher than the thresholds estimated by the median+2MAD approach, for both raw and logarithmic transformed data sets (Carranza, 2008c; Reimann et al., 2005). Therefore, uni-element threshold concentrations (e.g. stream sediment data which often experience dilution effects) may be overestimated by the box and Whisker technique. As a result, higher thresholds estimation (e.g. by the box plot) may subsequently obscure the geochemical anomalies. Thus, the median+2MAD which is a direct analogue to the [mean+2standard deviation] is the choice for this case study, to define the threshold concentration and classify the geochemical

data for geochemical anomaly identification and mapping. The median absolute deviation (MAD) is given by:

$$\text{MAD} = \text{median} [ | (X - X_{\text{median}}) | ] \quad (4.1)$$

Where  $X_{\text{median}}$  is the median of variable X. MAD is estimated as the median of the absolute deviations of all data values for a given uni-element (e.g. Au) from the median of that uni-element. First, the median of a uni-element is computed, next, the absolute deviation of each uni-element value from the median is calculated and finally, the median of all the absolute deviations (now the MAD) is determined (Peter Verboon and Willem, [www.datatheory.nl/pdfs/88/88\\_07.pdf](http://www.datatheory.nl/pdfs/88/88_07.pdf)). Table 4.2 gives the different uni-element thresholds and anomaly classes based on this method.

Table 4.2: Upper class boundaries of Uni-element background and anomaly based on threshold = Median+2MAD for both mafic and felsic facies in the BGF. All units are in ppm except for Au (ppb) and SiO<sub>2</sub>, Al<sub>2</sub>O<sub>3</sub>, Fe<sub>2</sub>O<sub>3</sub>, MgO and TiO<sub>2</sub> (%)

	Median		MAD		Background		Anomaly	
	Felsic	Mafic	Felsic	Mafic	Felsic	Mafic	Felsic	Mafic
SiO <sub>2</sub>	74	66.4	6.7	6.25	87.4	78.9	93.6	87.9
Al <sub>2</sub> O <sub>3</sub>	13.3	15.3	1.23	1.23	15.8	17.8	29.4	29.1
Fe <sub>2</sub> O <sub>3</sub>	6.5	9.9	1.48	1.32	9.4	12.5	37.7	21.1
MgO	0.4	0.6	1.32	1.32	3	3.2	2	2.4
TiO <sub>2</sub>	1.3	1.7	1.17	1.23	3.6	4.2	4.3	3.9
P <sub>2</sub> O <sub>5</sub>	1274	1548	1.4	1.3	1277	1551	8267	6836
Li	10	14	1.8	1.5	14	17	138	50
B	48	48	1.3	1.4	51	51	296	573
V	118	245	1.3	1.3	121	247	561	578
Cr	80	162	1.3	1.3	82	165	478	513
Co	25	45	1.4	1.4	28	48	284	191
Ni	52	93	1.2	1.3	54	96	233	217
Cu	37	80	1.4	1.4	40	83	217	226
Zn	70	96	1.3	1.2	73	98	219	424
Sr	55	55	1.3	1.3	58	58	302	358
Y	39	45	1.3	1.3	41	48	488	122
Nb	72	79	1.3	1.2	75	82	428	193
Mo	4	3	1.5	1.5	7	6	17	10
Ba	287	202	1.4	1.5	290	205	1422	880
Ce	93	96	1.5	1.3	96	98	721	240
Pb	16	14	1.4	1.3	19	17	224	71
Zr	450	406	1.3	1.2	453	408	2208	1108

#### **4.2.1.3. Spatial distribution of uni-elements in stream sediment geochemical data**

Unlike soil samples, stream sediments are not representative of the sample sites from where they are taken. Rather, they are natural composites of the weathering and erosion drainage materials from individual catchment basins above each sample location. Thus the geoinformation embedded in each stream sediment sample would fairly be visualized in terms of drainage catchments (Alidu, 2007; Bonham-Carter, 1994; Carranza, 1994). However, the BGF is relatively flat with an altitude ranging from 1070-1400 m. Moreover, the 1400 m features are only a few isolated hills formed by the ferruginous quartzites (BIFs), volcanic rocks (e.g. Sukulu Carbonatite) as well as granites (Figure 2.2). This makes it extremely hard to generate representative catchment basins for the BGF. On the other hand, the fairly flat landscape of the BGF implies that the stream sediments are not transported far from their sources. Because of the above reasons, coupled with the clustering or regionalization for almost all the uni-elements (Figure 4.2A) the uni-elements for this geochemical data set can be contoured with minimal errors. The contouring conundrum and arguments regarding contouring of geochemical data (Stanley, <http://www.appliedgeochemists.org/events/iges2005/presentations/24%20Stanley%20Cliff.pdf>) are minimized by the regionalization of the geochemical data. Examples of the mostly used algorithms or ways for contouring geochemical data include: 1) nearest neighbour, 2) local mean, 3) inverse distance weighting and 4) kriging. These algorithms are provided by most of the modern computer programs or geographic information systems e.g. ArcGIS or ILWIS.

Therefore, in addition to the bulb plots for identifying anomalies, spatial associations as well as multi-element-association in uni-elements, the geochemical data were interpolated using inverse distance weighting (IDW) method. IDW was done for Au for better visualization of the target anomalies, since Au prospectivity mapping is the sole purpose of this research. IDW is a moving average interpolation method that estimates cell values by averaging the values of sample data points in the neighbourhood of each processing cell. The closer a point is to the centre of the cell being estimated, the more influence or weight it has in the averaging process. This method assumes that the variable (or property e.g. Au prospectivity) being mapped decreases in magnitude with distance from the sampled location.

Using the defined uni-element classes (i.e. background and anomaly, Table 4.2), the different uni-elements and PC scores were plotted on the geological map using bulb plots in order to identify uni-elements anomalies. Results of uni-element anomaly mapping show moderate to high Au anomalies (except for a few cases) to be strongly associated with the

amphibolites facies and  $\text{Al}_2\text{O}_3$ ,  $\text{Fe}_2\text{O}_3$ ,  $\text{TiO}_2$ ,  $\text{P}_2\text{O}_5$ , V, Co, Ni, Cu and Zn as opposed to  $\text{SiO}_2$ . Additionally, Au anomaly mapping by IDW interpolation of Au data (Figure 4.2B) exposes about four (4) NW and NNW striking groups of anomalies.

The spatial association between Au and amphibolites (mafic volcanics) suggests that Au deposits are preferentially hosted by lithologies that provide iron for sulphidation and Au precipitation reactions (Kuehn et al., 1990), with the most favourable host rock being the one with the highest Fe content. The little or no quartz in amphibolites (Lapidus, 2003) plus its mafic nature explains the observed spatial distribution between Au (which is associated with the amphibolites) in relation to  $\text{SiO}_2$ ,  $\text{TiO}_2$ ,  $\text{P}_2\text{O}_5$ , V, Co, Ni, Cu and Zn since Au is associated with the amphibolites. The spatial association between  $\text{Al}_2\text{O}_3$  is possibly due clay alteration minerals. The apparent Au- $\text{P}_2\text{O}_5$  interrelationship is logical support of the idea of a sedimentary basin (characteristic of a granite-greenstone terrane e.g. the BGF) where phosphorus dissolved from rocks accumulates as calcium phosphate (*phosphorite*). Thus, the observed spatial association between Au and  $\text{P}_2\text{O}_5$  is a possible coincidence of lode deposits associated with the BGF greenstone belts as well as a suitable sedimentary environment (i.e. the BGF basin) for phosphorite precipitation. The NW-SE alignment of Au anomalies possibly implies spatial association between Au deposits and the NW-SE and NNW-SSE lineaments. The observed spatial distribution of and association between uni-elements above are further investigated using principle component analyses in the following section with the aim of Au prospectivity mapping.

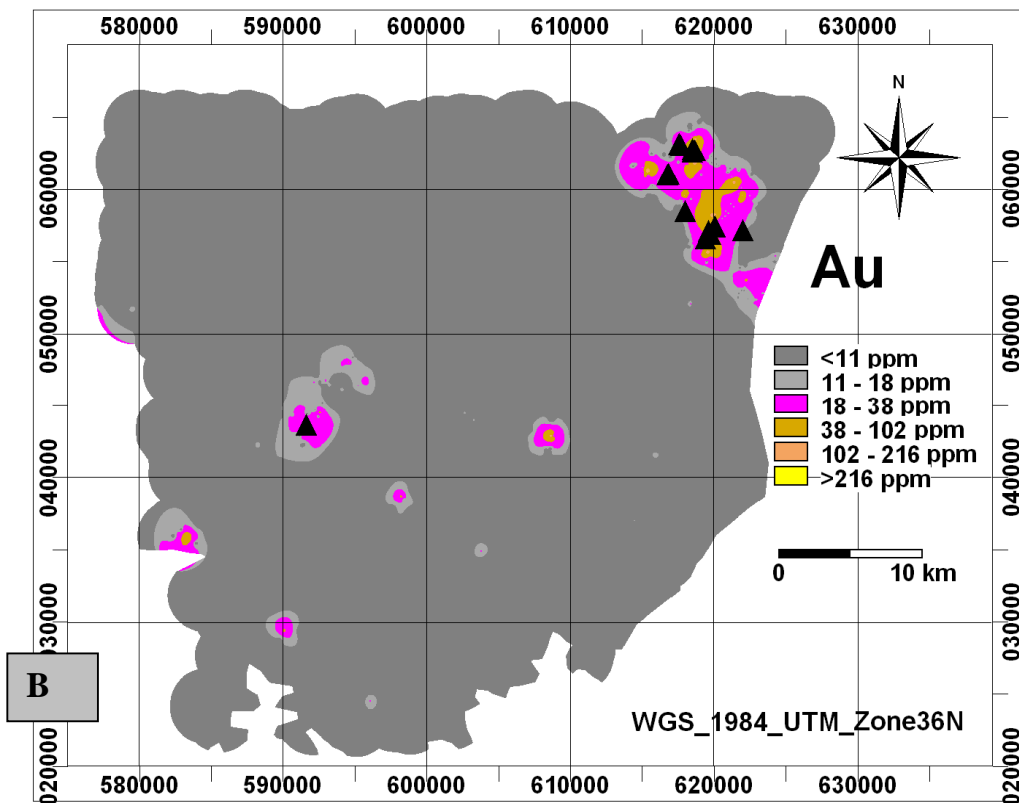
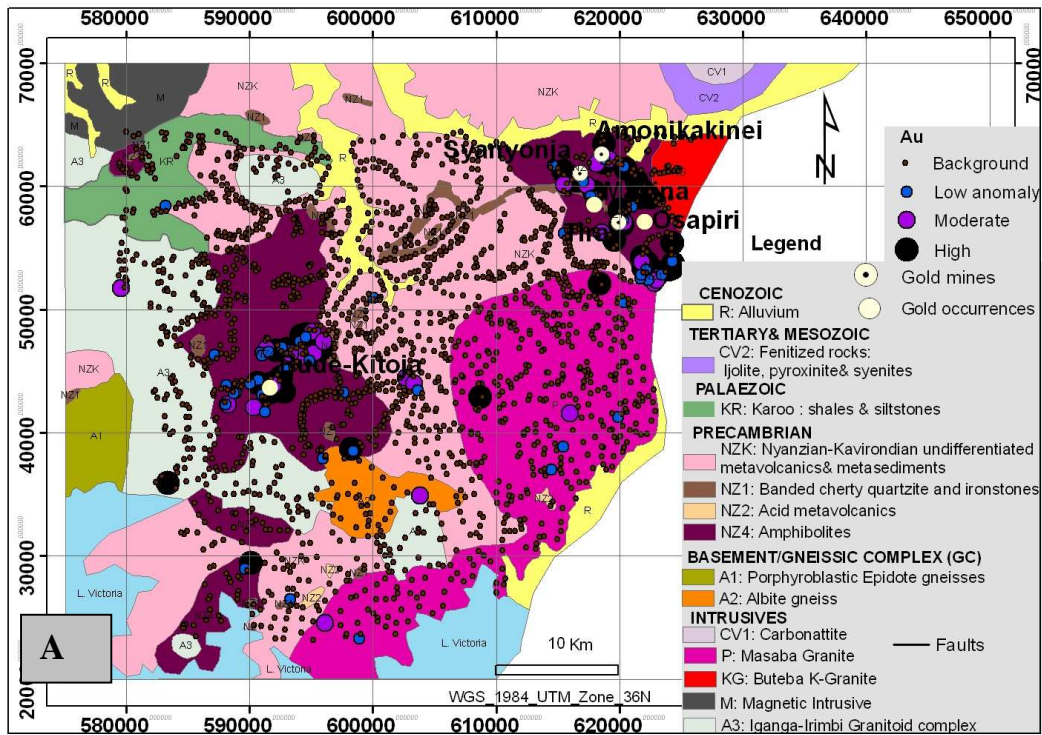


Figure 4.1: Au anomalies in log transformed geochemical data. Figure: 4.2A and 4.2B are bulb plots and IDW interpolation Au data. Black triangles are respectively Au mines and Au prospects.

#### **4.2.2. Multivariate anomalies in stream sediment geochemical data**

Multivariate analysis comprises a set of statistical techniques dedicated to the analysis of data sets with more than one variable at a time (Abdi, 2003). Such techniques include: principle component analysis, cluster analysis, logistic regression, simple linear regression, Poisson regression, discriminant analysis etc. The special case of two variables (e.g. correlation analysis) is known as bivariate analysis. The choice of the technique depends on the study, objectives and variables. Of these techniques, the use of principle component analysis in revealing the mutual inter-relationships and variability among uni-elements in a geochemical data set is demonstrated in this research.

##### **4.2.2.1. Principle component analysis (PCA)**

PCA is one of the oldest methods whose objective is to decompose a data set with correlated measurements/variables into a new set of uncorrelated (i.e., orthogonal) variables by using a covariance matrix to calculate linear combinations between the eigenvectors and the input variables. That is to say, a smaller set of “synthetic” variables that explains the original set is generated. These variables are known as principal components (PC). Since each linear combination (PC) explains all the variance in each variable (e.g. uni-element), each PC carries a different piece of information which is uncorrelated with other PCs. Thus, each PC is assigned a set of scores which corresponds to its projection onto all the variables at any given sample site. Consequently, PCA uncovers relationships among many variables (e.g. those inherent in a set of uni-elements), thereby reducing the amount of data required to define the relationship. Such relationships (for geochemical data) may include: lithology type, presence of mineralization, Fe/Mn oxides/hydroxides-scavenging effect etc. The first PC accounts for as much of the variability in a data set as possible with each succeeding PCs also accounting for as much of the remaining variability as possible. The PCs are interpreted in terms of the relationships that may be inbuilt in the input variables by using the magnitude and sign of the eigenvector loadings.

Before carrying out PCA, the  $\text{Log}_e$  transformed stream sediment geochemical data were standardized first. Standardisation of uni-element geochemical data sets via a more robust technique is an important step prior to modelling of multi-element signatures through application of multivariate analytical techniques (Carranza, 2008), which require proper estimation of the multivariate covariance (or correlation) matrix. By using the median and MAD (obtained in 4.2.1.2), the  $\text{Log}_e$  transformed geochemical data were standardized according to equation 4.2 (Carranza, 2008). Equation 4.2 is analogous with the classical statistical standardization algorithm in accordance with equation 4.3. The standardized

geochemical data (Z) were then subjected to PCA. Table 4.4 gives PCA loadings of the standardized Log<sub>e</sub> transformed stream sediment geochemical data for 23 uni-elements in each of the 1924 samples taken.

$$Z = [(X - \text{Median})/\text{MAD}] \quad (4.2)$$

$$Z = [(X - \text{Mean})/\text{std.dev}] \quad (4.3)$$

Where X is the observed uni-element content at any given sample location.

PCA results (Table 4.4) are in line with the above (4.2.1.3) uni-element anomaly mapping. PC1 representing Fe-Ni-Cr-Co-Cu-Zn-V-Ti-Al association and explaining 26.62% and 30.43% for felsic and mafic rock types respectively, is a plausible Fe-metal scavenging effect. Scatter plot of Log<sub>e</sub> Fe<sub>2</sub>O<sub>3</sub> against PC1 for both rock types (Figure 4.3) supports the Fe-scavenging effect. Al<sub>2</sub>O<sub>3</sub> associated with PC1 may be due to formation of clay minerals due to effects of hydrothermal alterations in the shear/fracture zones in the BGF greenstone belts.

PC2 characterized by Zr-Ce-Nb-Y association and accounting for 15.47% and 15.78% variance for mafic and felsic rocks respectively is possibly indicative of the potassic centres for example characteristic of the granitic terranes or felsic metavolcanics in the BGF. Whereas PC3 for the felsic rocks characterized by moderate to high positive loadings on (V-Cr-Ni-Cu) seem to point to a mafic lithological PC, PC3 for the mafic rocks does not suggest any plausible relationship. The rest of PCs each explaining a specific variance in the geochemical data may be due to other multi-element interrelationships such as associations reflecting minor (and hence negligible) geological-geochemical processes in the study area as well as errors in the data variables.

To identify the PC or multi-element group associated with Au mineralization, only Au values above the detection limit (i.e. excluding censored values) were plotted (on scatter plots) against the PC scores associated with the same sample location. This was because Au was excluded in PCA due to the high number of censored values (>90%). Figure 4.2 show no significant linear association ( $R^2$  0.0-5.7% for all PC) between Au and all PCs for both rock types. A linear association between Au and a given PC would imply a multi-element association occurring together with Au and hence a pointer to the Au mineralization.

To investigate the conceived idea that there is no multi-element association between Au and other elements, Au data excluding censored values were plotted on scatter plots against the uni-elements which appear to be spatially associated with Au which at same time bear high

and positive scores on PCs. Similarly, results (Appendix 4) show no significant ( $R^2 = 0.0 - 5.1\%$ ) association between Au and the uni-elements. Finally, to investigate which rock type hosts the gold mineralization, Au data excluding censored values were plotted on the box and whiskers plots. Results (Figure 4.4) indicate that the mafic rocks constitute the highest number of Au anomalies. Out of 150 valid Au values (i.e. excluding censored values), 112 values are located in the mafic rocks and only 38 in the felsic rocks, yet mafic rocks constitute about 25% of the entire study area. Mafic rocks also have more Au anomalies (10) than felsic rocks (3). It should also be noted that of the three (3) Au anomalies in felsic rocks, two (2) are associated with the banded iron quartzites (BIFs) overlying the amphibolites (mafic rocks). Additionally, out of the ten anomalies in the mafic rocks, seven (7) are higher than those in the felsic rocks.



Table 4.3: PCA of standardised (z) Log<sub>e</sub> transformed stream sediment data for 1924 samples, i.e. 492 and 1432 samples from mafic and felsic rock suits respectively

	Principal components (PC)											
	PC1		PC2		PC3		PC4		PC5		PC6	
	Felsic	Mafic	Felsic	Mafic	Felsic	Mafic	Felsic	Mafic	Felsic	Mafic	Felsic	Mafic
SiO <sub>2</sub>	-0.852	-0.791	-0.240	-0.241	-0.136	0.080	0.182	0.294	0.128	0.135	-0.034	0.137
Al <sub>2</sub> O <sub>3</sub>	0.716	0.752	0.561	0.549	0.098	-0.104	0.035	-0.058	-0.041	-0.018	0.062	-0.064
Fe <sub>2</sub> O <sub>3</sub>	0.916	0.871	0.087	0.204	0.054	-0.058	-0.134	-0.257	0.011	-0.128	-0.017	-0.074
MgO	0.315	0.392	-0.224	-0.321	0.621	0.709	0.278	0.128	0.410	0.049	0.047	0.016
TiO <sub>2</sub>	0.431	0.477	0.432	0.347	-0.518	-0.584	0.285	0.089	0.006	-0.015	-0.101	-0.026
P <sub>2</sub> O <sub>5</sub>	0.773	0.652	0.225	0.229	0.267	0.268	-0.105	-0.156	0.098	0.267	-0.091	-0.052
Li	0.411	0.353	0.221	0.517	0.268	0.153	0.189	-0.035	-0.078	-0.295	0.074	0.117
B	-0.372	-0.110	0.051	0.040	-0.071	-0.142	0.481	0.932	0.062	0.071	-0.218	-0.032
V	0.839	0.849	0.016	0.146	-0.125	-0.204	0.306	-0.050	-0.063	-0.191	-0.052	-0.056
Cr	0.264	0.753	-0.012	0.251	0.097	0.015	0.880	0.315	0.008	-0.042	0.017	0.033
Co	0.816	0.817	-0.090	0.073	-0.009	-0.090	0.065	-0.015	-0.019	-0.121	0.009	-0.054
Ni	0.681	0.847	-0.117	0.160	0.010	-0.090	0.535	0.114	-0.023	-0.165	0.034	-0.049
Cu	0.791	0.888	0.030	0.233	-0.173	-0.201	0.366	0.013	0.151	-0.010	-0.134	-0.114
Zn	0.744	0.753	0.253	0.111	0.175	0.092	0.120	0.060	0.194	0.322	-0.055	-0.040
Sr	0.021	-0.182	0.000	0.010	0.878	0.888	0.165	-0.136	0.022	0.008	-0.039	0.013
Y	0.191	0.523	0.846	0.687	0.072	-0.184	0.051	-0.056	-0.023	0.133	0.062	-0.094
Nb	0.184	0.294	0.865	0.768	-0.048	-0.295	-0.026	0.028	0.061	0.278	0.105	0.005
Mo	-0.002	-0.171	0.021	0.172	-0.036	-0.003	0.008	0.073	0.952	0.797	0.081	0.081
Ba	0.100	-0.415	0.149	0.116	0.715	0.519	-0.217	-0.310	-0.149	-0.256	0.134	0.129
Ce	0.398	0.398	0.667	0.709	0.245	0.216	-0.130	-0.117	-0.083	-0.153	0.245	0.173
Pb	-0.154	-0.208	0.319	0.098	0.106	0.049	-0.078	-0.033	0.120	0.072	0.909	0.968
Zr	-0.216	0.003	0.837	0.793	-0.121	-0.255	-0.008	0.191	0.003	0.329	0.042	0.037
Variance (%)	30.27	35.07	16.08	15.35	10.44	10.82	8.62	6.22	5.57	5.99	4.70	4.87
Σ Variance (%)	30.27	35.07	46.35	50.42	56.79	61.23	66.41	67.46	70.99	73.45	75.68	78.32

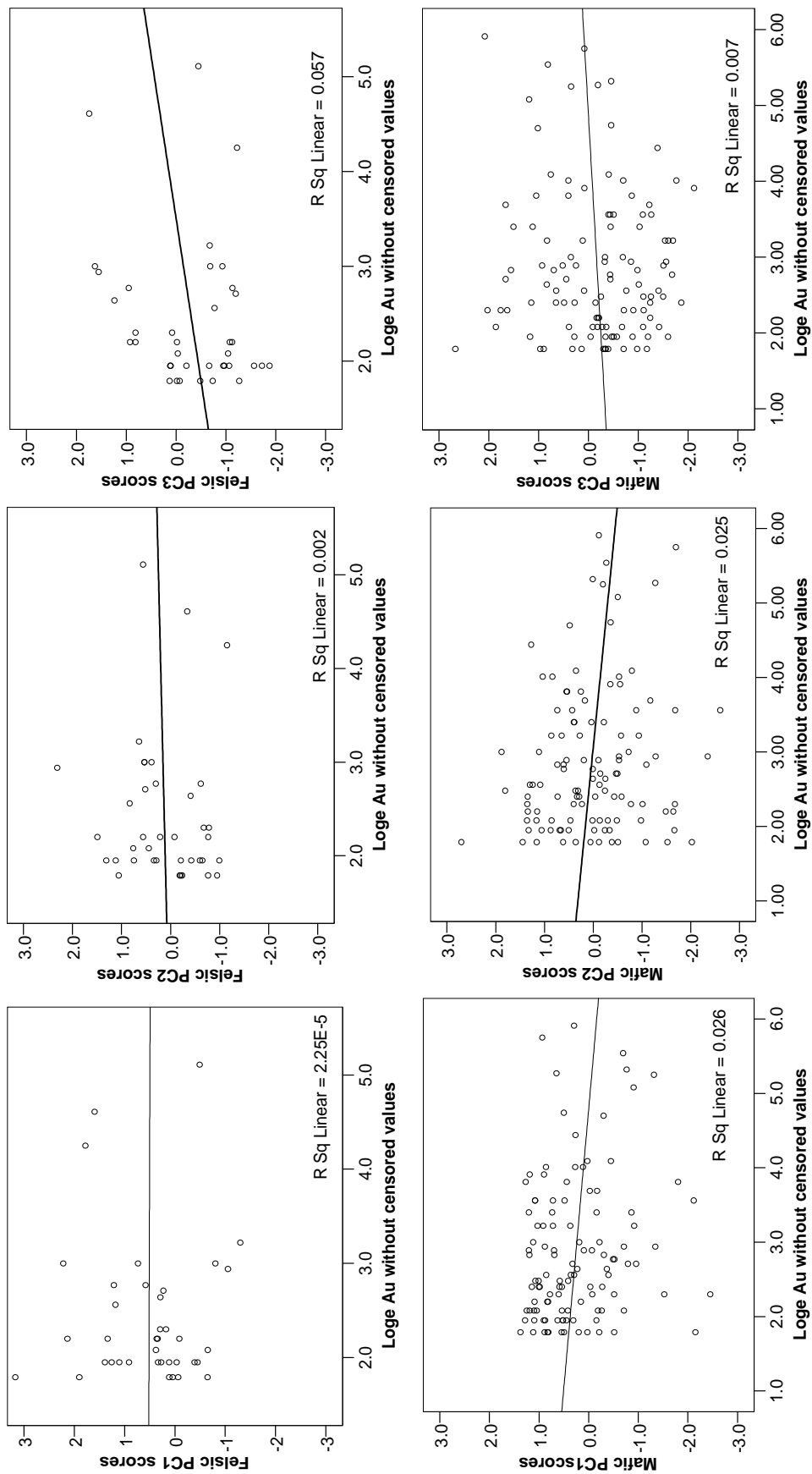
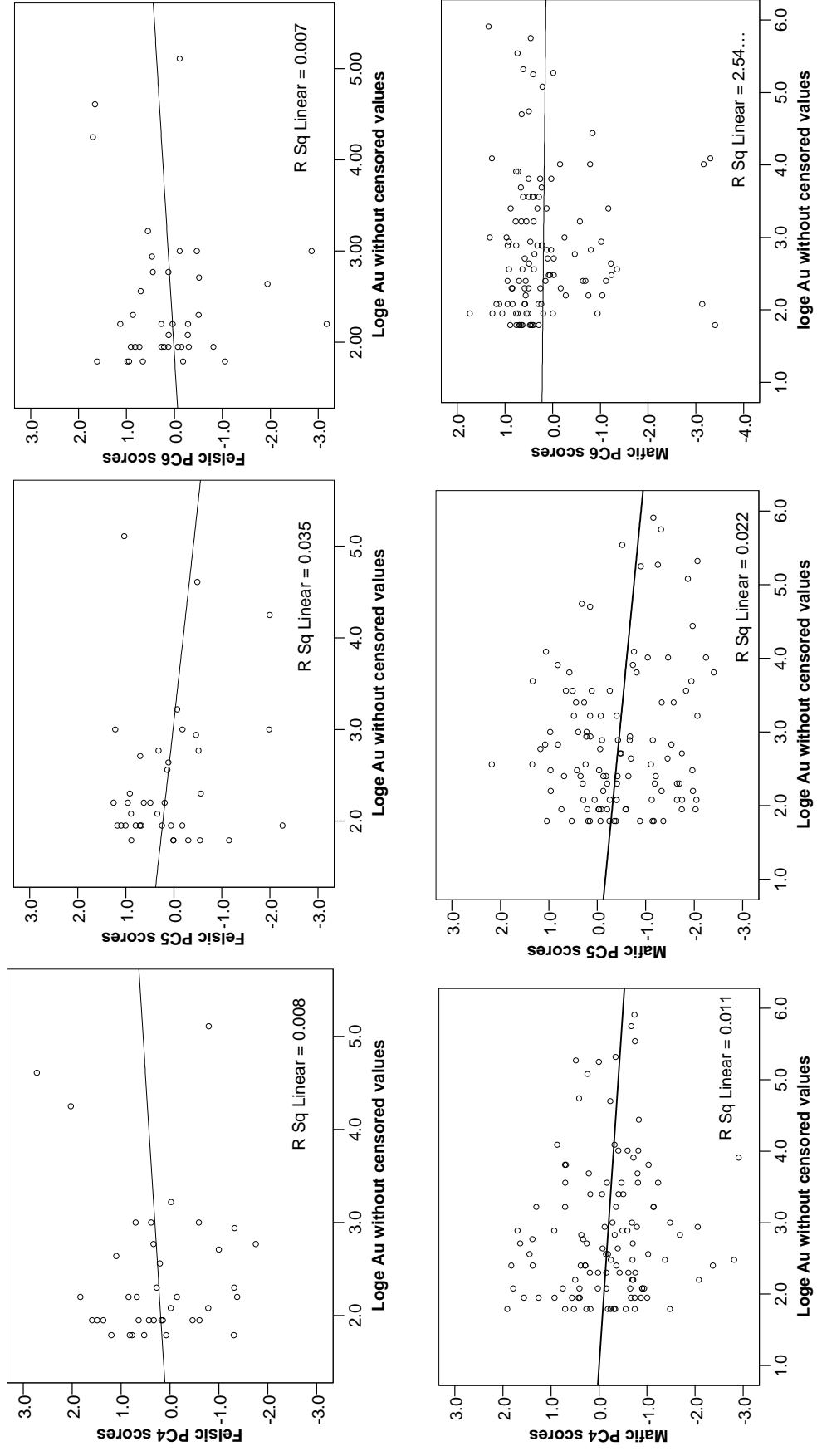


Figure 4.2: scatter plot of Log<sub>e</sub> Au censored values versus PC1, PC2 and PC3 scores for both the felsic and mafic rock suites.



**Figure 4.3:** scatter plot of Log<sub>e</sub> excluding Au censored values versus PC4, PC5 and PC6 scores for both the felsic and mafic rock suites

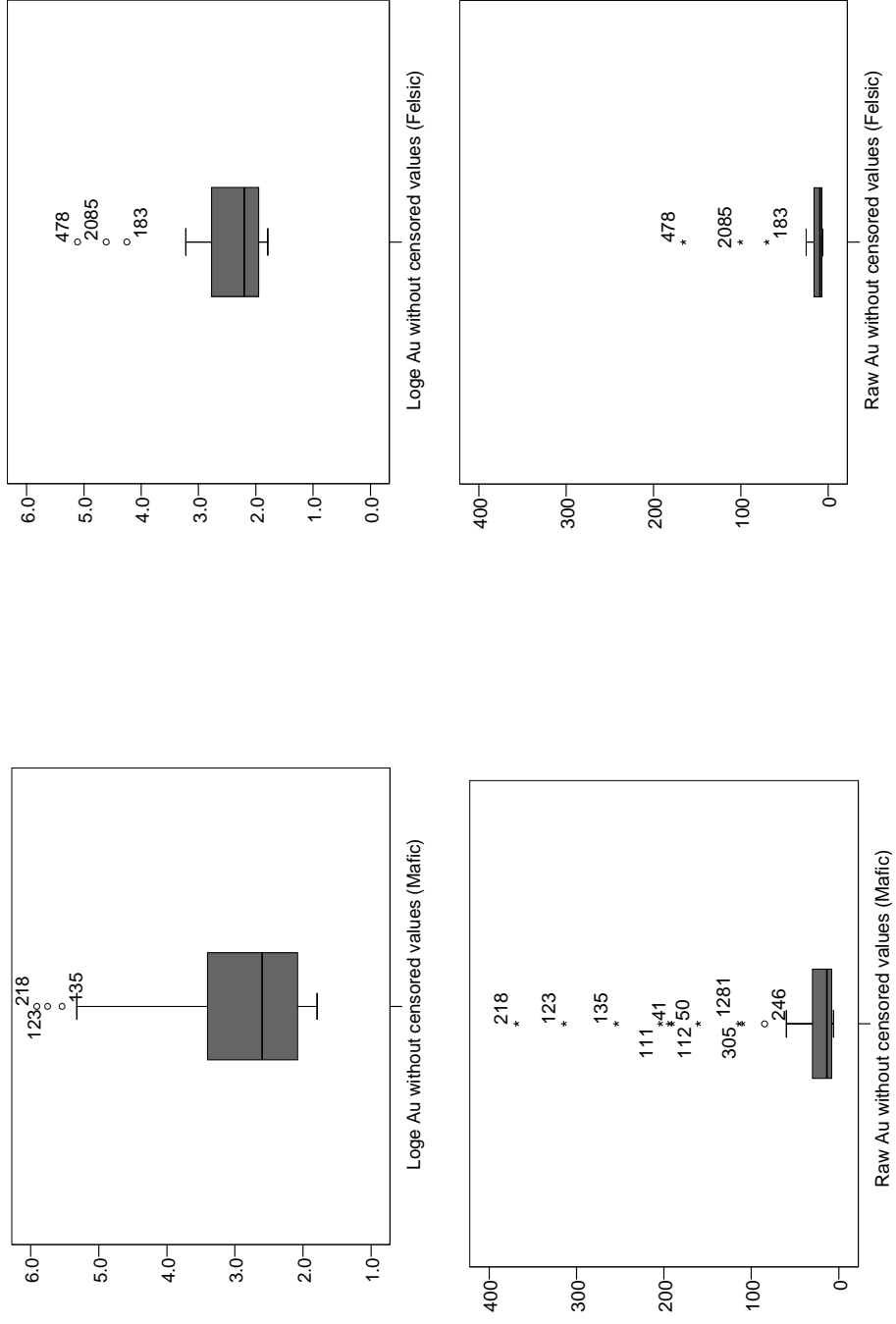


Figure 4.4: Box and Whiskers plots for raw and Log<sub>e</sub> transformed Au excluding censored values for both felsic and mafic rock suites. N = 38 and 112 for felsic and mafic rock suites respectively. All units are in ppb and natural logarithmic numbers for raw and Log<sub>e</sub> transformed Au data respectively. The number assigned to each outlier is its corresponding sample location number for easy identification and followed up.

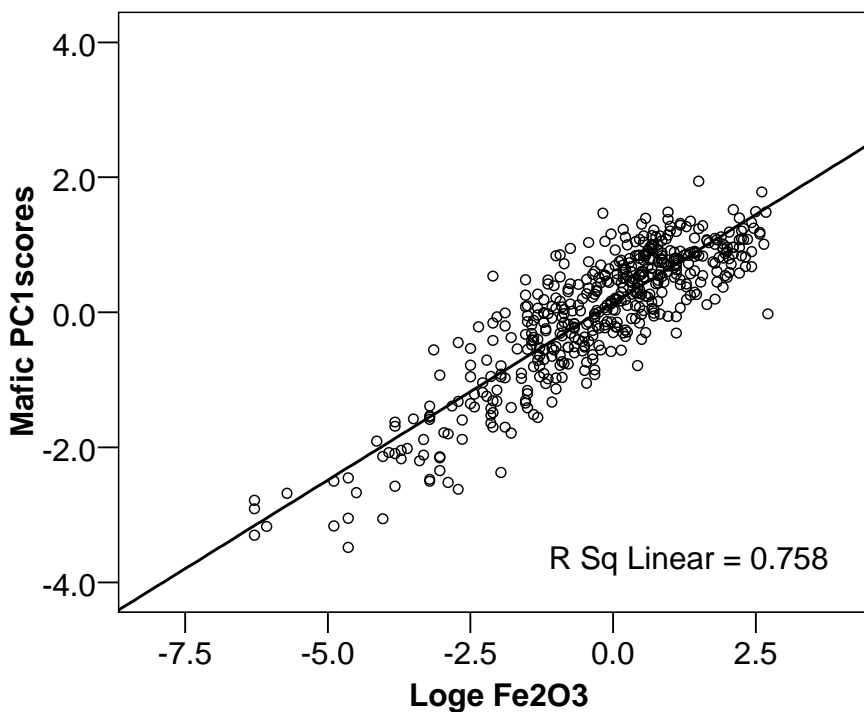
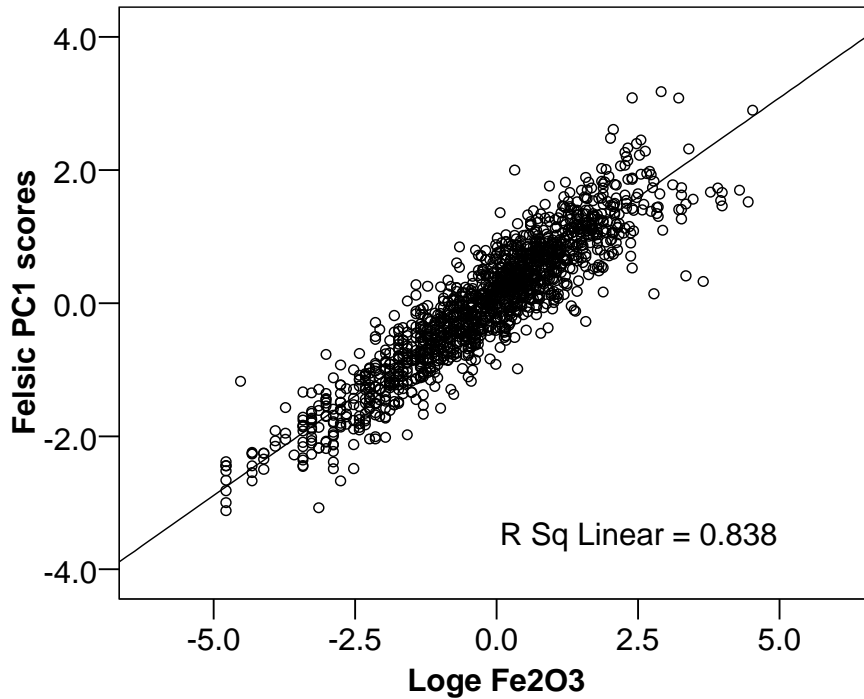


Figure 4.5: Scatter plots of  $\log_e \text{Fe}_2\text{O}_3$  versus  $\log_e \text{PC1}$  scores of standardized stream sediment geochemical data for both felsic and mafic rock suites. Note the linear ( $R^2 = 83.8\%$  and  $75.8\%$  for felsic and mafic suites respectively) association between Fe and the PC1 scores.

### 4.3. Discussion and conclusions

The results of the geochemical data analyses carried out above indicate that the variability in the geochemical data is highly influenced by lithology. This may be due to the fact that the chemistry of the rocks plays a big role in the classification of rocks. That is to say, whereas basic/mafic rocks are characterized by relatively high concentration in elements such as Ni, Cr, V, Ti, Mg, Cu, Fe etc, felsic rocks are enriched in the lighter elements, such as SiO<sub>3</sub>, Al, Ba, Sr etc. Because of the complexity of lithologies characteristic of an accretionary environment such as the Nyanzian greenstone belts of which the BGF is part, the chemical complexity is apparent and hence the variability in the data.

Another significant factor accounting for the variability in the geochemical data is the Fe-metal scavenging effect. This is attributed to presence of Fe-oxides/hydroxides generated by oxidation of the Fe in pyrite (FeS<sub>2</sub>), arsenopyrite (FeAsS) and sphalerite ((Zn, Fe) S). The reddish brown soils (Appendix 5) in the study area are the appropriate manifestation of presence of Fe-oxides/hydroxides which are responsible for metal scavenging. The Fe-metal scavenging effect is possibly supplemented by the Mn-oxides/hydroxides scavenging effect. Although Mn is not part of the geochemical data set, evidence for MnO<sub>2</sub> is attributed to the smoky (gray-black colour) quartz pebbles (Appendix 5)

The NW-SE and NNW-SSE trending anomalies in Au data are possible support the previous findings that Lode gold mineralization in the Busia gold field is associated with the NNW and NS faults (Schumann, 2007).

The association of almost all gold anomalies with the mafic rocks concurs with previous work that gold-bearing quartz veins are hosted by amphibolites. However, the absence of gold anomalies in some areas characterized by the presence of amphibolite (metabasalts) suggests a special geologic environment within the amphibolites with which the gold anomalies and hence gold deposits are associated. Since geochemical interpretation evidences above further support the presence of lode gold mineralization in the BGF, then the special geologic environment should be shear/fracture zones. Lode gold deposits are sited proximal to major accretionary structures (e.g. shear/fracture zones) (Campbell and Kerrich, 1998). This is supported by the geological knowledge that metabasalts are indicators of a paleo-volcanic-activity-environment which is (normally) associated with weak (shear/fracture) zones. The spatial association of lode gold (i.e. vein-hosted Au) mineralization with amphibolite metabasalts in the BGF therefore, leads to the conclusion that amphibolites are spatial vectors to shear zones with which the lode gold mineralization is

associated. That is to say, the presence of amphibolites may be an indicator for the presence of shear zones and/or lode gold mineralization. The presence of some anomalies in felsic rocks supports the findings that lode gold deposits may occur in any lithology (Campbell and Kerrich, 1998).

The lack of significant linear association between Au and PCs and the individual Fe, Ti, V, Cr, Cr, Ni, Cu and Zn uni-elements indicates that although these uni-elements and the multi-element appear to be spatially associated with the gold anomalies and known gold deposits, they are only of lithological significance (i.e. amphibolites) which hosts the gold-bearing quartz veins. They are not directly related with the lode gold mineralization and therefore can only be used as tertiary indicator features to the lode gold mineralization. This is supported by the geological knowledge that lode Au deposits are generally associated with enrichment in Au, Ag ( As, Sb, Te, W, Mo, Bi, B), with low enrichments of Cu, Pb, Zn relative to the background abundances (Campbell and Kerrich, 1998).

Finally, the results also suggest that no multi-element association or uni-element may be used as evidence for lode prospectivity for this geochemical data set except the Au data. As already observed above however, Au data excluding censored values is not representative of the whole area since only less than 10% (i.e. 150 out 1924 samples) are valid values. Notwithstanding the negative consequences of using non representative Au data in gold prospectivity mapping, Au data together with structures and lithology are further used in mapping of prospectivity for gold deposits in the next chapter.

## 5. Mapping of prospectivity for Au deposits

### 5.1. Introduction

It is widely known (e.g. in Uganda) that people who have previously worked in mines (i.e. mineral deposits) have later on “*accidentally*” discovered a number of mineral deposits of the type they used to mine. By means of the knowledge about a particular mineral one may discover mineral deposits even if not on exploration campaign for any mineral deposit (i.e. accidentally). This knowledge or conceptual model of the mineral deposits sought is of paramount importance in mineral exploration and particularly for GIS-based mineral prospectivity mapping which is an office or desk activity. As already observed (in chapter 1), a conceptual model is an idealized set of characteristics attributed to a group of mineral deposits (Bonham-Carter, 1994). Systematic analysis of the spatial association between mineral deposits and geological features or recognition criteria may lead to mapping of the prospectivity for mineral deposits of the type sought.

Predictive mapping of prospectivity for mineral deposits is carried out using two groups of methods i.e. the *conceptual* and *empirical* methods. Conceptual methods involve subjective (i.e. knowledge-driven) weighting of evidential maps based on geological expertise whereas empirical methods involve objective (i.e. data-driven) weighting of evidential maps based on measured spatial association between locations of known mineral deposits and indicative geologic features, (Bonham-Carter, 1994). Unlike the conceptual methods, data-driven methods require that target the variables (e.g. gold deposits) are sufficient (for statistically significant results) so that they can be divided into a training and a testing set (Carranza, 2008; Carranza et al., 2007). Using the training set, the relationships between the target and predictors (e.g. proximity to lineaments) are quantified and then used for prediction. The testing set is then used to test for the predictive capacity of the generated model (e.g. gold prospectivity map).

Considering the small number of known gold deposits/occurrences in the BGF therefore, conceptual methods are the most appropriate for this case study. This chapter therefore is concerned with: 1) spatial association analysis to define the prospectivity recognition criteria for lode gold deposits in BGF and 2) Knowledge-guided data-driven mapping of prospectivity for Au deposits. Since conceptual methods are mainly descriptive and or diagrammatic

(Bonham-Carter, 1994), the gold deposits in the BGF are further described in the next subsection. This is aimed at establishing the spatial recognition criteria for gold deposits on which gold deposits prospectivity mapping in a GIS is based in this chapter.

## **5.2. Spatial association analysis to define prospectivity recognition criteria**

Lode gold deposits (chapter 2) are known in the BGF, a granite-greenstone belts terrane and part of the gold province in the Nyanzian greenstone belts of East Africa. They occur in the Nyanzian formations which have been intruded and folded by granites during the Precambrian era. The deposits are similar in type with those known in Lake Victoria gold field of Tanzania and Kavirondo areas in Kenya (Gabert, 1990; Kuehn et al., 1990).

The principal spatial characteristics relevant to mineral prospectivity mapping in a GIS are described as follows. Known gold deposits are located in the amphibolite metabasalts. Consequently, amphibolites ought to be a lithological vector to gold mineralization. The gold occurs as native (free) metal as well as pyrite and auriferous arsenopyrite, with much rarer galena (PbS) and sphalerite ((Zn, Fe) S). Thus, Au, As plus anomalies and Fe should be good pathfinder/indicator elements for gold in stream sediment geochemical data. On the contrary, Fe shows no significant linear association with Au (i.e.  $R^2 = 0.3\%$ , Appendix 4) and not a good predictor for Au mineralization in this case. Gold appears as small flakes or coatings on joint surfaces or cracks and is unevenly distributed within the quartz veins (Barnes, 1961; Byamugisha et al., 1994; Mroz et al., 1991b). Further more, Schumann (2007) along with field observations indicate that the NW-SE, NNW-SSE as well as the N-S quartz veins are the principal hosts for gold deposits. This implies that faults or lineaments in general, with NW-SE, NNW-SSE as well as the N-S strikes are significant structural controls to the gold mineralization.

Given the compiled geological map, stream sediment geochemical data and faults interpreted from both satellite imagery and airborne magnetic data therefore, the prospectivity recognition criteria for lode gold deposits in the BGF are as follows:

- 1) Presence of or proximity to amphibolites
- 2) Presence of or proximity to NW faults interpreted from satellite SRTM and ASTER DEM images, geological map and airborne magnetic data
- 3) Presence of or proximity to NS faults interpreted from satellite SRTM and ASTER DEM images, geological map and airborne magnetic data
- 4) Proximity to high Au concentrations in stream sediment geochemical data

With the gold prospectivity recognition criteria in place, the next step is to: 1) produce a series of gold prospectivity maps in accordance with each criterion above and 2) combining the evidential maps to generate the overall prospectivity map for lode gold deposits in the BGF and 3) validation of the gold prospectivity map produced by overlaying of known Au deposits and prospects.

### **5.3. Knowledge-guided data-driven mapping of prospectivity for Au deposits**

#### **5.3.1. Introduction**

For areas where a number of mineral deposits of the type sought have already been discovered, predictive mapping of other prospective zones involves weighting and integration of geological, geochemical, or geophysical evidences (Carranza, 2007). The higher the number of discovered deposits, the more robust the evidential weights and hence the higher predictive capacity of the resultant mineral prospectivity map. This approach however, is not applicable in areas with few (e.g. the BGF) or no known mineral deposits of the type sought. Therefore the knowledge-guided data-driven approach to gold prospectivity mapping is taken. By use of knowledge about the spatial association between geological, geochemical and or geophysical features and known mineral deposits, the evidential features are subjectively scored. The wildcat method for predictive mapping of mineral prospectivity in areas with no discovered mineral deposits of the type sought (Carranza and Hale, 2002g) is used to score the distance proximity maps to faults. The wildcat approach has been recommended for vein-hosted mineral deposits of which lode deposits are part. The lithological units are also score subjectively according to their relevance to the prospectivity of the mineral sought. The fuzzy logic method for modelling mineral prospectivity as describe by (Bonham-Carter, 1994) is applied in this case for integration of the set of weighted evidential maps in order to generate a gold prospectivity map in the BGF. The predictive capacity of the resultant prospectivity map is then tested by how many known gold deposits it predicts.

#### **5.3.2. Preparation of evidential features for gold prospectivity mapping**

##### **5.3.2.1. Structural evidential maps**

NW, NNW and NS trending faults are known to be associated with Lode gold mineralization and therefore NW and NS faults are used as evidences in this case. All the NW and NNW faults have been all generalized as NW faults. Structural evidential maps were obtained by: 1) rasterizing the interpreted NW and NS faults, 2) creation of distance maps from the faults, 3) classifying the distances to the faults into proximity classes using equal-percentile

distance intervals, 4) dividing the distance corresponding to each percentile by two (i.e. into two halves or median distance  $d$ ) and 4) finally scoring the proximity percentile classes by equation 5.1 as below:

$$S_c = (1/d) C \quad (5.1)$$

Where  $S_c$  = score of each percentile class and  $C$  = hypotenuse of the pixel size of the map. The pixel size in case is 50 X 50m, big enough for the computer to perform the calculation faster considering the size of the map (2500Km<sup>2</sup>). Tables 5.1 and 5.2 are summaries of the above steps in scoring geological features in mineral prospectivity mapping using the wildcat method.

Percentiles are used to classify proximity distances to geological features because they are robust in classifying continuous data of any distribution. Similarly, the median instead of the mean distance is used because of its robustness in estimating the central data (Carranza and Hale, 2002g). The hypotenuse of pixel size is taken because it is the maximum distance across the pixel on a raster. Figure 5.2 shows resultant evidential maps. The inverse of the distance (to geological features) used in the wildcat technique is a measure of favourability, i.e., the closer to a geological feature, the greater the chances of finding mineral deposits of the type sought. With inverse distance therefore, proximal classes have higher degrees of favourability compared to distal classes.

This way of scoring evidential features is referred to as the *wildcat* method for predictive mapping of mineral prospectivity in areas with no discovered mineral deposits of the type sought (Carranza and Hale, 2002g). Based on the general qualitative characteristics of the geological environment of the mineral deposit type sought (Carranza, 2002c), the wildcat modelling of mineral potential involves blindly pursuing mineralization by use of limited geological information. The method uses the geological knowledge that mineral deposits occur in a particular environment characterized by anomalous geological characteristics compared to its surroundings. Such anomalous environments are characterised by a set of special geological features (Bonham-Carter, 1994) for example enrichments in uni-elements and/or multi-element association, silicification (e.g. in Au-bearing quartz veins), hydrothermal alterations etc.

It is evident (see Figure 5.1, 5.3 and 5.7) that scoring of evidential features using the wildcat results in evidential scores that decrease exponentially with decreasing proximity to geological features suggesting that, mineral deposits preferably occur only in areas closest to geological features. This is on the other hand not realistic. Normally, in several examples

of data-driven predictive mapping of mineral prospectivity, evidential weights tend to decrease parabolically. However it has been shown (Carranza, 2007) that the wildcat technique is suitable for vein-type deposits modelling and hence the reason for the choice of the method for this research, to model the prospectivity for lode gold deposits in the BGF. Tables 5.1 and 5.2 summarize the scoring process while Figures 5.2 and 5.4 are the weighted/scored curvilinear evidential features.

Table 5.1: proximity classes and scores of the distance to NW trending faults

Proximity class/Km	proximity class median	Scores
0.00-0.20	100	0.707
0.20-0.40	200	0.354
0.40-0.61	305	0.232
0.61-0.86	430	0.164
086-1.11	555	0.129
1.11-1.40	700	0.101
1.40-1.74	870	0.081
1.74-2.178	1089	0.065
2.178-2.84	1420	0.05
2.84-16.51	8255	0.009

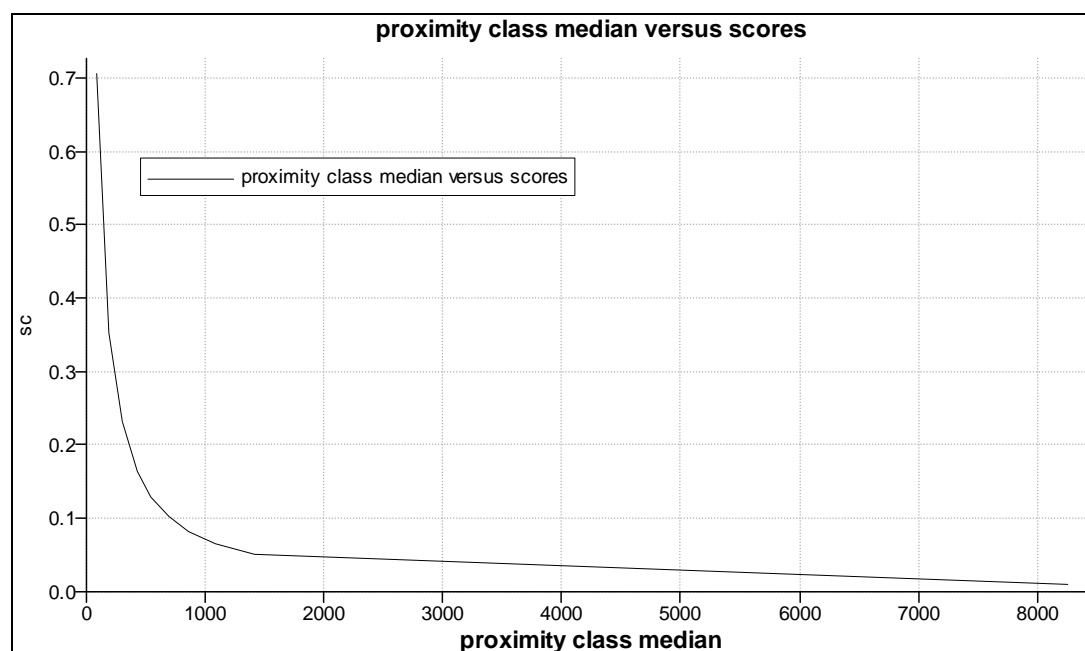


Figure 5.1: Graph of class median of proximity to NS trending faults versus scores

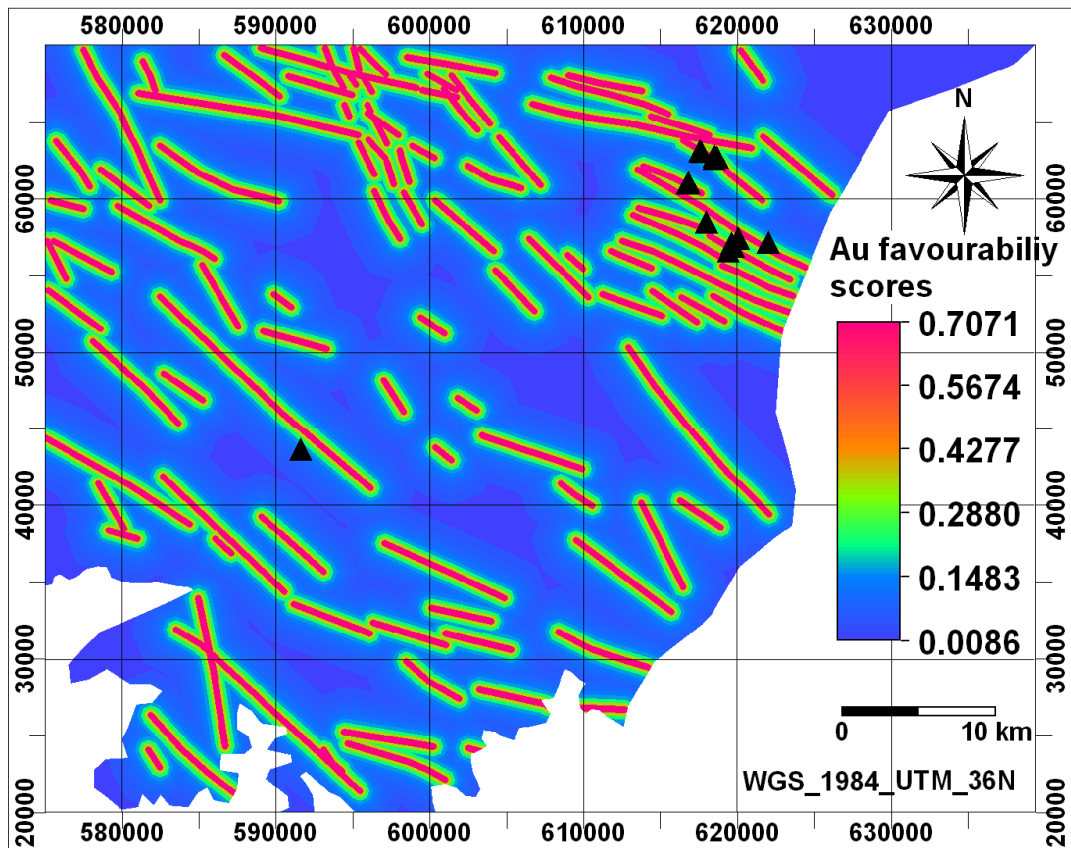


Figure 5.2: Au prospectivity map based on the NW faults. The black triangles are known gold occurrences.

Table 5.2: proximity classes and scores of the distance to NS trending faults

Proximity class/Km	proximity class median	Scores
0.00-91	455	0.1554
0.91-1.64	820	0.0862
1.64-2.32	1160	0.061
2.32-3.02	1510	0.0468
3.02-3.82	1910	0.037
3.82-4.74	2370	0.0298
4.74-5.94	2970	0.0238
5.94-7.47	3735	0.0189
7.47-10.81	5405	0.0131
10.81-21.2186	10609.3	0.0067

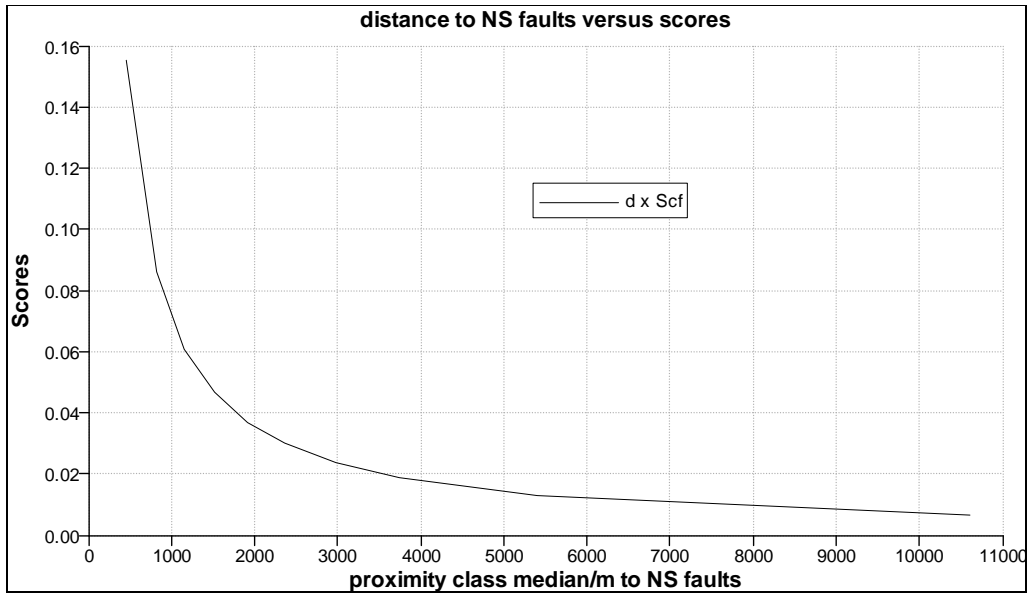


Figure 5.3: Graph of scores versus class median of proximity to NS trending faults

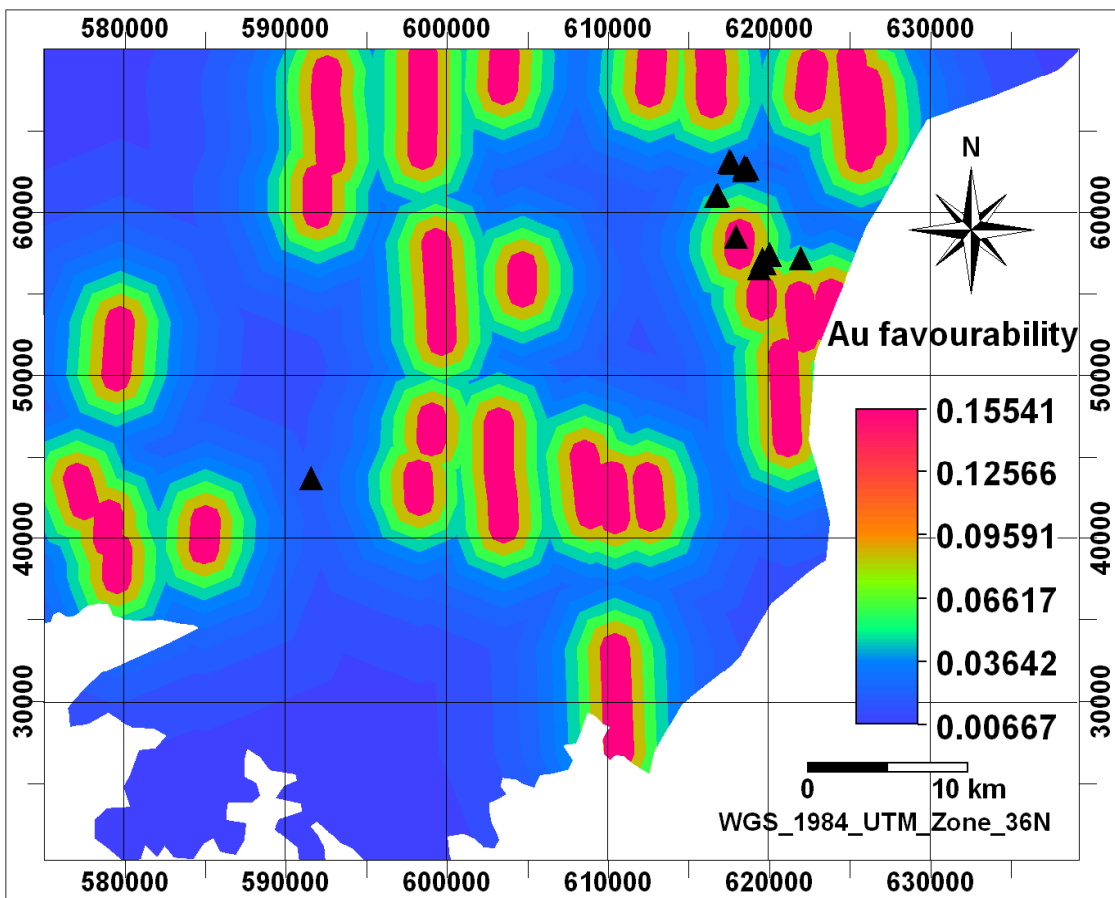


Figure 5.4: Au prospectivity map based on the NS faults. The black triangles are known gold occurrences.



Figure 5.5: Possible stratigraphic column with respect to Amphibolites, Banded Iron quartzites (BIFs) and Undifferentiated Nyanzian-Kavironidian metavolcanics and metasediments. Direction of younging is upwards.

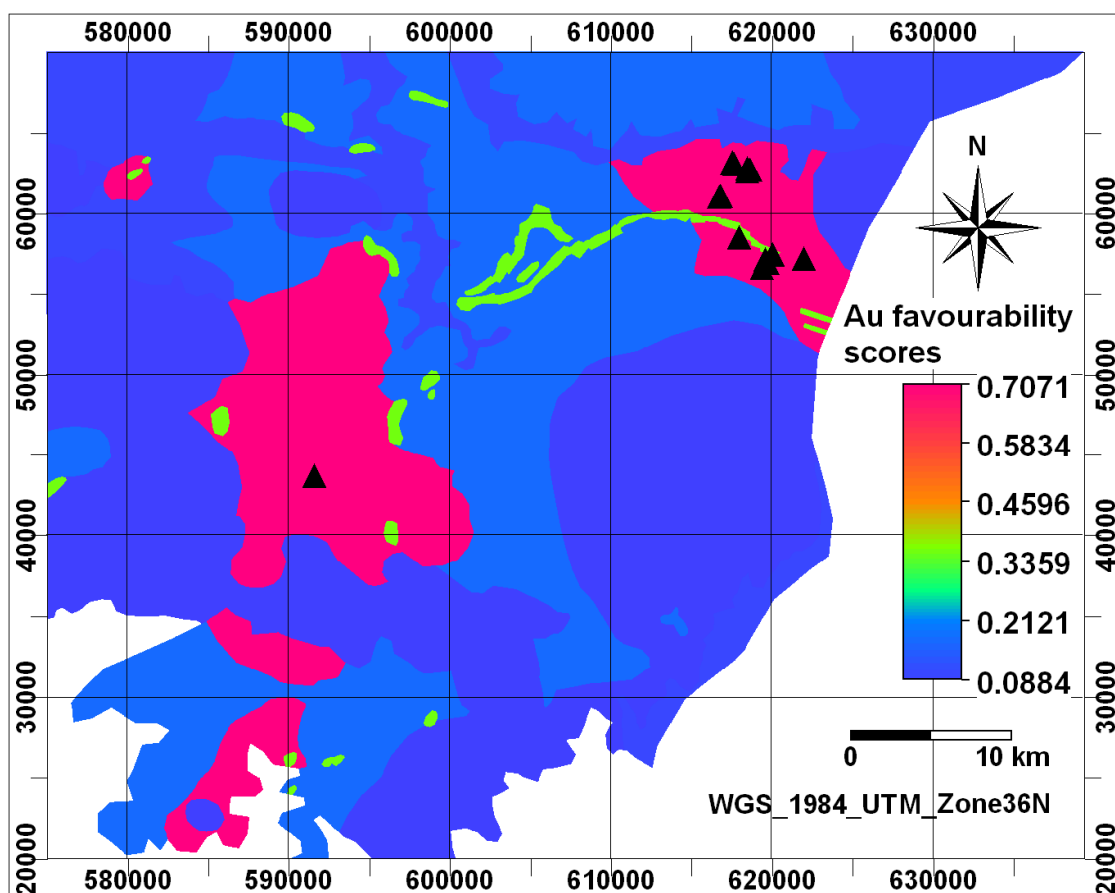


Figure 5.6: Au prospectivity map based on lithology. The black triangles are known gold occurrences.

### 5.3.2.3. Geochemical evidential map

Only gold data is used as lode gold prospectivity evidential layer. Because of the positive skewness of the Au data even after loge transformation, the robust box and whiskers plots (Carranza, 2008) together with the histogram (Figure 5.7) were used to identify the populations in the gold data so as to score them appropriately. From the histogram, at least six (6) populations are evident. Consequently, the Au data were sub-divided into six populations (Table 5.3). The populations: 1) above the upper whisker (UW) were considered anomalous, 2) between UW and (UH upper hinge) as high background, 3) between UH and LH (lower hinge) as background and 4) below very low background. However, to give particular importance to the observed populations in the high background and background classes, the individual populations in these classes were considered and scored separately.

Like with the previous evidential features above, scoring of the Au data was also via the wildcat method. The process involved: 1) classifying data, 2) estimation of the class median, 3) assigning the anomalous class median a value equal to that of the first proximity class of the curvilinear evidential features and generating the evidential scores for the succeeding classes by way of halving the preceding class scores. It should be noted that after estimating identification of the individual population, the corresponding loge transformed Au data were reconverted to normal values to portray the real picture of the data. Figure 5.8 is a graph showing variation of the Au class median with the Au scores whereas 5.9 is a weighted Au data map.

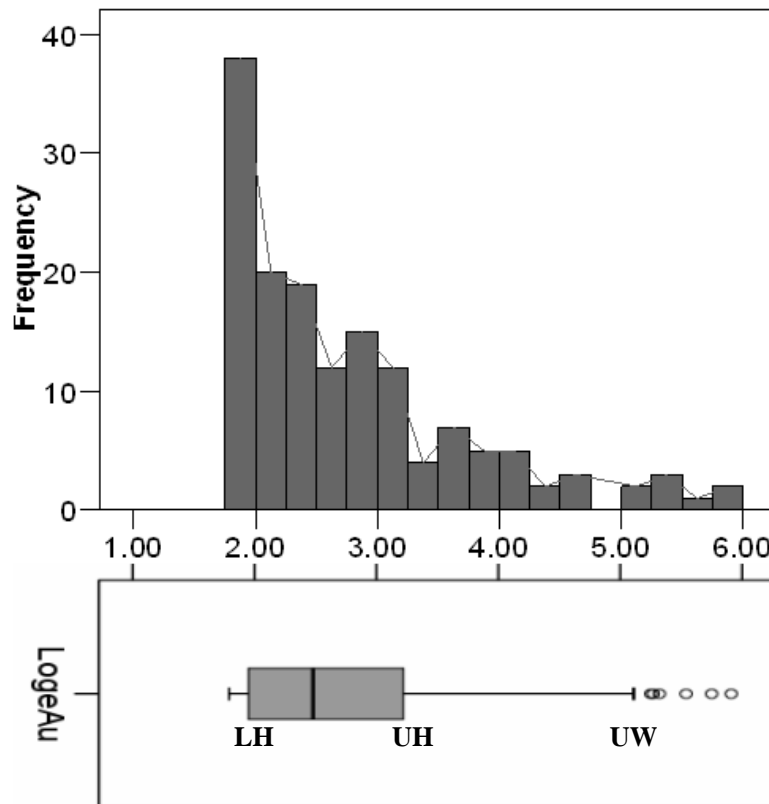


Figure 5.7: Histogram and box plots showing populations in the loge transformed Au data excluding censored values (N =150).

Table 5.3: Au data classes and scores

Au/ppb	Au class median/ppb	score
5-11	5.5	0.0221
11-18pp	9	0.0442
18-38	19	0.0884
38-102	50.5	0.1768
102-216	108	0.3536
216-271.2	135.6	0.7071

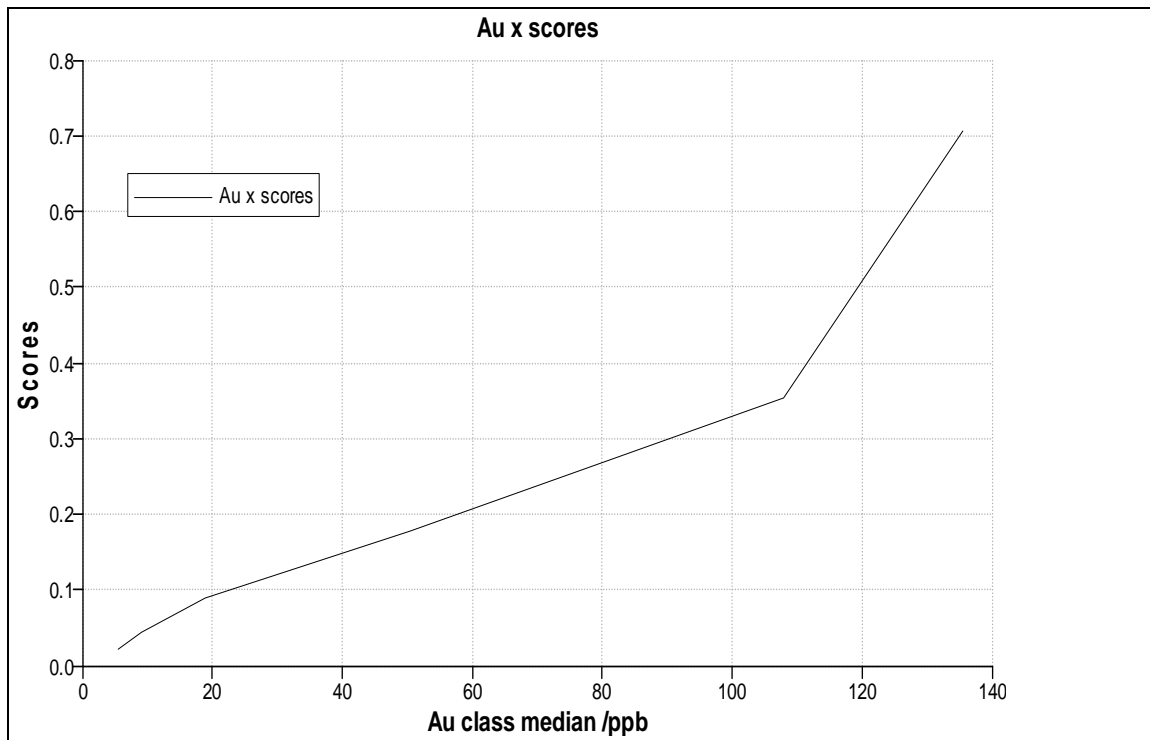


Figure 5.8: Graph showing the variation of Au scores with the Au class median

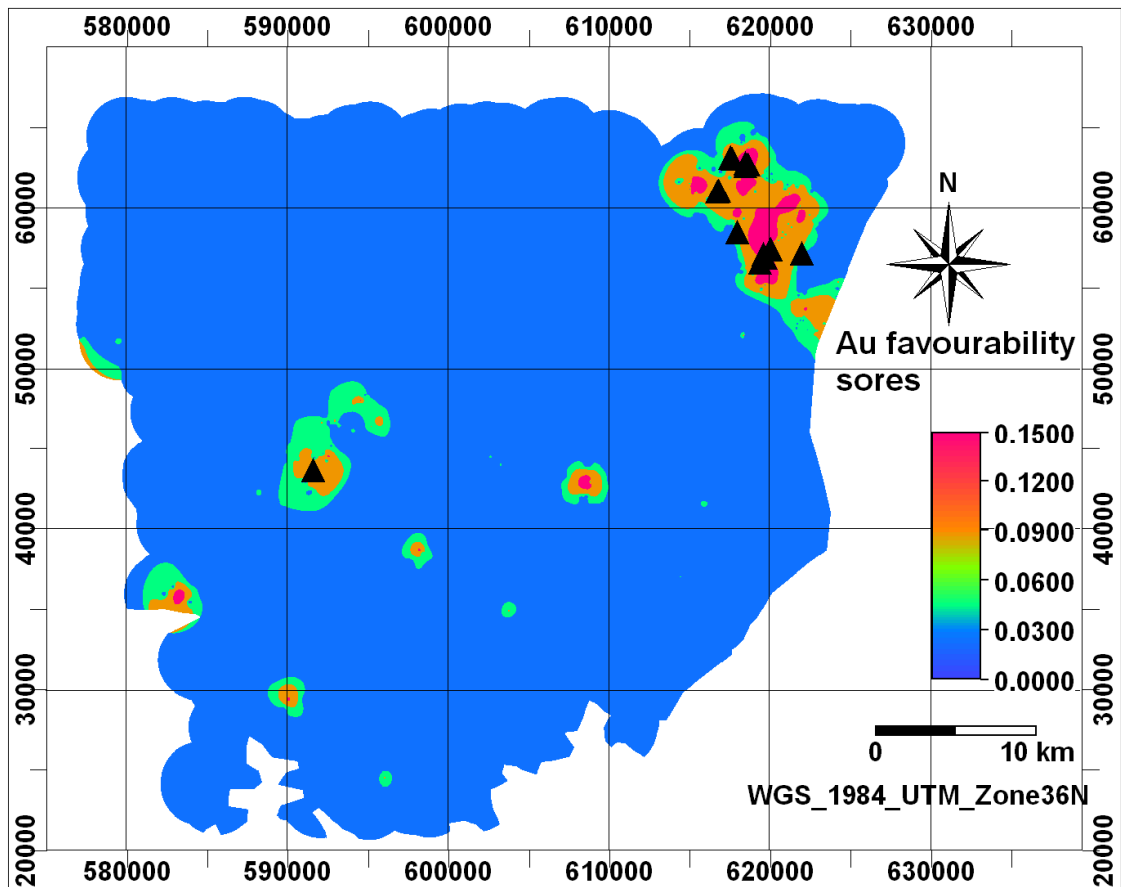


Figure 5.9: Au prospectivity map based on Au geochemical data. The black triangles are known gold occurrences. Note that the maximum favourability score is 0.7071 but for visualization purpose, the favourability scores were stretched between 0.00 and 0.15.

#### 5.3.2.4. Integration of the evidential map

The fuzzy logic method for modelling mineral prospectivity as described by (Bonham-Carter, 1994) is applied in this case for integration of the of weighted evidential maps in order to generate a gold prospectivity map in the BGF. The predictive capacity of the resultant prospectivity map is then tested by how many known gold occurrences it predicts.

There is a variety of operators used in combining the membership evidential maps derived (An et al., 1991; Bonham-Carter, 1994). These include fuzzy AND, fuzzy OR, fuzzy algebraic product, fuzzy algebraic sum and Fuzzy gamma operator. Whereas the fuzzy AND is an equivalent of the Boolean AND (intersection), the fuzzy OR is similar to the Boolean OR (union). It can be therefore realized that in the fuzzy AND, the output is controlled by the smallest or minimum fuzzy membership values while the fuzzy OR generalizes whereby maximum membership values control the output map. Hence fuzzy OR is helpful in areas

where evidences for mineral prospectivity are scarce whereby the presence of either of the evidences gives an indication of the favourability.

The fuzzy algebraic product is defined is also an equivalent of the algebraic product unlike the Fuzzy algebraic sum. The fuzzy algebraic product is however more effective than the fuzzy AND and the fuzzy OR in integrating evidential maps although the values of the resultant map are much smaller than either of the input maps due to multiplication of such small numbers less than one (1). But since all the pixel values are affected the, the effect is distributed all over the output map with no loss of information.

The fuzzy algebraic sum operator results in larger than or equal to the largest contributing fuzzy membership value. The evidential maps reinforce one another and the combined evidence results in more support than any of evidential map input. Hence it may not suitable for mineralization where the mineral resource is scarce.

Lastly, there is the fuzzy gamma operator defined as the algebraic product of the fuzzy algebraic product and the fuzzy algebraic sum. It is characterized by subjective choice of gamma value for which reason the fuzzy algebraic product has been preferred for integrating the evidential maps for this case study.

### **6.2.2 Application of the fuzzy logic method to the Busia gold field**

The fuzzy algebraic product was used to combine the evidential maps by algebraically multiplying the evidential maps as below:

$$\mathbf{AuP_{overall} = A1 * A2 * GG * Au_{p\_geochem}} \quad \mathbf{(5.3)}$$

Where AuP<sub>overall</sub> = Overall gold prospectivity map, A1 and A2 = respectively the gold prospectivity map based on NW and NS trending faults and GG = gold prospectivity map based on lithology and Au<sub>p\_geochem</sub> = gold prospectivity Au in the geochemical data.

Because mineral resources (e.g. gold) are rare natural resources, the predictive capacity of the knowledge based gold prospectivity map produced was tested at a 97.5% confidence level. The favourability scores were reclassified into percentiles and all scores below 97.5% were considered unfavourable whereas those above (i.e. the top 2.5%) were considered favourable zones for gold prospectivity. Selecting 2.5 % of the highest favourability scores as favourable for gold prospectivity was based on one of the procedures recommended for selecting threshold levels (97.5% in this case) in order to identify anomalies in geochemical statistical analyses (Hawkes and Webb, 1962; Reimann et al., 2005). That is to say, ordering

the data (e.g. Au favourability scores) and then selecting the top 2.5% of the data for further inspection. This is also in line with the classical [mean + 2standard deviations] for estimating about 2.5% of the upper extreme values for further inspection.

The results (Figure 5.3) show that apart from one (Bude-Kitoja-A), all the known gold occurrences (i.e. Amonikakinei-B, Syanyonja-C, Makina-D, Tiira-E and Osapiri-F) are predicted by the prospectivity map. Moreover, the unpredicted occurrence is also close (about 1/2Km) to favourable zones. Also two areas (i.e. N1 and N2) are predicted as favourable zones. Whereas the N1 zone is associated with the banded iron formations (BIF), the N2 zone is associated with the contacts between the Masaba granite and the undifferentiated Nyanzian-Kivirondian lithologies.

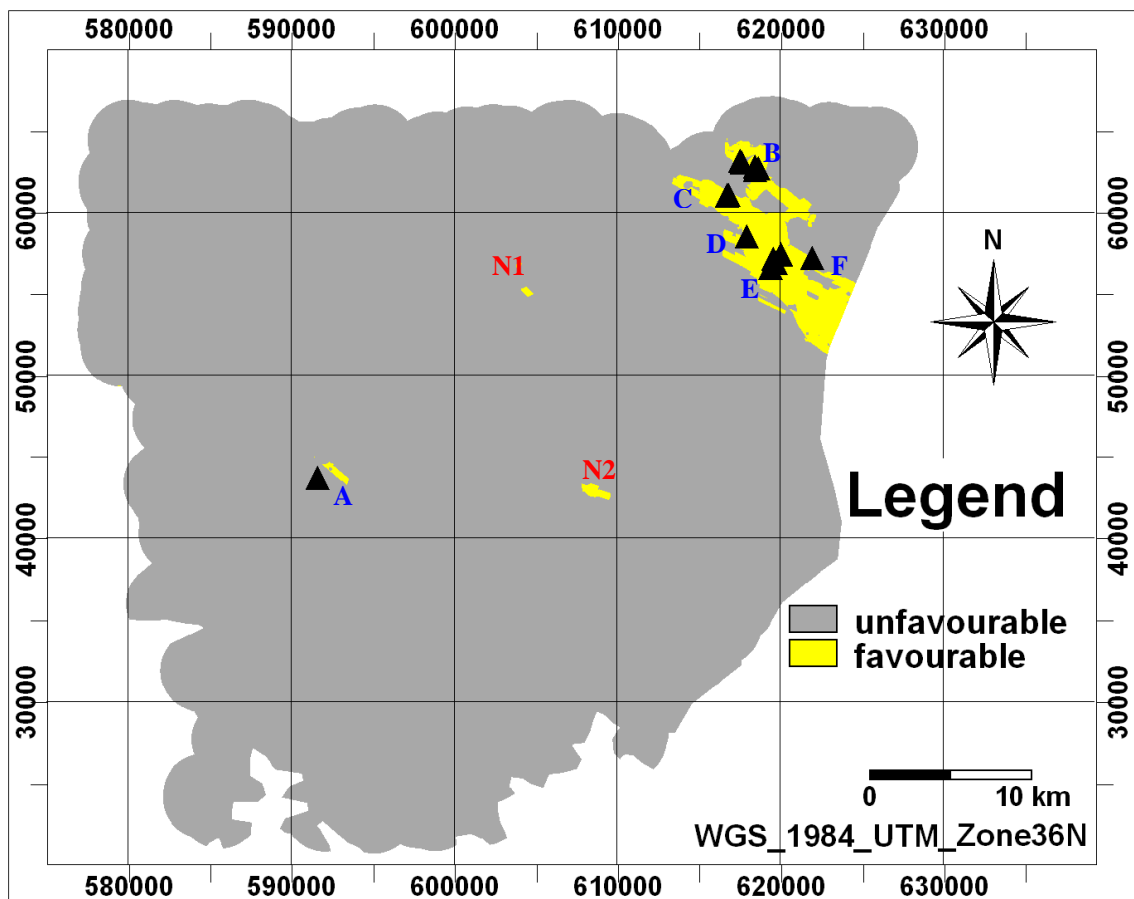


Figure 5.10: Overall gold prospectivity map for the Busia gold field base on all evidential features. Black triangles are known gold occurrences. N1 and N2 zones are predicted as favourable.

#### **5.4. Discussion and conclusions**

The results from knowledge-guided data-driven mapping of prospectivity for Au deposits in the Busia gold have demonstrated the capacity of GIS-based representation and integration techniques for mapping mineral (e.g. gold) prospectivity. The predictive capacity of the overall gold prospectivity map derived suggests that it can be used to predict other areas for lode gold deposits. The location of all favourable zones (except at N2) in the Nyanzian greenstone belts lithologies is consistent with the geological knowledge that lode gold deposits are distributed in belts of great geological complexity (characterized by gradients of lithology, strain and metamorphic grade) and proximal to major accretionary structures (Campbell and Kerrich, 1998). This is in turn indicative of the potential for lode gold prospectivity of the Busia greenstone belts, which are such an environment. The ability of the overall gold prospectivity map to predict all zones known for gold mining in the BGF (i.e. Tiira, Syanyonja and Amonikakinei) implies high lode prospectivity at Makina, Osapiri as well as Bude-Kitoja which are also predicted by the same map. The less known N1 and N2 which are as well predicted as favourable zones should therefore be investigated. Because N2 is also associated with a geochemical anomaly (Figure 5.4 above) unlike N1, the former seems to be more prospective than the latter.

The conformance of the current results to results of past gold prospectivity work in the Busia goldfield suggests that: 1) inverse distance weighting is a good method for interpolating geochemical data provided the data is auto-correlated, 2) the wildcat method is a good technique for quantifying and scoring the spatial association between geological features and zones of high prospectivity for mineral deposits such as lode gold mineralization/deposits in order to generate intermediate or evidential maps, 3) Fuzzy algebraic product is a good method for integrating evidential maps to generate an overall mineral (e.g. gold) prospectivity map and finally 4) ground-collected and remotely-sensed datasets are useful for mapping geological features that are essential predictors for lode gold prospectivity

## 6. Overall Conclusions and Recommendations

### 6.1. Overall conclusions

To answer the research questions posed earlier on in chapter 1, the following conclusions which are based on observations from the available data, data analysis and interpretations can be made:

- 1) Busia gold field is a prospective area for lode gold mineralization whose exploration requires the use of structures and lode gold pathfinder elements (i.e. enrichment in Au, Ag and (As, Sb, Te, W, Mo, Bi, and B)).
- 2) The Lode gold mineralization in the Busia gold field is structurally controlled and the principal or primary geological features with which lode gold mineralization is associated are the NW and NS faults.
- 3) Although the multi-element association Fe-Ti-V-Cr-Cr-Ni-Cu-Zn as well as individual uni-elements appear to be spatially associated with the gold anomalies and known gold occurrences, they are only of lithological significance (i.e. amphibolites) which hosts the gold-bearing quartz veins. They are not directly related with the lode mineralization and therefore can only be used as tertiary indicator features to the lode gold mineralization. Geochemical analysis shows no significant linear association between Au and other uni-elements (Fe-Ti-V-Cr-Cr-Ni-Cu-Zn) with which it appears to be spatially associated have proved
- 4) The Amphibolites (mafic metavolcanics) in the Busia gold field are spatial vectors to shear zones with which lode gold mineralization
- 5) Inverse distance weighting is a good method for interpolating geochemical data provided the data is auto-correlated
- 6) The wildcat method is a good technique for quantifying and scoring the spatial association between geological features and zones of high prospectivity for mineral deposits such as lode gold mineralization/deposits in order to generate intermediate or evidential maps.
- 7) Fuzzy algebraic product is a good method for integrating evidential maps to generate an overall mineral (e.g. gold) prospectivity map
- 8) Ground-collected and remotely-sensed datasets are useful for mapping geological features that are essential predictors for lode gold prospectivity

## **6.2. Recommendations**

- 1) Detailed geological mapping is recommended in order to identify major structures and belts of great geological complexity (i.e. characterized by gradients of lithology, strain and metamorphic grade) reflecting an accretionary environment which is the special geologic environment associated with hydrothermal fluids transport and deposition responsible for lode gold mineralization.
- 2) Special attention should be given to lode gold pathfinder elements during geochemical surveys especially if the mineral deposits type pursued is lode gold deposits type. The more the pathfinder/indicator elements, the higher evidence and the better predictive capacity of a mineral prospectivity generated.
- 3) A follow-up investigation of the favourable areas (N1 and N2) is recommended. Since only stream sediment geochemical data was used in this research, trenching through the regolith up to or close to the bedrock may possibly yield zones for drilling could betray locations of lode gold mineralization/deposits.

## 7. References:

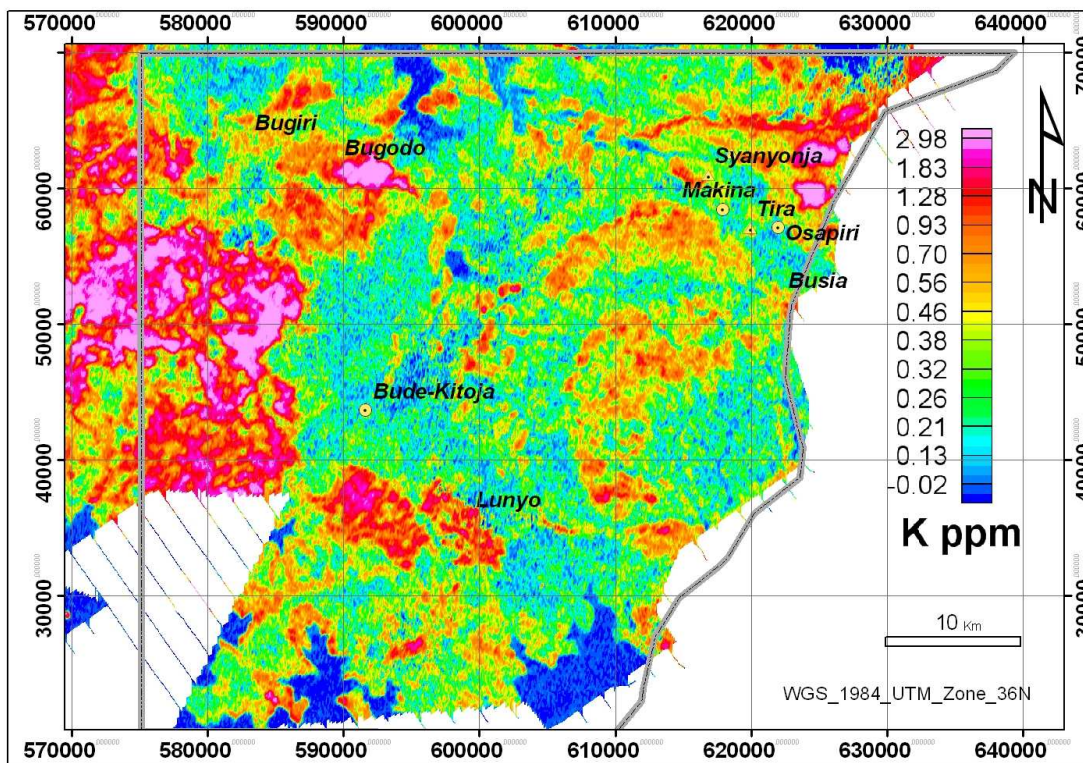
- Abdi, H., 2003, *Multivariate Analysis*.
- Alidu, S., 2007, *Classification of Birimian gold occurrences using their geological and geochemical attributes : case study in South Ashanti belt, Ghana, ITC, Enschede, 67 p.*
- Amor, S., <http://dirtbagger.golinfo.com/data1.pdf>, *Data presentation and interpretation requirements for geochemical exploration*
- An, P., W. M. Moon, and A. N. Rencz, 1991, *Application of fuzzy set theory to integrated mineral exploration: In: Canadian journal of exploration geophysics, 27(1991)1, pp. 10-11.*
- Barnes, J. W., 1961, *The mineral resources of Uganda, Bulletin. No. 4, Department of Geological Survey and Mines, Entebbe.*
- Bonham-Carter, G. F., 1994, *Geographic information systems for Geoscientists, Modelling with GIS: Computer methods in the Geosciences, v. 13, 398 p.*
- Byamugisha, S. S., A. Kebede, and D. B. A. Galimaka, 1994, *Follow up investigations in Bude-Kitoja EPL No. 4100 Iganga District, South-East, Uganda. RMC report. , Department of Geological Survey and Mines, Entebbe, Uganda*
- Campbell, M., T., and R. Kerrich, 1998, *P--T--t--deformation--fluid characteristics of lode gold deposits: evidence from alteration systematics: Ore Geology Reviews, v. 12, p. 381-453.*
- Carranza, E. J. M., 1994, *catchment basin approach to the analysis of reconnaissance geochemical - geological data from Albay province, Philippines, ITC, Delft, 191 p.*
- Carranza, E. J. M., 2002c, *Geologically - constrained mineral potential mapping : examples from the Philippines, ITC, Enschede, 480 p.*
- Carranza, E. J. M., 2007, *Predictive mapping of mineral prospectivity in areas without known mineral deposits: In: Map Asia 2007 : 6th annual international conference and exhibition on geographical information technology and applications : proceedings, 14-16 August 2007, Kuala Lumpur, Malaysia. art MA07 PN 203. 7 p.*
- Carranza, E. J. M., 2008, *Geochemical anomaly and mineral prospectivity mapping in GIS: Handbook of exploration and environmental geochemistry;11: Amsterdam, Elsevier, 366 p.*
- Carranza, E. J. M., 2008c, *Geochemical anomaly and mineral prospectivity mapping in GIS: Handbook of exploration and environmental geochemistry;11: Amsterdam, Elsevier, 366 p.*
- Carranza, E. J. M., and M. Hale, 2002e, *Where are porphyry copper deposits spatially localized? : a case study in Benguet Province Philippines: Natural resources research, v. 11.*
- Carranza, E. J. M., and M. Hale, 2002g, *Wildcat mapping of gold potential, Baguio district, Philippines: Transactions of the Institution of Mining and Metallurgy : Section B : Applied earth science, v. 111.*
- Carranza, E. J. M., M. Hale, and C. Faassen, 2007, *Selection of coherent deposit - type locations and their application in data-driven mineral prospectivity mapping: In: Ore geology review, (2007)In Press, 67 p.*
- Carranza, E. J. M., F. J. A. van Ruitenbeek, C. Hecker, M. van der Meijde, and F. D. van der Meer, 2008b, *Knowledge-guided data-driven evidential belief modeling of mineral*

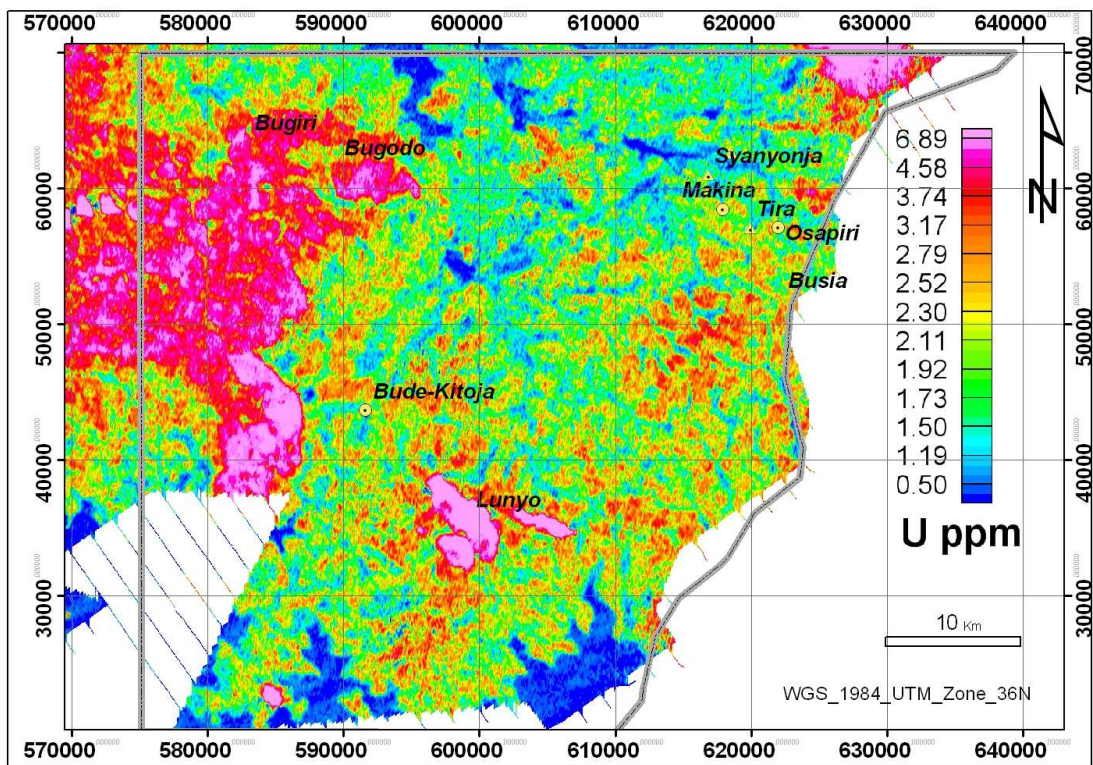
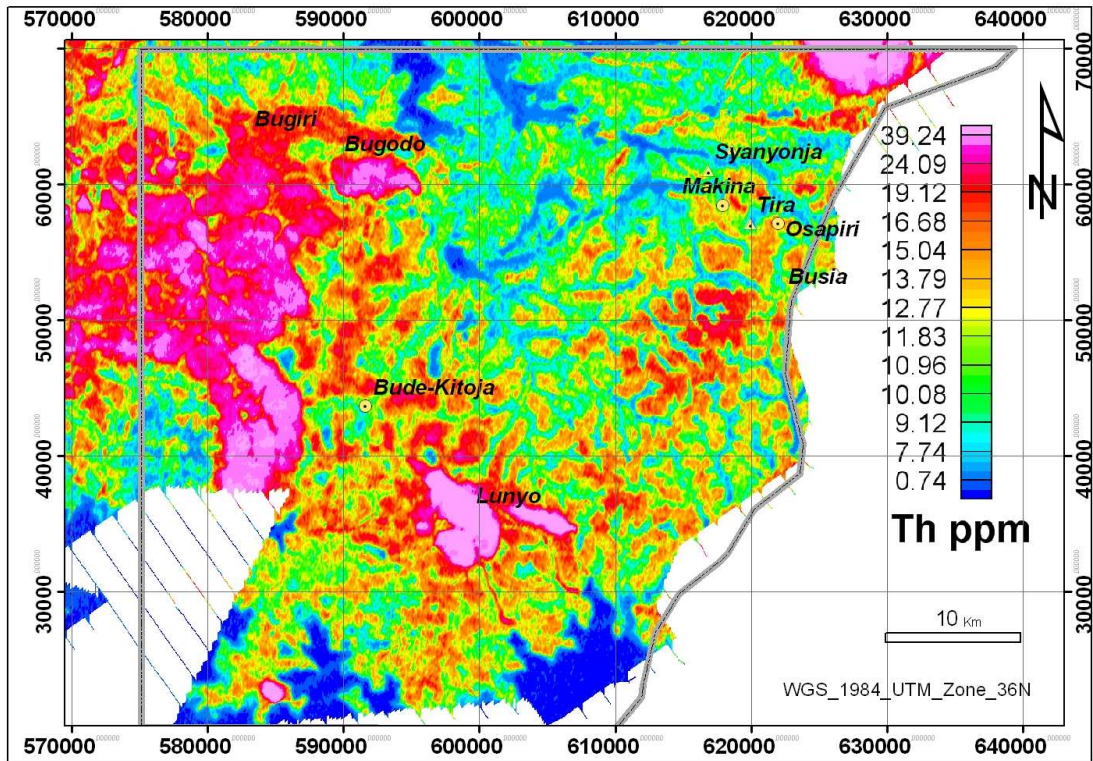
- prospectivity in Cabo de Gata, SE Spain: *International Journal of Applied Earth Observation and Geoinformation*, v. In Press, Corrected Proof.
- Chernicoff, C. J., J. P. Richards, and E. O. Zappettini, 2002, Crustal lineament control on magmatism and mineralization in northwestern Argentina: geological, geophysical, and remote sensing evidence: *Ore Geology Reviews*, v. 21, p. 127-155.
- Davies, 1934a, 1:50,000 scale geology map of Samia-Bukoli sector , : Department of Geological Survey and Mines Entebbe, Uganda.
- Davies, K. A., 1934b, Geology of parts of samia (Budama) and Bukoli (Busoga), Eastern Province Uganda Department of Geological Survey and Mines, Entebbe, Uganda.
- Eilu, P., and E. J. Mikucki, 1998a, Alteration and primary geochemical dispersion associated with the Bulletin lode-gold deposit, Wiluna, Western Australia: *Journal of Geochemical Exploration*, v. 63, p. 73-103.
- Eilu, P., E. J. Mikucki, and D. I. Groves, 1998, Wallrock alteration and primary geochemical dispersing in lode - gold exploration : notes from a short course presented at the 4th biennial meeting of the Society for Geology Applied to Mineral Deposits SGA, Turku, Finland, August 11-13, 1997: *Freiberg, The Society for Geology Applied to Mineral Deposits (SGA)*, 65 p.
- Gabert, G., 1990, Lithostratigraphic and tectonic setting of gold mineralization in the Archean cratons of Tanzania and Uganda, East Africa: *Precambrian Research*, v. 46, p. 59-69.
- GARS-DBM-TEAM, GSMD, and MARC, 1998, 1:250 000 Geology map of Jinja: compiled by McDonald and published by GARS-DBM-TEAM, GSMD and MARC (1:250 000).
- Grünfeld, K., 2004, Dealing with outliers and censored values in multi-element geochemical data - a visualization approach using XmdvTool: *Applied Geochemistry*, v. 20, p. 341-352
- Hawkes, H. E., and J. S. Webb, 1962, *Geochemistry in mineral exploration*, New York7 Harper.
- Hester, B., W. Boberg, J. T. Tuhumwire, J. Odida, E. Katto, and J. Nyakaana, 2006, Opportunities for Mining Investment, in G. S. Mines, ed., Entebbe, Ministry of Energy and Mineral Development of Uganda through Brian W. Hester Inc., p. 68.
- Hodgson, C. J., 1989, The structure of shear-related, vein-type gold deposits: A review: *Ore Geology Reviews*, v. 4, p. 231-273.
- Isabirye, M., E, 2005, 1:250 000 Jinja Geology map (1:250 000).
- Keays, R. R. e., W. R. H. e. Ramsay, and D. I. e. Groves, 1989, geology of gold deposits : the perspective in 1988: *Economic geology : monograph*,6: New Haven, The Economic Geology Publishing Company, 668 p.
- Kuehn, S., J. Ogola, and P. Sango, 1990, Regional setting and nature of gold mineralization in Tanzania and southwest Kenya: *Precambrian Research*, v. 46, p. 71-82.
- Lapidus, D. F., 2003, Collins Geology dictionary, in W. Isobel, ed.
- Mikucki, E. J., 1998, Hydrothermal transport and depositional processes in Archean lode-gold systems: A review: *Ore Geology Reviews*, v. 13, p. 307-321.
- Moore, D. S., and G. P. McCabe, 1998, *Introduction to the practice of statistics*: New York, Freeman, 854 p.
- Mroz, J. P., P. Urien, Z. Baguma, and L. Viallefold, 1991a, 1:100 000 Litho-geochemical map of the Busia Goldfield area (1: 100 000): Department of Geological Survey and Mines
- Mroz, J. P., P. Urien, Z. Baguma, and L. Viallefold, 1991b, Gold exploration in Busia area Uganda. BRGM Rep. No. 32761, Orleans , France., Department of Geological Survey and Mines, Entebbe, Uganda.
- Old, R. A., 1968, *The Geology of part of south east Uganda*: PhD thesis, Leeds University.
- Reimann, C., P. Filzmoser, and R. G. Garrett, 2005, Background and threshold: critical comparison of methods of determination: *Science of The Total Environment*, v. 346, p. 1-16.

- Rose, A. W., H. E. Hawkes, and J. S. Webb, 1979, *Geochemistry in mineral exploration: London etc.*, Academic Press, 657 p.
- Sango, P. M., 1995, *Controls on mineralisation in the Lake Victoria goldfield, Tanzania*, ITC, Delft, 142 p.
- Schumann, A., 2007, *Summary of the geology of the Tiira area, its gold mineralization, and current and future exploration targets with a note on recent exploration results from McAllister's reef on EL 0030*, BUSITEMA MINING CIE LTD Reports, p. 11.
- Stanley, C. R., <http://www.appliedgeochemists.org/events/iges2005/presentations/24%20Stanley%20QCliff.pdf>, *Univariate Data Presentation: The Contouring Conundrum and Philosophical Arguments Regarding the Contouring of Geochemical Data*, p. 38.
- van Roij, A., E. J. M. Carranza, M. Hale, and E. A. Owusu, 2006, *Geological remote sensing and gold prospectivity mapping in Kibi area, Ghana: In: AARSE 2006 : Proceeding of the 6th AARSE international conference on earth observation and geoinformation sciences in support of Africa's development, 30 October - 2 November 2006, Cairo, Egypt. Cairo : The National Authority for Remote Sensing and Space Science (NARSS), 2006. ISBN 1-920-01710-0. 8 p.*
- Yusta, I., F. Velasco, and J.-M. Herrero, 1998, *Anomaly threshold estimation and data normalization using EDA statistics: application to lithochemical exploration in Lower Cretaceous Zn-Pb carbonate-hosted deposits, Northern Spain: Applied Geochemistry*, v. 13, p. 421-439.

## 8. Appendices

Appendix 1: Radio-element grid maps for K, Th and U

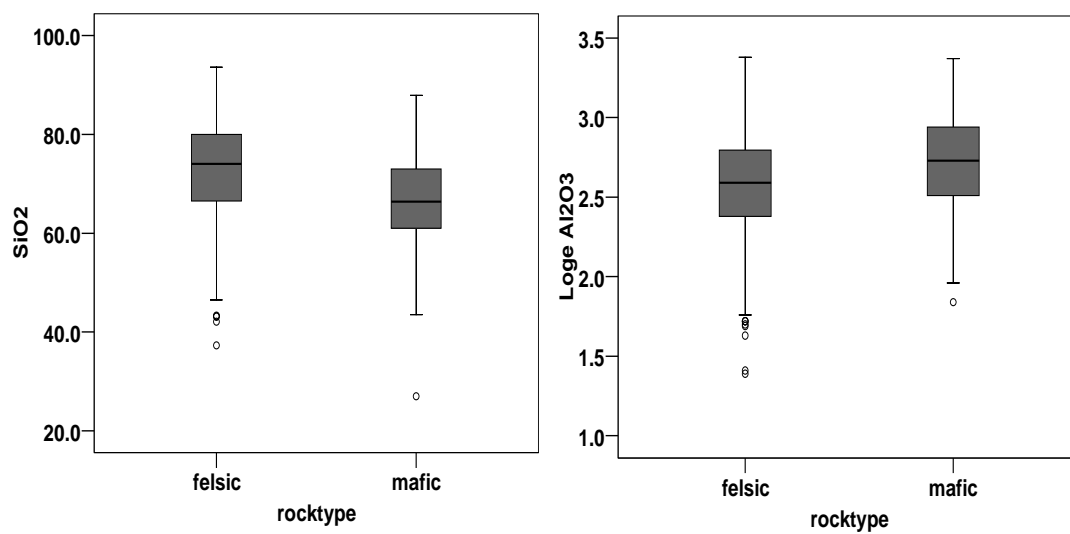


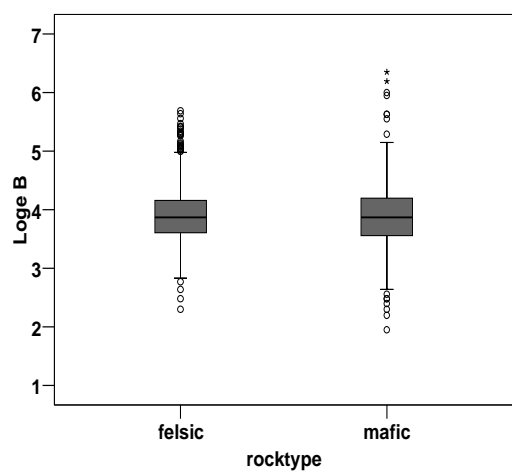
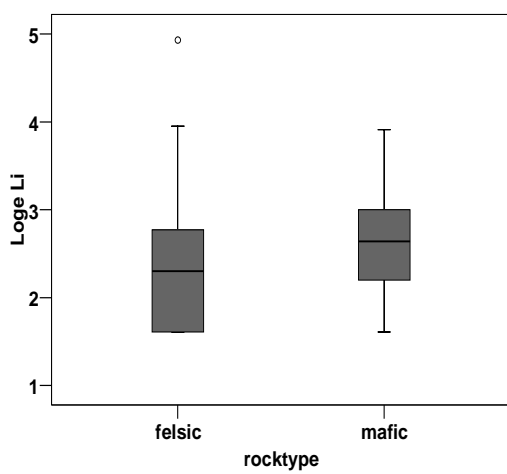
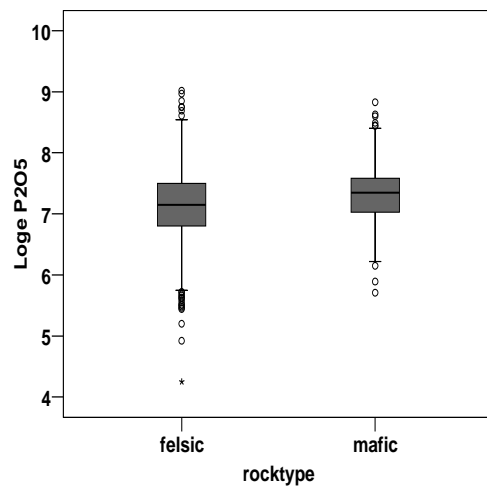
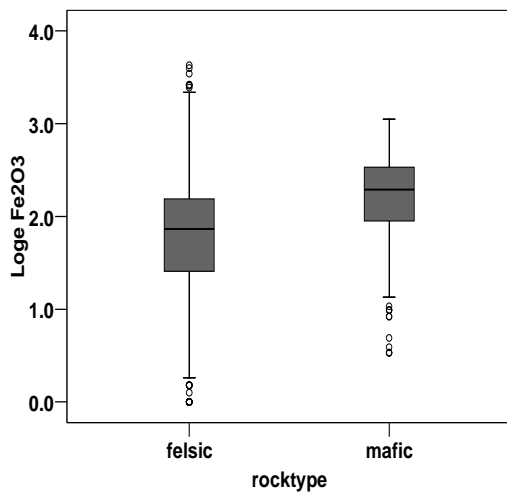
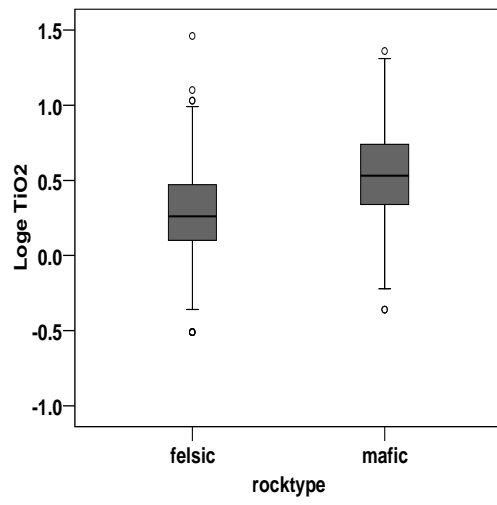
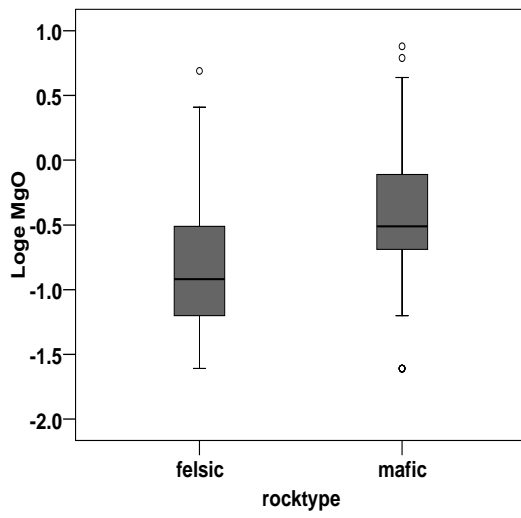


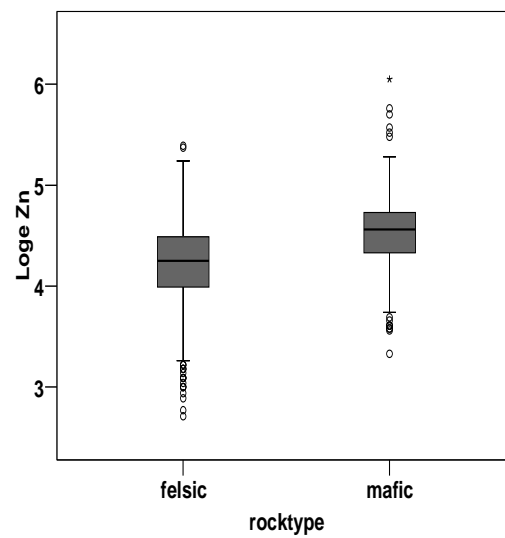
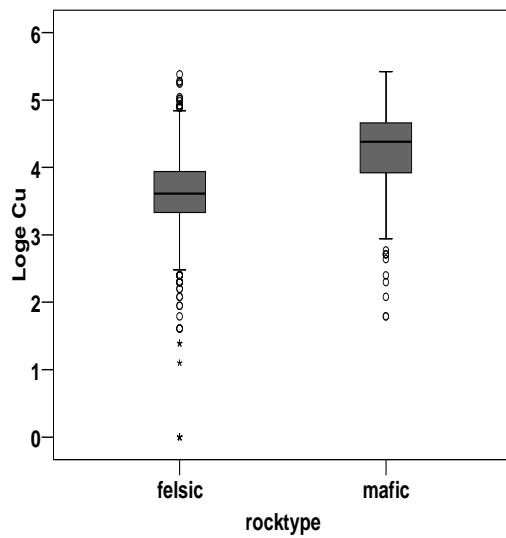
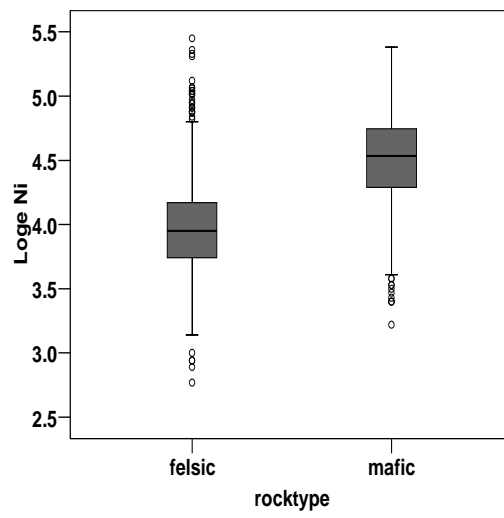
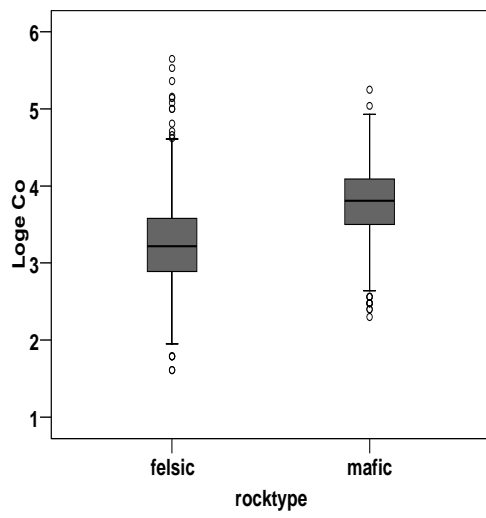
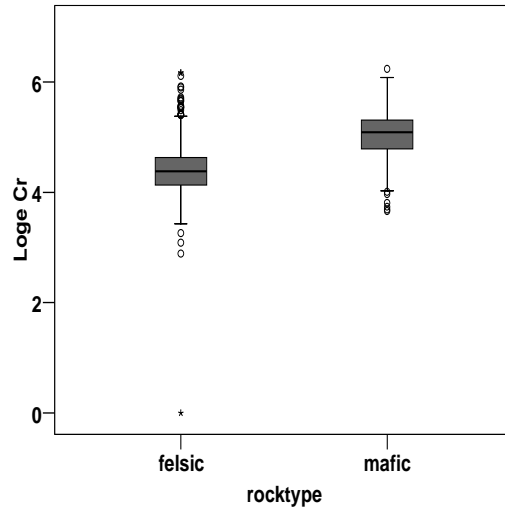
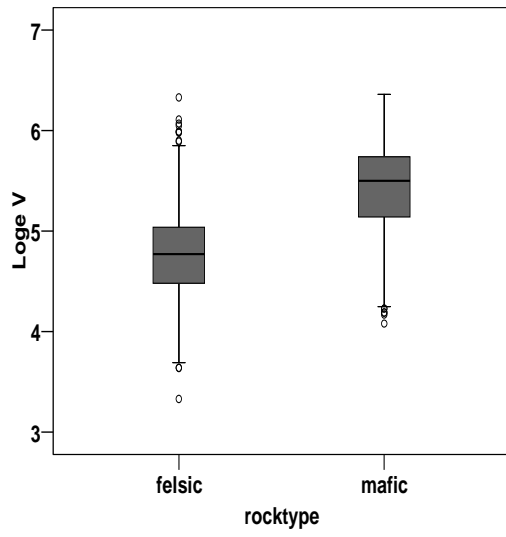
Appendix 2: Photograph taken on top of the Buteba granite. Note the K-rich medium grained grey feldspars.

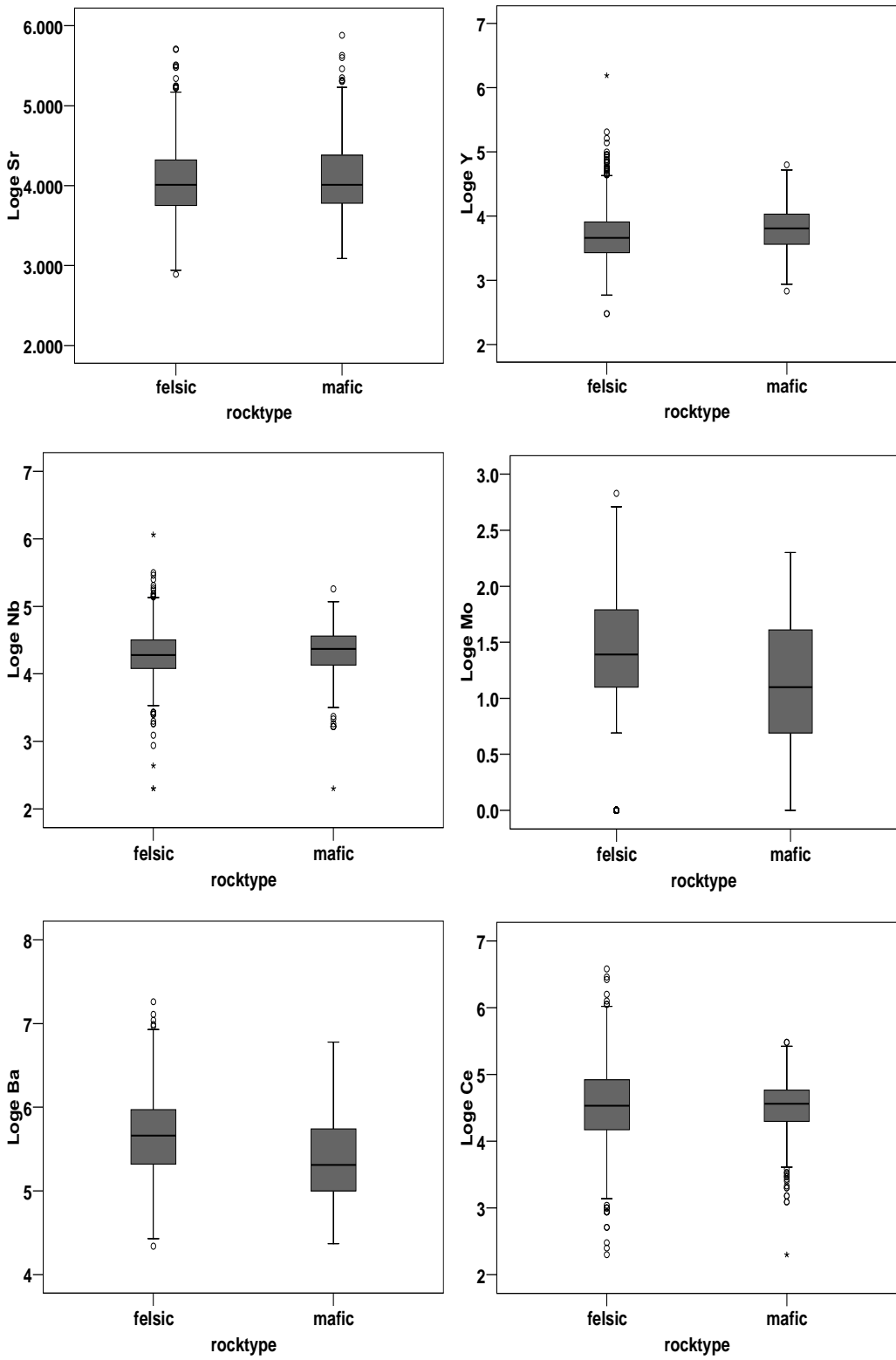


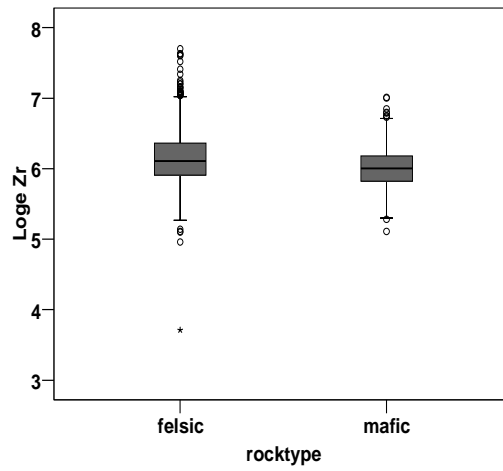
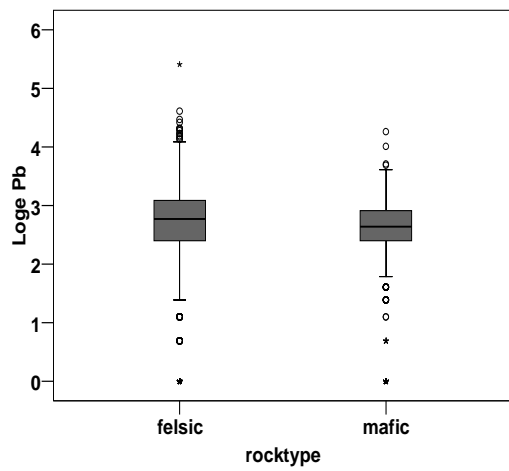
Appendix 3: Uni-element box and whiskers plots for both felsic and mafic rock suits



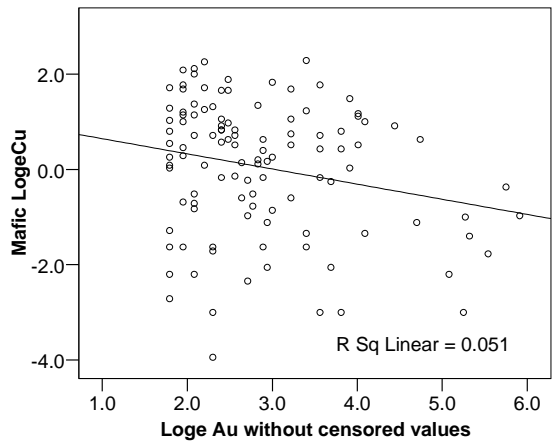
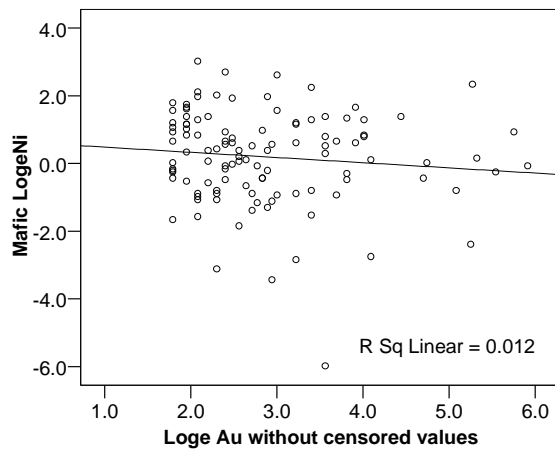
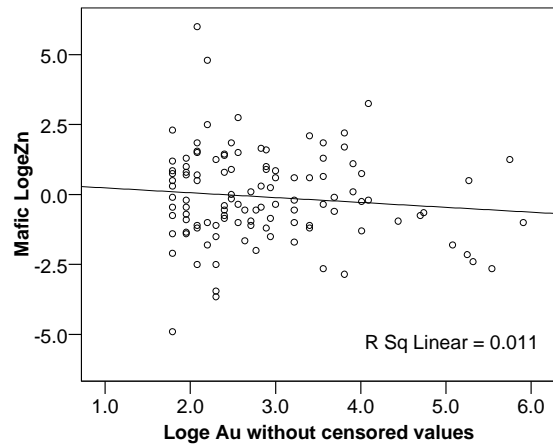
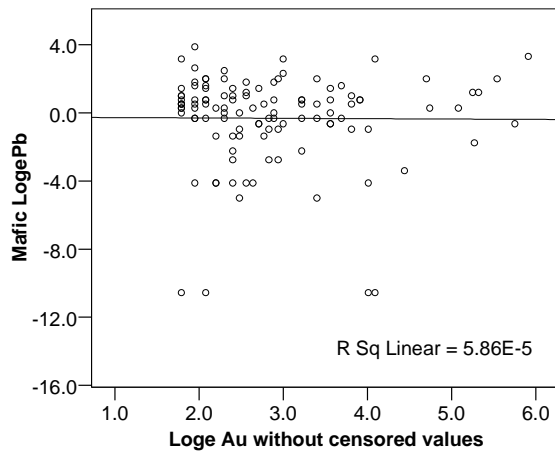


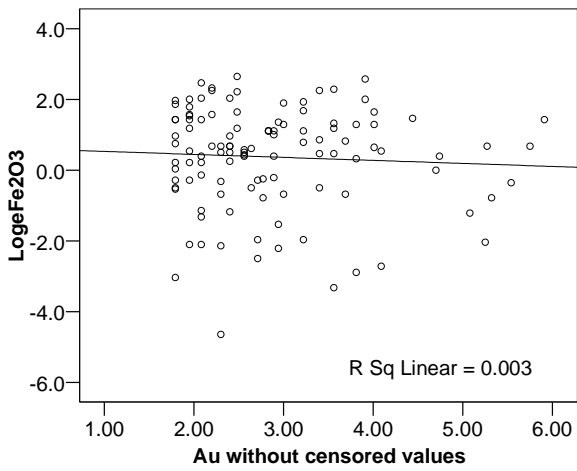
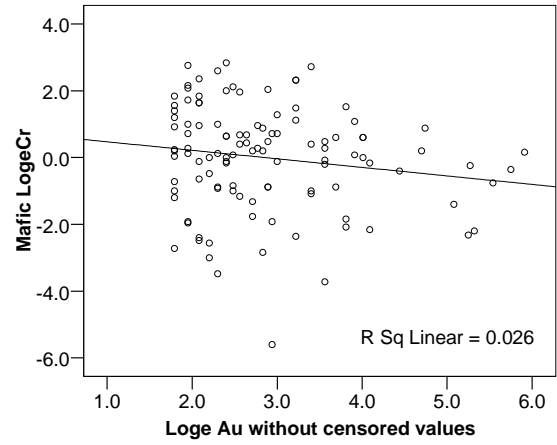
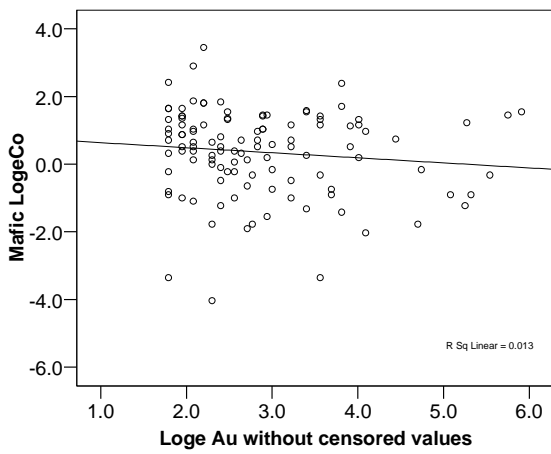






Appendix 4: Scatter plot of Au versus selected elements





Appendix 5: Photos at some of the Tiira mine opencast mining pits showing Fe-oxide/hydroxide-rich reddish brown soils and MnO<sub>2</sub> overprints on to quartz pebbles

